T.C.
ISTANBUL GEDİK UNIVERSITY
INSTITUTE OF GRADUATE STUDIES

HYDROLOGICAL EVALUATION OF SPILLWAY IN EARTH DAM, A CASE STUDY: KHANAS DAM IN IRAQ-DUHOK

MASTER's THESIS

Suzan Nazmy HUSEEIN

Civil Engineering Department

Master in Civil Engineering English Program

JUNE 2023

T.C.
ISTANBUL GEDİK UNIVERSITY
INSTITUTE OF GRADUATE STUDIES

HYDROLOGICAL EVALUATION OF SPILLWAY IN EARTH DAM, A CASE STUDY: KHANAS DAM IN IRAQ-DUHOK

MASTER's THESIS

Suzan Nazmy HUSEEIN
(211282003)

Civil Engineering Department

Master in Civil Engineering English Program

Thesis Advisor: Assoc. Prof. Dr. Redvan GHASEMLOUNIA

JUNE 2023

T.C.
İSTANBUL GEDİK ÜNİVERSİTESİ
LİSANSÜSTÜ EĞİTİM ENSTİTÜSÜ MÜDÜRLÜĞÜ

Yüksek Lisans Tez Onay Belgesi

Enstitümüz, Civil Engineering Department İngilizce Tezli Yüksek Lisans Programı (211282003) numaralı öğrencisi Suzan Nazmy HUSEEIN'nin "Hydrological Evaluation of Spillway in Earth Dam, A Case Study: Khanas Dam in Iraq-Duhok" adlı tez çalışması Enstitümüz Yönetim Kurulunun 01/06/2023 tarihinde oluşturulan jüri tarafından *Oy Birliği* ile Yüksek Lisans tezi olarak *Kabul* edilmiştir.

Öğretim Üyesi Adı Soyadı

Tez SavunmaTarihi: 01/06/2023

1) Tez Danışmanı: Doç. Dr. Redvan GHASEMLOUNIA

2) Jüri Üyesi: Dr. Öğr. Üyesi Mert TOLON

3) Jüri Üyesi: Dr. Öğr. Üyesi Hasan Bozkurt NAZİLLİ

DECLARATION

I, Suzan Nazmy Hussein, declare that this thesis titled " Hydological Evaluation of Spillway In Earth Dam, A Case Study: Khanas Dam In Iraq-Duhok", is original work done by me for the award of the master's degree in the Faculty of Civil Engineering. I also declare that this thesis or any part of it has not been submitted and presented for any other degree or research paper in any other university or institution (01/06/2023)

Suzan Nazmy HUSEEIN

DEDICATION

I dedicate my research to all my dedication to my lovely family, my wonderful and great mom (MRS.Samiye Rasheed Ibrahim), my dear brother (Mohanad Nazmy Hussein),my husbunad (Engineer Mustafa Sameer Algburi), my husband's father and my second father (Pr.Dr.Sameer Saadoon Algburi), my husband's mother and my second mom (Mrs.Wahbiye Ahmed Mohameed) my childrens (Haytham, Tim and Tia) and favourite Dam engineer Mr. Abdulkadir Mohammed Salih (Duhok Dam Directorate).

PREFACE

Foremost thanks to Allah, the most beneficent and merciful, who helped me to complete this study and to submit it in such a way.

I would like to express my thanks, appreciation, and gratitude to my supervisor, Assoc. Prof. Dr. Redvan Ghasemlounia for his concern, guidance, and advice.

June 2023 Suzan Nazmy HUSEEIN

TABLE OF CONTENT

Page

ABBREVIATIONS

AVM : Assistance Vector Model
FFORD : Formula of First-Order Dependability
FSORD : Formula of Second-Order Dependability
HD : Hypothetical Design
IONM : Initial Order Next Moment
PDD : Polynomial Disorder Development
PM : Part Modeling
PCE : Probability-based Criticality Evaluation
LSF : Limit State Function
LSS : Limit State Surface
UF : Unidentified Field
MT : Moment Techniques
MPFP : Most Probable Failure Point
MCM : Monte Carlo Modeling
SS : Significance Sampling
SF : Safety Factor
SAO : Several Autocorrelation Operates
WCD : World Conservation Union

LIST OF TABLES

Page

LIST OF FIGURES

Page

HYDROLOGICAL EVALUATION OF SPILLWAY IN EARTH DAM, A CASE STUDY: KHANAS DAM IN IRAQ-DUHOK

ABSTRACT

The execution of the embankment requires a significant amount of time, as well as a significant amount of Hydrological resources and experience. As a result, it is necessary for it to be planned, developed, and constructed in accordance with severe requirements in order to achieve a strong structure and high efficiency while maintaining a safe operating environment in order to preserve human contributions.

An investigation of any dam site needs a feasibility study for the site as four parts: Preliminary study (Geophysical, Geological and Surveyor study), if this part is evaluated and decision makes, then the second part will be started such as (Geotechnical, Surveying, hydrological, Hydraulically and geological, in details, Then Analysis for design of the dam will be started, and in the final part, the design must be checked and evaluated.

In this research Khanas dam Project was evaluated hydrologically after analyzing rainfall data using Hyfran software by 11 models; the best one, according to our analyzing data using comparison by AIC and BIC, is the Exponential (maximum likelihood) model and the maximum estimated rainfall for 24 hours is (265) mm as shown in Table no.1, and maximum flood discharge according to our research is (1,853.44) m^3/s for return period (2000) years (for the same return period of the original Khanas dam design).

While the Spillway maximum flood in the original design of Khanas dam (947) m3/s and the maximum flood discharge calculated by this research it's about two times of the design value, therefore the Spillway dimensions are not adequacy to pass flood safely in the same return period, and Khanas dam Project in Risk.

Keywords: *Embankment, Feasibility Study, HYFRAN, Spillway, Return Period*

TOPRAK BARAJINDAKİ DOLUSAVAKIN HİDROLOJİK DEĞERLENDİRİLMESİ, BİR ÖRNEK İNCELEMESİ: IRAK-DUHOK'TAKİ KHANAS BARAJI

ÖZET

Herhangi bir dolgu barajı projesinin uygulama aşaması uzun zaman almaktadır, ayrıca çok miktarda hidrolojik kaynağa ve pratik tecrübeye ihtiyaç duyar. Güçlü bir yapıya ve yüksek verili bir baraj yapmasını sağlamak amacıyla, aynı zamanda güvenli bir işletme ortamı yaratmak için, özel gereksinimlere göre planlaması, geliştirilmesi ve inşa edilmesi gerekmektedir. Barajın inşaatı için bir fizibilite çalışmasının dört aşamada yapılması gerekiyor; Ön çalışma (jeofizik, jeolojik ve ölçme çalışması), ikinci aşamada detaylı olarak (jeoteknik, kadastral, hidrolojik, hidrolik ve jeolojik) gibi bu kısımda başlar, üçüncü aşamada (baraj tasarımı için analizlere başlayacak) ve dördüncü aşamada ise tasarım incelenir ve değerlendirilir. Bu araştırmada, Khanas Barajı projesi, 11 model kullanılarak Hyfran programı ile yağış verileri analiz edildikten sonra hidrolojik olarak değerlendirilmiştir; AIC ve BIC karşılaştırmasını kullanarak yaptığımız analiz verilerine göre en iyisi, Üstel modeldir (maksimum olasılık) ingilizce adı (maximum likelihood) ve Tablo 1'de gösterildiği gibi 24 saat için tahmini maksimum yağış (265) mm ve dönüş süresi için araştırmamıza göre maksimum taşkın deşarjı (1.853,44) metreküp / sn'dir (2000) yıl (Khanas Barajı'nın orijinal tasarımına dönüş ile aynı dönüş süresi için). Khanas Barajı'nın orijinal tasarımındaki savak (spillway) maksimum taşkın (947) m3/s ve bu araştırma ile hesaplanan maksimum taşkın debisi (maximum flood discharge) tasarım değerinin yaklaşık iki katı olup, bu nedenle su akıntısının boyutları aynı geri dönüş süresi için selin güvenli bir şekilde geçmesi için yeterli değil ve Khanas Barajı projesi kritik bir durumda olduğunu görebiliriz .

Anahtar Sözcükler: *Dolgu Baraji, Fizibilite, HYFRAN, Savak, Geri Dönüş Süresi*

1. INTRODUCTION

1.1 General Introduction

Dams with embankments are monumental structures that are built to serve a wide variety of human activities from both economically and protection viewpoints. The building of the embankment requires a significant amount of time, as well as a significant amount of resources and experience. As a result, it is necessary for it to be planned, developed, and constructed in accordance with severe requirements in order to achieve a strong structure and high efficiency while maintaining a safe operating environment in order to preserve human contributions.

The advancement in human activity was initially accomplished by the scientific method and in-depth research on all aspects of the fields that support and lead to progress. The investigation into the design and implementation of embankments represents the foundation for the establishment of water and infrastructure assignments. From this vantage point, the importance of conducting this study emerges, as does the requirement that those who deal with the designing of embankment dams be aware of what to anticipate in any geological setting, as well as have a grasp of the limitations of inquiry and design methods, as well as building procedures.

Because of the potential for catastrophic consequences in the event of a dam's failure, conducting safety assessments is an absolutely essential part of the dam-building process. When it comes to earth dams, there are primarily three types of failure modes: two of which are connected to structural collapses (piping and slope weakness), and one of which is caused by flood overtopping.

Zhang et al. (2009) provided a statistical overview of the embankment-dam collapses that had occurred prior to the year 1986. The authors emphasized that the piping is the primary cause of structural collapses for these dams, and they made this fact clear in their discussion. Additionally, they discovered that the parameters of the zoning play a significant contribution in the incidence of piping collapses.

For instance, up until the year 1986, there were no reports of the collapse of pipelines in embankment dams that are outfitted with a central core. On the other hand, this particular sort of failure has caused the destruction of 16 huge homogenous earth-filled dams. Consequently, the piping should not necessarily be the primary consideration for central core earth dams, and the issue of stabilization of slopes ought to be given serious thought when planning or appraising this type of dam. Both of these problems should be taken into consideration (Foster et al., 2022).

In the past, the variability of the soil was taken into consideration by "penalizing" the soil strength characteristics using partial factors that were either advised by qualified professionals or mandated by design standards. This ensured that the designs or computations were as conservative as possible. On the other hand, if there is a great amount of variability, this method might result in risky constructions.

In other instances, the designs, which are dictated by partial elements, might be too cautious, making them economically infeasible. The probabilistic evaluation is a powerful approach that, by presenting complementary findings, makes it possible to more effectively handle the challenges outlined in the previous paragraph (Azam and Li, 2010).

1.2 Dams and Sustainability

The primary function of dams is to collect water and control the flow of rivers. The water that is stored in dam reservoirs can be used for a variety of purposes, including agriculture, human and industrial consumption, and the generation of electricity through hydropower. Several dams are built with the purpose of distributing water to different areas.

Over (57,000) major dams are currently operational across the globe. The “International Commission of Large Dams” describes these as those with a storage capacity that is larger than 3 million cubic meters or having a height that is higher than 15 meters. The starting of the previous century saw the beginning of the period of huge dams. In the globe today, there are around (5,000) such dams that are more than (50) years old. Just a single river out of every four that is longer than one thousand kilometres in the world does not have any dams on it and is therefore regarded to be a free-flowing river that is least impacted by human activities. These

rivers are the equivalent of wildness in the freshwater environment. The “Greater Zab” is thought to be the last river in “Mesopotamia” that still flows freely, and it may be found in the “Kurdistan Region of Iraq”.

The use of hydropower is the most prevalent form of renewable energy production across the globe. It is common practice to portray large hydroelectric dams in a positive light. Studies have shown that a significant number of these large-scale water infrastructure constructions in “Europe” and “United States” have had a negative impact on the environment. Even though they would lead to an increase in the proportion of renewable energy used globally, dams have a challenging association with the “Sustainable Development Goals” established by the United Nations (Bartle,2002).

Dams almost always cause irreversible harm to the rivers on which they are built. The initial expenditures of dams are typically large, and there is typically a long wait among the authorization of a project and the beginning of execution. As a result, the risks connected with like water infrastructure are significant. It has been demonstrated that the majority of these buildings that have been erected across the world turned out to be priced higher than what was expected, and its environmental and social implications are frequently not taken into consideration, typically because of the potential of low-cost electricity generating hydropower.

In point of fact, industries are the ones that reap the greatest benefits from dam construction projects. Both a lack of due care in handling human and environmental infractions and a lack of unbiased assessment of the socio-environmental repercussions are frequent among the parties involved in dam construction initiatives (Chang et al., 2010).

1.2.1 Environmentally effect

Dams prevent the natural migration of fish as well as the movement of sediments and nutrients. This causes a significant disturbance to the natural functioning of the environment. Dam reservoirs have an effect not only on the temperature and quality of the water but also on the patterns of river flow. This may result in disturbances further downstream of the river. The impact of habitat loss and degradation is greatest on freshwater ecosystems, which are also the most threatened. The quantity and quality of the water, as well as how well it is connected to the rest of the system,

the state of the habitat, and the kinds of plants and animals that live there all have a role in determining its overall health.

Because of this, wildlife and forests might be wiped out if a dam's reservoir were to overflow and flood the surrounding area. Dams may hasten the progression of climate change. The construction of river dams disrupts the rivers' natural flows, which can lead to a shortage of water in communities further downstream. As a result of other impacts and releases of greenhouse gases, it has the potential to disrupt and modify the hydrosphere, which is the most susceptible portion of the climate system. Dam reservoirs are responsible for the transmission of such methane releases.

The building of dams and the associated extraction industries can lead to the destruction of forests, which are important places for the absorption of carbon. Dams, in and of themselves, are susceptible to the effects of climate change; they could become inoperable as a result of flooding or drought. In the context of climate-changing processes, such as the Green Climate Fund, various civil society organizations from around the world have argued for the removal of financial incentives for the development of new hydroelectric projects (Sangal et al.,2013).

1.2.2 Social effect

When their territory becomes drowned, the local communities are forced to relocate. Dam reservoirs have resulted in the forcible relocation of up to 80 million people all across the world, with little provision for compensation. Communities that may be adversely affected by dams often do not have a voice in the development of dams in their region.

People whose livelihoods depend on the river downstream from the dam will also be negatively impacted; one example of this is the loss of revenue that will be experienced by those whose livelihoods depend on fisheries. In many cases, the effects on people located further downstream are not taken into consideration.

In most cases, the construction of dams has been accompanied by the building of access roads, immigration, the seizure of land, logging, deforestation, and mining. The fact that many dam projects have been developed without prior consultation or approval from local dam-affected populations has contributed to the prevalence of socioenvironmental conflicts that, on numerous occasions, have resulted in violent conflict. Dams are frequently promoted as being good to the areas in which they are

located; however, research has shown that this is not the case. Constructors frequently fail to address important problems such as governance and long-term sustainability. In many cases, local populations are promised benefits like as cheaper energy, new jobs, and upgraded infrastructure; nevertheless, these benefits frequently do not materialize (Ledec and Quintero,2003).

In the case of the “Belo Monte” and “Jirau Dams” located on the “Amazon River” at Brazil, the price of energy increased, and the majority of the newly created positions were filled by people from outside the area. These jobs disappeared after a few years. As a result of the construction of dams, local populations may also experience a loss of their cultural legacy. There have been numerous instances in which water infrastructure has posed a risk to cultural heritage monuments. There have been 51 “UNESCO World Heritage” sites that have been damaged or are in danger due to water infrastructure all across worldwide.

The old town of “Hasankeyf” in Turkey was flooded due to the installation of the Ilisu Dam, which is an example of the destruction of legacy that can occur as a result of dam construction. The development of upstream dams on the “KRI” poses a risk to the marshlands of “Southern Iraq”, which are a “World Heritage Site”.

1.2.3 Economic effect

The World Bank and other IFIs, the need for energy in emerging economies, "South-to-South" investment and trade, and bilateral agreements and objectives are all factors that the International Hydropower Association (IHA) that reflects the global hydropower industry sees as driving an expansion of hydropower dams. Hierarchical decision-making systems that lack transparency, community participation, and strategic consideration are typically where big dam projects are planned.

It is ideal to promote complete assessments, which take into account all of the social, environmental, and economic costs and benefits. The social and environmental implications of dam construction are frequently minimized in studies that are commissioned by private dam construction corporations. Environmental impact assessments, on the other hand, are typically carried out by dam proponents who are primarily concerned with showing the profitability of the project.

In this particular context, the suggestions made by the World Commission on Dams (WCD) are particularly pertinent. The World Conservation Union (WCD) was an

autonomous international group that brought together representatives from a variety of sectors, including governments, industries, academic institutions, and civil society. The environmental and social implications of major dams were examined and addressed in this report (Whitney et al., 1997).

1.3 Iraq and Water Legislation

For the purpose of controlling the flow of water through dam reservoirs, a number of authorities have argued in favour of preserving and encouraging environmental flow regimes that are supported by scientific evidence. These environmental fluxes are used to characterize the amount, frequency, and quality of drinking water flows and concentrations that are required to maintain aquatic environments, which in turn support societies, economies, and sustainable ways of life and well-being. Even while the preservation of environmental flows is written into the legislation in many nations, the law's application is frequently highly skewed in favour of dam constructions.

This is a problem that has to be addressed. Neither Iraq nor the KRI has any laws that specifically address the flow of water. The use of hydropower, which is currently one of the alternatives to fossil fuels, is responsible for the greatest number of adverse effects on both the natural world and human beings. By damming waterways, wind power, solar energy, and biomass power plants may create electricity that has minimal carbon emissions. Alternatives like this should be taken into consideration by decision-makers so that energy sources can be diversified. In addition, the lifespan of a dam is not infinite (Yousuf et al., 2018).

Dam removal is becoming increasingly prevalent throughout the industrialized world, despite the fact that numerous new dams are currently under construction or are in the planning stages in Africa and Asia. The vast majority of them are of a small to medium dimension.

Dam dismantling is a complicated process that may result in significant environmental shifts, yet, it may be up to three times less expensive than dam repair and may help to restore ecosystems dependent on drinking water. The structures of dams, to the tune of thousands, have been demolished all over the world in an effort to restore ecosystems (Sulaiman et al., 2019).

1.4 Khanas Dam

The place of “Khanas Dam” is located in a mountainous region that is found in the northern section of the “Kurdistan” region in Iraq, as shown in figure (1-1). A significant portion of the foundation rock component is composed of limestone, whereas the majority of the foundation rock material is composed of “claystone”, “marl”, “limestone”, and the infrequent occurrence of gypsum at elevations. The “Pilaspi Limestone Formation”, which dates back to the Late Eocene, serves as the foundation for the dam's axis, which is tilted roughly 12 degrees to the south-west. The underlying geotechnical assessment was performed by investigating the core of eight dug boreholes with an overall length of 193 meters. Four of the boreholes were sunk along the longitudinal direction of the dam, two were drilled in ahead, one was dug in the downstream direction, and one was drilled in the region wherein the infrastructures connected to the dam are going to be erected (Askar, 2018).

During the site evaluation processes, uniform and suitable site evaluation techniques were utilized to ensure that precise, trustworthy, and representative information would be gained. This was done so that a small earth-fill dam of fifteen meters in height could be constructed on the Gomel perennial river, which has a discharge that ranges from (3 to 4) (m^3/s) when it is dry and (40 to 50) (m^3/s) when it is rainy (Al-Khateeb and Capigian, 2010).

Figure 1.1: Khanas Dam

1.5 The Aims of the Research

The research provides a control situation for the Khanas Dam, determines the supposed longevity of the dam, and determines, in the case of a flood, the amount to whether the dam will be capable to survive the flood or cannot.

- An investigation on the hydrological analysis of the Khans dam.
- Evaluation and planning of floods are expected to occur during the next 24 hours.
- Flood management, regardless of the degree to which the dam can accommodate the water.
- Investigation on the sediments that are being brought to the dam.
- The default life expectancy of the dam was calculated.
- Manage the flow of water entering the system.
- Utilize a program that does frequency analysis hydrological.

1.6 The Scope of the Research

The following is a synopsis of the approach and methodology that the study takes:

- Assessment of the helpful investigations and research that were done in the planning, construction, and assessment of the embankment and adoption of the overall standard for the establishment of a phased planning and assessment strategy.
- Gather any and all data that may be relevant to the existing embankment that is being investigated for this particular research.
- Implement the research plan that was designed in order to gather the missing as well as actual knowledge and statistics for the embankment that is being considered.
- Discussing and analyze the findings obtained from every possible source of data as well as the results of the experiment that was carried out.
- Describe the shortcomings of the current embankment that was examined in terms of its design and construction in order to assess the level of performance that can be anticipated from it in the future.

1.7 Structure of the Study

The structure of the study is as follows:

Chapter One: In this section, a broad introduction is offered, in which the reasons, aims, and organization of the current study are discussed.

Chapter Two: the durability methodologies that are typically utilized in the actual construction of geo-structures, in addition to the probabilistic evaluation of earth dams. Furthermore, the probabilistic assessment methods that were utilized in this work or modified specifically for the dam problem are discussed in this study.

Chapter Three: An overview of prior research on the main sources of the water are perennial streams which flow mainly in the synclinal valleys beside the rainfall and spring, snow covers some of the high mountains, which supply a good quantity of water after melting.

Chapter Four: Study the future projections for the development of hydraulic infrastructure, statistical and stochastic methods employed in analysing historical data on hydrologic variables to ascertain their properties in order to predict their future values.

Chapter Five: Results and Discussion

Chapter Six: Conclusion and Recommendation

2. LITERATURE REVIEW

2.1 General Review

One definition of an embankment dam is "any dam established of materials from excavation placed without including binding materials apart from those inherent components." The materials are typically acquired locally or in close proximity to the location of the dam.

The impounding of water for multiple purposes, including water supply, protection, and the construction of dams to resupply groundwater, is the objective of embankment dams.

The goals of this chapter are twofold: Firstly, give an overview of prior research on the probabilistic evaluation of earth dams by providing an overall review of durability evaluation methodology typically used in geotechnical technology, including a full discussion of the probabilistic methods applied; and secondly by presenting the probabilistic methodologies used in this study in particular.

The probabilistic methods used in this study are then discussed at length. In this section, we discuss the procedures for doing a probability-based criticality evaluation (PCE), a global sensitivity evaluation (Sobol index), and spatial modelling (various Unidentified Fields).

In addition to introducing the Latin Hypercube Sampling technique, this section also discusses iso-probabilistic conversion and variogram evaluation. The earlier probabilistic research on earth dams is evaluated at the end of this chapter and is organized into three categories, focusing on the leaking stability of slopes and interior deformation.

2.1.1 Embankment dam varieties

The earth-fill and rock-fill dams are the two most common types of embankment dams. They are differentiated from one another based on the major fill material

utilized during construction, and their characteristics are outlined in the following paragraphs (Froehlich, 2008).

- **Earth Dam:** The right soil for an earth dam can be collected from borrow regions or by doing the necessary excavation, and then it is mechanically compressed in layers to form the dam. Typical portions of earth dams illustrate zoning for several kinds of fill materials and volumes, as well as various ways to prevent seepage.
- **Rock Dam:** Dams that are made primarily of rock and have an impervious core are referred to as rockfill dams. A series of points of transition that are constructed out of material that has been appropriately graded lie between the core and the rock. Two broad categories of rockfill dams are described here.

2.2 Considerations for Dam Design and Construction

The designing of an embankment dam is difficult because of the lack of information regarding the footing and the resources that can be used in its construction. The accumulation of prior knowledge demonstrates that embankment dams may be (simply) adapted to meet the specific demands of a project in terms of its geologic site characteristics and operational necessities (Adamo et al., 2020)

In addition, practical experience has traditionally been an essential component in the construction of embankment dams. The comprehensive evaluations of embankment dams must be carried out utilizing a wide variety of factors, which will enable one to gain an understanding of how sensitive the particular study is to the material qualities and the geometric layout (Martin and McRoberts, 1999).

When designing and building new dams, as well as when assessing the safety of existing dams, having a solid comprehension of the factors that can lead to failure is an essential component of the process. The collapse of previously constructed dams might be taken into consideration for efforts in the field of dam protection and dam construction, as well as for the creation of an inventory of construction considerations and guidance. This section addresses the design idea from and beyond the collapse modes and their Probability of occurrence, as well as the general factors and limitations that need to be taken into account in the process of designing and building dams (Adamo et al., 2020).

2.2.1 Collapse mode evaluation

The described project design is based on the project specifications, geology evaluation and site description, one-of-a-kind project attributes, loading situations, and specifications for the dam and connected components. As the design process moves on, an analysis of the dispersion of the materials and the construction of an initial part of the embankment is carried out. The last stage is to carry out a preliminary collapse mode evaluation, which entails determining the modes of collapse that are most likely to occur for the dam, the basis, the abutments, and the associated structures as they were intended (Martin and McRoberts, 1999).

It is essential to have a comprehensive grasp of the historical reasons for collapse and the Probability associated with each of those causes. After this has been accomplished, the collapse modes should be identified in the order of the possibility that each one will occur. The collapse modes are examined and modified while the ultimate design is being worked on. It has recently become possible to classify the many types of collapses into one of three primary groups, thanks to the assessment reports that were conducted on the vast majority of the previous collapses:

- Hydraulic collapse.
- Seepage collapse.
- Structure collapse.

2.2.1.1 Hydraulic collapse

a. Overtopping: the foundation of the dam has a chance of being overtopped if the amount of water that was designed for it is overestimated or if the capacity of the spillway is insufficient. Overtopping can also be caused by other factors, such as inadequate freeboard or settlement of the foundation or embankment.

b. Corrosion at the toe: Corrosion at the toe may take place for one of two reasons: (1) erosion caused by tailwater or (2) corrosion caused by stable currents that may originate from overflow buckets or from existing areas of outlets. By constructing strong riprap on the upstream area, up to a height that is somewhat higher than the level of the tailwater, it is possible to prevent corrosion.

c. Gullying: A severe rainstorm can cause gullies to form on a slope, which can cause the slope to crumble. It is important to supply the downstream side with suitable cultivating and a good drainage system in order to minimize failure caused by gullying.

d. Corrosion Caused by Waves has the effect of notching out dirt from the upstream slope when there is not sufficient safety for the slope in the shape of a riprap.

2.2.1.2 Seepage collapse

The collapse of seepage could be caused by either (a) piping or (b) cavern.

a. Piping: The passage of water through the structure and the base of the earth dam can lead to piping or the gradual corrosion of a concentrated leakage, both of which can result in a large amount of catastrophic collapses.

The following are examples of the negative effects that seepage across the embankment can have:

I. The seepage of water causes erosive forces, which remove particulates from the soil arrangement and cause movement of the particles to spaces between bigger grains.

II. Seepage water is a potential source of groundwater contamination.

III. Because of the flow and the related differential pressure within the pores, a piece of the soil mass may be lifted, which may cause boiling.

IV. Interior corrosion of the soil structure leads to the construction of open conduits (channels) across the soil. This happens when there is increasing backwashing from the location of the exit.

V. The interior pressure in the soil moisture can diminish the portion of the soil's strength that is created by interior friction, which in turn leads to a reduction in the volume of the soil's strength as well as can even cause it to fail by shear. Poor construction management may have been the most common reason for embankment collapse in the past.

This can result in insufficiently compacted or previous layers within the embankment, as well as inferior compaction and connection between the

embankment and the base or connections. Cracks in the embankment that are caused by differential settling have also been a significant source of the problem (Bai et al., (2013).

b. Cavern: A failure that occurs as a result of progressive shaving or ravelling is closely connected to the piping. If the reservoir is totally full, the area downstream will continue to be moist and may experience erosion, which could lead to a slight slump or slip. This situation is possible. This minor slide leaves behind a rather steep face, which is subsequently wet by seepage from the reservoir, causing it to fall once more, leaving a considerably higher and more unstable slope. This process continues until the face reaches the level of the reservoir. This process of movement can continue until the remaining portion of the dam is not thick enough to withstand the water pressure, at which time there will be an abrupt full failure (Ou et al., 2013).

2.2.1.3 Structural collapse

The following are some of the possible causes of the structural collapse:

1. Slope collapse upstream as well as downstream as a result of construction pore stress. When a dam is constructed out of very impervious and collapsible soil, drainage is exceedingly sluggish, and extra pore pressure develops both during and shortly after construction, impairing the soil's ability to support its own weight.
2. Upstream slope collapse with abrupt drawdown. For those on the downstream slope, the critical situation occurred when the reservoir abruptly emptied without allowing any suitable reduction in the water flow beneath the saturated soil structure. This stage is referred to as the rapid drawdown step.

When the reservoir is completely drained, the hydrostatic force that was working along the upstream slope when the reservoir was full is eliminated since there is no longer the hydrostatic pressure on the slope to counterbalance it.

3. A slip on the downstream slope amid conditions of full reservoir When the reservoir is completely filled, and the rate of percolation is at its highest, a critical condition exists for the slope of the downstream area.

In other words, the pressure created by pore water operating on soil mass beneath the saturation line tends to reduce the actual stress that is responsible for mobilization shearing resistance. This happens because the pattern of seepage tends to decrease stabilization.

4. Foundation collapses (spontaneous liquefaction) When an earth dam has a foundation of small silt or silt soil, it is possible for it to slide fully on occasion.

If a soft and fragile clayey seam exists under the foundation, the dam may slide over it, causing it to fail. Unbalanced conditions that lead to foundation failure can also be caused by an excessive amount of water pressure acting on constricted seams of sand and silt in the foundation.

5. Failing due to the spread. Collapse by spreading has only been seen in relation to fill that is positioned above layered deposits that include layers of soft clay.
6. Failure brought on by the earthquake.
7. Slope protection failure Over a layer of gravel or a filter blanket, riprap is typically used to protect slopes.

This riprap can be manually laid or dropped. Waves that are riding the surface of the reservoir during a severe storm continually collide with the slope that is located just above the stage of the reservoir. This action could potentially have two impacts:

i. The wave may travel through the spaces in the riprap and wash away the filter layer, which will cause the riprap layer to settle and will leave the embankment vulnerable to wave corrosion.
ii. If the typical size of the riprap is not hefty, it has a greater chance of being washed out of the covering by the hydraulic force that is generated by the waves.

2.3 Evaluating Reliability: A Quick Review

This part provides a high-level overview of the most typical approaches to ensuring dependability. Approximation techniques, sampling strategies, and surrogate

modelling are broken down into subcategories for easier understanding. First, we describe and explain some fundamental ideas in dependability evaluation.

2.3.1 The fundamentals of dependability

In the field of civil engineering, the collapse of a structure component happens when one of the system reactions (such as displacement or fracture length) is beyond a permissible limit amount. Collapse can be caused by a number of different factors. Failure can be caused by unusual loadings such as earthquakes and hurricanes, or it can be caused by a weakening of the material's capacity over time. When examining a system's behaviour that can be specified by a random vector (x) made of M random variables (x1, x2,..., xM), there are then two zones in the input area defined by the x: safe Rs and collapse Rc. Both of these regions are denoted by the letters Rs and “Unidentified Field "Uf, respectively.

The Limit State Surface (LSS) is the curve (with M equal to 2), surface (with M equal to 3), or hyperplane (with M more than 3) that describes the border among the two domains (Rs and Rc). After that, it is possible to design a function called g(x) that is capable of giving positive or negative estimations for the safe or collapse domain (see equation 2.1).

As a consequence of this, g(x) will equal 0 if the value of x is found on the LSS. The name "Performance Function" or "Limit State Function" (LSF) is given to this function g(x).

$$Rs\text{: } (\boldsymbol{x}) > 0$$

$$R\text{c: } (\boldsymbol{x}) \leq 0 \qquad \textbf{(2.1)}$$

The collapse probability of a structure, abbreviated as Pc, is defined as the likelihood of having a performance that falls within the collapse domain. The Pc can be defined as following if the incoming random variable can be characterized by a joint probabilities density functioning (fj(x)):

$$Pc = \int_{Rc} fj(x)dx \qquad \textbf{(2.2)}$$

Because the LSF is assumed to be implicit in engineering issues that are relevant to the actual world, it is not possible to identify the failure domain Rc in a straightforward manner. As a direct consequence of this, a variety of methods have

been presented with the purpose of estimating the Pf in either an approximation approach (such as FFORD) or by extensive sampling in the data space (such as MCS). In the next section, various geotechnical reliability evaluation methodologies that are utilized frequently will be offered for your perusal.

The topics discussed above are illustrated in a two-dimensional format in Figure (2.1). The LSS, represented by the bold black line in the L1 - L2 plane, is the path that brings one to the equation g(x) = 0. The ellipses, which indicate the contours of the split PDC fj(x), are created by projecting the fj(x) onto the level. This results in the joint PDC being plotted on the plane. According to this depiction, the Pc is the volume that lies beneath the joint PDC in the Rc region.

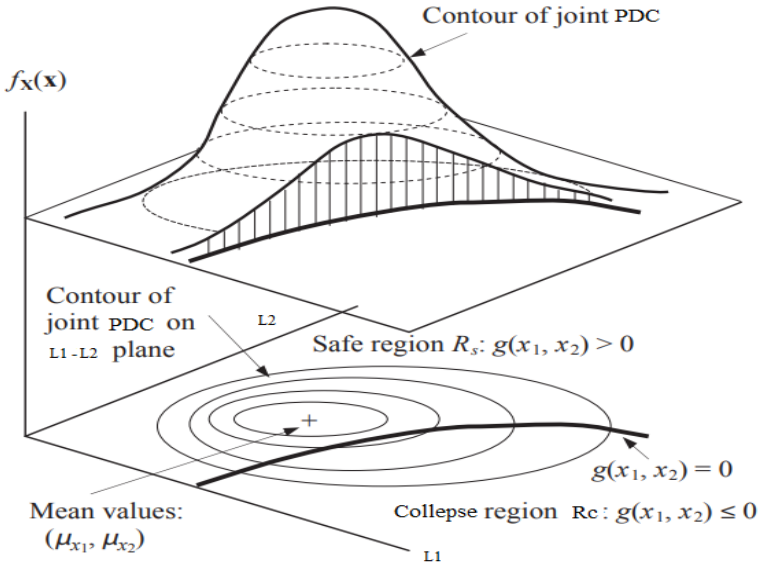

Figure 2.1: Display of the Safe/Failure Area, LSS, Joint PDC, and Pc.

Source: Emmerich and Deutz, (2018)

2.3.2 Approximation procedures

This category of dependability methods calculates the Pc by calculating an approximation of the LSS regionally at a benchmark point using either a linear or nonlinear expansion. The benchmark point is also referred to as design point P and is regarded as the "Most Probable Failure Point" (MPFP) in the system.

2.3.2.1 The formula of first-order dependability (FFORD)

Utilizing the iso-probabilistic conversion approach, the arbitrary input variable x is first changed into a standard normal variable u in the FFORD (Li et al., 2021). This

is done in order to ensure that the results are accurate. The design point P is therefore described as the point on the LSS that is situated in the position that is nearest to the basis of the standard normal area. The collapse probability Pc is directly connected to the average of P, which is referred to as the "Hasofer-Lind dependability index

"(β_{HL}) (Li et al., 2021).

$$Pc \approx \emptyset_{SN}(-\beta_{HL}) = \emptyset_{SN}(-||P||) \quad \textbf{(2.3)}$$

Where $\emptyset_{SN}$ Denotes the normal cumulative distribution function of the standard normal distribution. The assumption behind Eq. (2-3) is that the LSF is ongoing, smooth, and distinguishable in the MPFP region. This hypothesis is supported by the fact that the LSF is approximated by a hyperplane which is tangent to the LSS at P.

Figure 2.2 presents an illustration of the terms linked to the FFORD that was mentioned before in an ordinary, normal space that is determined by the two variables u1 and u2. The length OP represents the "Hasofer-Lind" dependability index (denoted as in Figure 2.2), and the vector a demonstrates the path that must be taken to reach the design location from the location of origin.

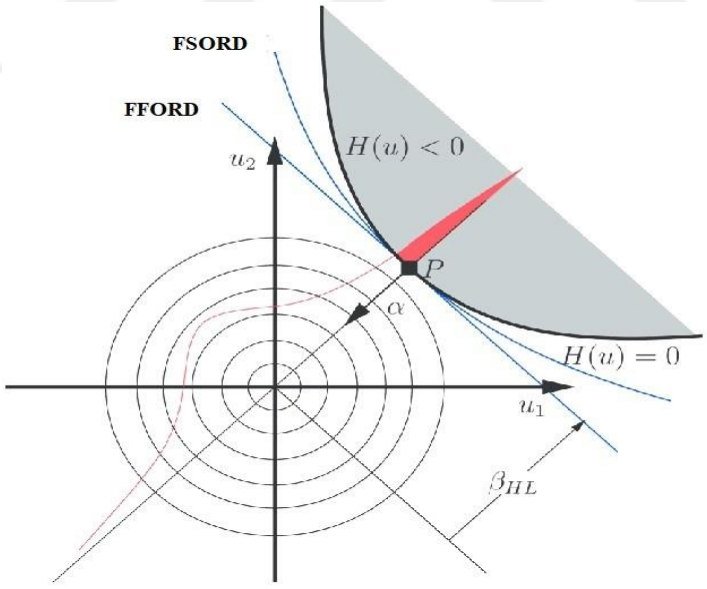

Figure 2.2: LSS Estimate Using FFORD and FSORD

Source: (Li et al., 2021)

According to Melchers and Beck (2018), there are a number of different approaches that might be taken to solve the optimization problem described above. The majority of them depend on an ongoing search technique, and for each repetition, a search direction, as well as a step duration, should be defined.

The search route is closely connected to the value of the LSF, and it is possible to evaluate it using finite differences by selecting an appropriate perturbation stage. This decision has a substantial bearing on the rate at which the process techniques converge while solving equations (2.4).

In terms of the LSS, the G(u) is the one that should be considered the genuine one. The G1(u) and G2(u) values represent the approximation that was created by FFORD and FSORD, respectively, and will be provided in the following paragraph.

It is clear that the primary focus of FFORD is on finding the design point P by the application of an appropriate optimization technique that is derived from the equation that is presented below:

$$P = argmin\{||u||, G(u) \leq 0 \quad \textbf{(2.4)}$$

2.3.2.2 The formula of second-order dependability (FSORD)

The FORM approach was first refined, and then the FSORD was refined to the second level. At the design value P that is identified by FFORD, it creates an approximation of the LSS using a vector hyper paraboloid. When the curvatures of the hyper-paraboloid are taken into consideration, the failure possibility of the FSORD can be thought of as a modification to the result obtained by the FFORD.

The Breitung equation (Breitung, 2006) can be used to predict the collapse probability Pc for minor curvatures of ki that are less than one.

$$Pc_b = \emptyset_{SN}(-\beta_{HL}) \prod_{i=1}^{N-1}(1 + \beta_{HL}\, k_i)^{-0.5} \quad \textbf{(2.5)}$$

Where N is the total number of parameters that were fed into the system, the Hohenbichler equation, which was published by Hu et al., (2021), provides a more precise method for computing Pc as follows:

$$Pc_b = \emptyset_{SN}(-\beta_{HL}) \prod_{i=1}^{N-1}(1 + \frac{\phi_{SN}\ (\beta_{HL})}{\emptyset_{SN}\ (-\beta_{HL})}\quad k_i)^{-0.5} \quad \textbf{(2.6)}$$

where ϕ_{SN} It is the PDC of the typical "Gaussian" distribution. It has been discovered that it is possible to approximate the curves of the hyper-secure by rotating the reference system in like a way that one of its planes is the direction. For additional information, viewers can look to Zuev, (2015).

2.3.3 Sampling techniques

The general concept underlying this family of approaches is to first determine an approximation of Pc based on the appropriate system responses in the resulting space and then to take samples from the associated PDC in a way that is either smartly or randomly chosen. In the following sections, you will find an explanation of four different sampling-based methodologies that are frequently utilized in the field of geotechnical reliability analysis.

2.3.3.1 Monte carlo modeling (MCM)

According to Sudret (2007), the MCS is a general method that may be used to assess complex fundamentals such as the one shown in equation (2-2). It provides a reliable and straightforward method for estimating the distribution of a system's response, which can then be followed by an evaluation of the Pc associated with that distribution. By inserting an indicator function. I_{MC}(x) of the collapse domain (i.e. I_{MC}(x) =1 if x is located in Rc and . I_{MC}(x) =0 otherwise), the Pc that is defined in equation (2-2) can be recast as follows:

$$Pc = \int_{Rc} fj(x)dx = \int I_{MC}(\mathrm{x}) \cdot fj(x)dx = \mathbb{E}[\, I_{MC}(\mathrm{x})\,] \qquad \textbf{(2.7)}$$

Where $\mathbb{E}[.]$ is the expected value in mathematics, the empirical norm of a wide set of IMC (x) values can be used to approximatively solve equations (2-7) in practice. The Pc is calculated as for a simple MCS with N_{MC} sample vectors on x:

$$Pc \approx \frac{1}{N_{MC}} . \sum_{i=1}^{N_{MC}} N_{MC}(X^{(i)}) \qquad \textbf{(2.8)}$$

To reliably estimate the Pc, it is necessary to have a sufficient number of NMC. The MCS Pc estimate's factor of variation (FoV) is calculated as follows (Feng et al., 2018):

$$FoV_{pc} = \sqrt{(1 - Pc)/(N_{MC}.Pc)} \; .100\% \qquad \textbf{(2.9)}$$

It is essential to emphasize the fact that the FoV_{pc} It is not reliant on the dimension of the issue (Priadko et al., 2016). When compared to alternative reliability approaches, like surrogate modelling, this independence is one of the most significant benefits offered by the MCS.

In addition, the MCS functions properly regardless of the level of detail of the LSC, which is another benefit it possesses over the FFORD /FSORD. However, the basic MCS has poor computing efficiency because of its lack of features.

2.3.3.2 Significance sampling (SS)

When dealing with issues that involve low failure probabilities, SS is a valuable technique that can lower the variance of the MCS estimation. The fundamental concept is to use a new joint PDC in place of the traditional one in order to increase the frequency with which the failure domain is populated.

In the framework of information theory, the equation given by (2-7) can be expressed in another alternative by introducing the following distribution HIS(x) that is conveniently chosen (this distribution is referred to as the SS PDC):

$$Pc = \int I_{MC}(x).f_j(x)dx = \int I_{MC}(x).\frac{f_j(x)}{H_{ss}(x)}.H_{ss}(x)dx \qquad \textbf{(2.10)}$$

The reliability of the SS-based Pc estimate, also known as Pc_{ss}, is determined by the H_{ss}(x) that is selected.

There is a best option for the IS PDC that, when selected, can result in the Pc IS variance being reduced to its smallest possible value.

In order to obtain the ideal H_{ss}(x), one possible method is to carry out an optimization procedure with the goal of reducing the Pc_{ss} Variance as much as possible. It is also possible to accomplish this goal by employing an adaptive adjustment to the SS PDC using samples that have been carefully chosen, as in the algorithm developed by El Methni et al., (2012).

Another option is to use the cross-entropy approach, which, according to Papaioannou and Straub,(2019), can be used to locate an H_{ss}(x) that is close to being optimal.

Barbu and Zhu, (2020) are the resources that readers are encouraged to look to for more information regarding the selection of the H_{ss}(x).

2.3.3.3 Part modeling (PM)

The PM, which is also known as flexible multilevel division, involves solving a succession of simpler issues related to reliability with intermediary collapse

thresholds (Bect and Vazquez, 2017) in order to calculate the Probability of an occurrence that is uncommon. This is done in order to determine how likely it is that the rare event will occur. The analyzed failure event E_{PM} is broken down into a series of intermediate events (E_{PM-1}, E_{PM-2},...., E_{PM-m}), each of which corresponds with a higher likelihood of occurrence and is hence simpler to estimate than the initial Pc value. It is possible to express the estimation of the ultimate Pc in the SS using the following formula (Betz et al., 2018):

$$Pc = P(E_{PM}) = P(E_{PM-1}) \prod_{i=1}^{m} P(E_{PM-i}|E_{PM}) \quad \text{.....(2.11)}$$

where $P(E_{PM-i}|E_{PM})$ represents the conditional Pc associated with the event $E_{PM-i}|E_{PM}$. When a starting threshold is provided, it is simple to calculate $P(E_{PM-1})$ using a rudimentary MCS in conjunction with N_{PM} samples. Estimating the remaining conditional possibilities can be done in the same manner, but the samples that are created need to fall within the related intermediate occurrence.

2.3.3.4 Moment techniques(MT)

According to Li et al., (2019), the MT can provide a distribution approximation by using the statistical moments of an RV. After the distribution has been found, the dependability index and collapse probability can be simply computed by establishing a threshold amount. This is done in order to simplify the process.

The second-moment estimation, often known as MT-2, is a well-known moment estimation (MT). It makes the assumption that the random model reaction follows a regular distribution and then uses the first two moments to calculate the dependability index, which may be written down as follows (Siacara et al., 2020):

$$\beta_{MT-2} = \frac{\mu_{pc}}{\sigma_{pc}} \quad \textbf{(2.12)}$$

Where β_{MT-2} is the dependability index calculated by the MM-2, μ_{pc} and σ_{pc} are correspondingly the mean and the average deviation of the amounts obtained from g(x).

2.3.4 Surrogate simulations methodologies

The basic idea behind a surrogate-based dependability analysis is to first build a surrogate model, which is also referred to as a meta-model, using only a limited number of calls to the determinate approach, and then to conduct a crude MCS

(Bhaskar et al., 2022) or any additional sampling technique (Athani et al., 2015) on the meta-model that was obtained. This is the first step in the process.

The primary goal is to cut down on the overall amount of time needed for computing a reliability analysis, particularly for situations involving models that are difficult to analyze or failure probabilities that are low.

There is a wide variety of mathematical software that may be used to construct approximation methods using a specific collection of samples. Kriging, algebraic chaos elongation, and support matrix system are the three approaches most frequently used in structural reliability assessment (Sica et al., 2019).

These techniques form the basis of the most prevalent methodologies used for structural reliability assessment. In the next sections, a concise explanation of each of these three surrogate modelling strategies is provided. In addition, the approach of utilizing learning, which can further improve the efficacy of these strategies in estimating Pc, is shown and commented on in this article.

2.3.4.1 Kriging

The hypothesis that the efficiency function g(x) is a representation of a "Gaussian Process" (GP) is the foundation upon which the Kriging theory is constructed. It determines the value of g(x) at unknown positions by combining g(x) at known points with an arbitrary function, which consists of a regression component and a stochastic procedure as described in the following way (Zhu and Du, 2016):

$$g(x) = Cr(x)^T \beta_{AK} + \varepsilon(x) \quad \textbf{(2.13)}$$

Where β_{AK} is a vector of undetermined parameters, Cr(x) is a vector of extrapolation functions, $Cr(x)^T \ \beta_{AK}$ is the trend of forecast or the average of the GP, and (x) is considered to be a Generalized Linear Model (GLM) with zero average and correlation.

For the creation of a "Kriging" surrogate approach, a set of Hypothetical Design (HD) requirements must be provided for the calculation of the hyper-parameters. This can be accomplished by an optimization technique (such as a genetic algorithm) that is done on the cross-validation mistake (Awad et al., 2015).

In the realm of advisable, the term (HD) describes a number of data samples and the predictive responses that correspond to those samples. These are the components that are utilized to identify a surrogate approach.

2.3.4.2 Assistance vector model (AVM)

One category of learning methods known as support vector machines, or AVMs, can divide the results of a random model into any number of categories that the user specifies. Specifically, binary categorization is of considerable importance for reliability studies since it may mark safety and failure zones; this makes binary categorization an extremely useful tool (Wang et al., 2018).

Let's start off by thinking about the scenario in which the data are linearly separable in the region where the provided random elements were originally stored. It is possible to identify an endless amount of hyperplanes that serve to separate the data. Taking into consideration a hypothetical hyperplane (the decision-making function of the AVM) (Andreini, 2019):

$$f_{AVM}(x) = w^T x + b = 0 \qquad \textbf{(2.14)}$$

Where W is orthogonal to the hyperplane, and b is a vector component. The hyperplane that has the greatest margin between itself and the nearby samples used for learning is the one that is considered to be the best option.

2.3.4.3 Polynomial disorder development (PDD)

In PDD, the meta-model is constructed by extending the system response on an appropriate foundation, which is a series of multidimensional polynomials. This is done in order to make the model as accurate as possible. The following is an expansion of what is meant by the notion of a model response that possesses a finite variance (Hadigol and Doostan, 2018):

$$Y \cong \sum_{a \in N^m} K_a \, \psi_a \, (\varrho) \qquad \textbf{(2.15)}$$

Where ϱ = { ϱ1, ϱ2,..., ϱM} are distinct RVs, $\psi_a(\varrho)$ are multichannel polynomials, K_a are unknown variables to be computed, and a= {a1,..., aM} is a multifunctional index. k are the unknown variables to be computed.

The multimodal orthonormal polynomial $\psi_a(\varrho)$ is constructed by taking the vector product of the unitary orthonormal polynomials $\psi_{ai}\,(\varrho i)$. According to Sudret

(2014), orthogonal multivariate polynomials can belong to any one of a number of families, including the Hermite polynomials and the Legendre coefficients.

2.3.4.4 Adaptive algorithmic techniques for surrogate simulation

It has been discovered that developing a surrogate simulation using only one set of Hypothetical Design (HD) is not sufficient in the sense that the area of interest is challenging to be covered unless a large sample size is supplied to the HD. The only exception to this is if the HD is given a lot of data to work with.

In the context of a reliability evaluation, this kind of region refers to the area immediately surrounding the LSS and, in most cases, indicates an area of low likelihood. As a result of this, the concept of developing a surrogate simulation by incrementally adding more information to an original HD was proposed. Over the course of the last ten years, a number of different algorithms have been created under this concept in order to improve the effectiveness and precision of surrogate-based reliability evaluations.

Examples can be obtained from Schöbi (2019) for the Kriging, PDD, and AVM, accordingly. These references are all cited in the previous sentence.

All of the created algorithms follow the same method in principle, which is depicted here in Figure (2.3) for your reference. An adjustable surrogate-based reliability evaluation requires two crucial components: a learning function and a halting condition.

The first step is to identify the subsequent sample that will be incorporated into the existing HD in order to enhance the performance of the meta-model while predicting the Pc.

The latter is utilized to put a stop to the HD enrichment procedure when the existing surrogate model reaches an adequate level of accuracy.

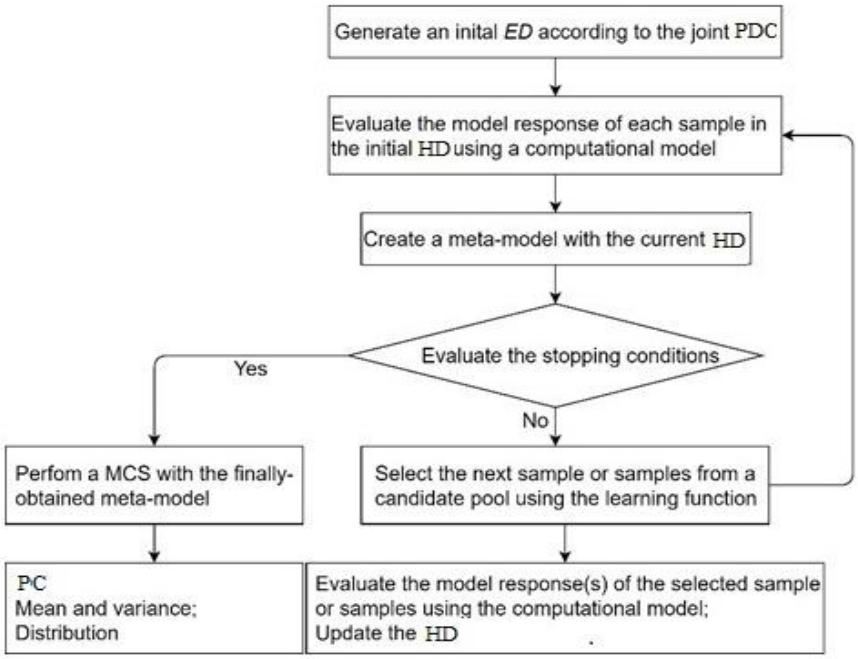

Figure 2.3: A Flowchart Illustrating An Adaptive Surrogate Simulation Mixed With MCS for the Purpose of Reliability Evaluation

Source: (Hasan et al., 2019)

2.4 Evaluation of Earth Dams Using Probability

In the following part, we will attempt to give an overarching summary of the previous research that has dealt with earth dam issues using a probabilistic framework. The relevant papers have been organized into three groups, each of which corresponds to one of the following three primary study subjects pertaining to earth dams:

1. A stochastic evaluation of seepage;
2. An examination of the reliability of the dam with relation to its stability; and
3. A probabilistic analysis of the breakdown of dams as a result of internal erosion.

In addition, other research that does not fall under any of the aforementioned three categories is also discussed in this part of the article.

2.4.1 Random flows

The primary group concentrates on the stochastic flows that occur inside earth dams by taking into account the variability of the soil's hydraulic properties. The free surface flow in earth dams was statistically explored by Mouyeaux et al., (2018),

who accounted for the geographical soil permeability heterogeneity in their research. Monte Carlo Modeling(MCM) framework was utilized in order to do the estimation of the flow rate parameters and the free area depression.

In addition, an empirical method was suggested as a means of estimating the mean and dispersion of the flow frequency in order to circumvent the necessity of carrying out a significant number of flow computations. The same researchers (Mouyeaux et al., 2018) resumed their work on analyzing stochastic flows within earth dams and concentrated on the fluctuation of hydraulic grades as their primary area of investigation.

Two identical dams, each containing a horizontal filtration drain, were under consideration. The findings indicated that a deterministic evaluation provided an estimate of the flow departure point that was on the cautious side. The authors also advised building filtered drainage that is longer than one-fourth of the dam foundation and has a permeability ratio that is one hundred twenty times higher than the lowest point of the dam structure. This would ensure that the interior flows of the dam are not susceptible to fluctuations in the permeability of the structure itself.

Guo, et al., (2019) used a finite element approach to investigate the free surface flow via earth dams. The study was primarily concerned with measuring the flow rate statistics. The lognormal UF modelling technique was used to simulate the hydraulic conductivity of the soil (Ks). It was discovered that expanding the horizontal dimension of the fluctuation led to a rise in the flow.

Tan et al., (2017) modelled the soil permeability (correlated with Ks and water storage) of an earth foundation by lognormal UFs and explored its impacts on the flow rates and time to achieve steady equilibrium in an unsaturated situation. They found that the soil porosity had a significant impact on both variables. They discovered that raising the standard variation or correlation duration of the porosity UF could result in a reduction in the mean amount of the amount of time required to attain a steady state as well as a rise in the mean amount of flow capacity.

By modelling the Ks as UFs, Sun et al., (2012) carried out a number of stochastic seepage evaluations on a homogeneous earth dam. The investigations led to the discovery that the dominating component of the flow vector was responsible for determining whether or not the autocorrelation distances had an effect on the seepage

behaviour. For instance, due to the fact that the predominant flow direction inside the dam structure is horizontal, the horizontal autocorrelation separation effect has a considerable impact on the mean flow rate. In addition, it was discovered that supposing two layers (i.e. two separate UFs) for the dam body resulted in more accurate average and standard variability estimations of the flow ratio in comparison to supposing a single layer. This was the case when comparing a single layer to supposing two layers.

Fattah et al., (2014) conducted research on the variation of the free flow surface that occurs within a uniform earth dam as a result of the regional variability of Ks. Figure (2.4) presents a result that was achieved by Fattah et al., (2014) as an illustration for this point. It illustrates the free surface as well as the contours of the water head for a random soil with regionally changing Ks values. The variation of Ks that is taken into account in the Core zone is greater than the variation that is taken into account in the Shell zone.

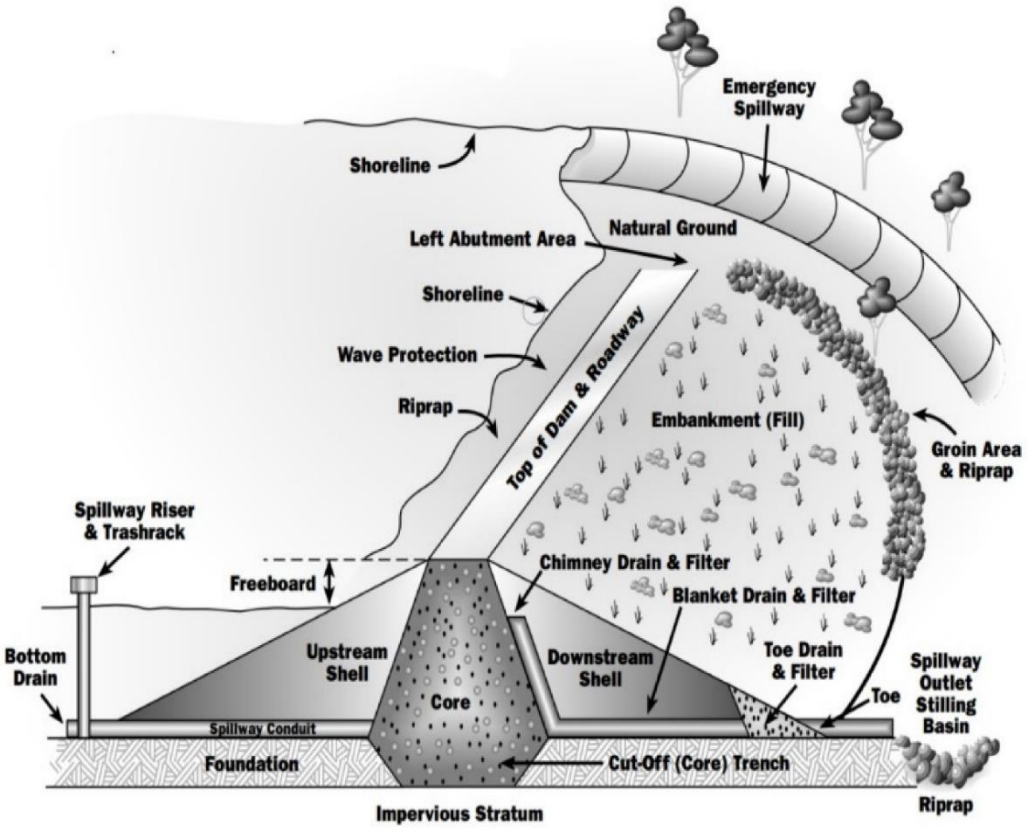

Figure 2.4: Dam Water Level Contours in Light of Spatially Variable Flow Rates

Source: (Fattah et al., 2014)

As a consequence of this, it results in an irregular phreatic surface within the clay zone, as demonstrated in the picture.

Refaiy et al., (2021) developed an UF depiction of the Ks for a real earth dam by utilizing field information in a geostatistical approach. This allowed them to create their model. After that, it was linked in a random finite element structure to predict the probabilistic variation of the pore fluid pressure and the advisable surface.

It was demonstrated there is a significant relationship between the Ks in the core component of a zoned dam and the flow rate that is allowed to pass through the dam. In the event that the core's mean Ks is sufficiently low, the degree of uncertainty in the flow rate will be minimal.

In their study on a seepage issue across an embankment, Liu et al., (2017) analyzed and evaluated Several Autocorrelation Operates (SAO). They came to the conclusion that the results supplied by the squared exponential ACF were more accurate and that the data provided by the single hyperbolic SAO may have been an underestimation of the seepage amount. According to the findings of this investigation, the discrepancies between the various SAOs do not constitute substantial distinctions.

2.4.2 Dam slope stiffness

The second category addresses the problem of earth dams' slope durability from the perspective of dependability assessment. The Initial Order Next Moment (IONM) and the advisable limit equilibrium approach were used in the methodology that Liang et al., (1999) presented in order to theoretically compute the dependability index. They used this methodology to analyze the "King Talal" embankment dam (as shown in figure 2-5) in order to determine the dependability of the dam in terms of the stability of both stream and outflow slopes during various loading situations (for example, rapid drawdown).

Nusier et al., (2002) conducted an investigation into the "Karameh Dam's" durability using a suggested probabilistic three-dimensional slope stability evaluation model that was based on the IONM. By analyzing the monitoring data, we were able to take into account the potential variations in the soil shear intensity parameters as well as the pore water stress.

Sengupta and Upadhyay (2009) solved a benchmark issue concerning earth dams by employing the polynomial anarchy depiction method. It was decided to use a rigorous safe condition for evaluating the Probability of a dam failing, and these

criteria stated that the dam was regarded to have failed if the "Mohr-Coulomb" requirement was fulfilled at a minimum one location along its body.

The impact of the Ks fluctuation on the slope durability of a uniform embankment dam was investigated by Richards and Reddy (2005), locating the critical failure surface in a slope stability analysis by genetic algorithm. The probabilistic evaluation was carried out with the help of the MCM, and the IONM was used to calculate the dam reliability level.

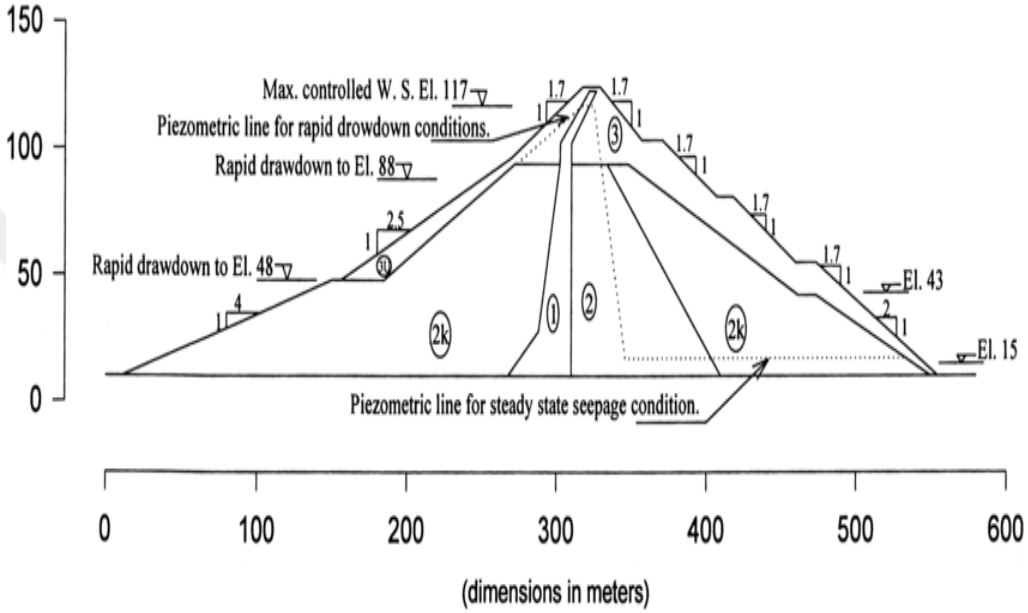

Figure 2.5: Cross-sectional view of the "King Talal" dam

Source: (Liang et al., 1999)

The reliability evaluation of a little earth-fill dam that was provided by Chen and Chang (2011) focused on the dam's stability (both its flow and outflow slopes). The IONM-based reliability analysis took into consideration, in addition to the soil variability, the uncertainties of the dam design (such as height and peak width), as well as the upper hydraulic loadings. This was done so that the analysis could be considered accurate.

By utilizing the Reaction Surface Approach (RSA) in conjunction with the IONM, Sachpazis (2013) were able to evaluate the dependability of four earth dams that had been renovated. They discovered that the variations in the geotechnical criteria, such as the highest possible ground acceleration amount and the full storage volume, had a considerable impact on the predictions of the dam dependability index. This was the case even though both of these factors were outside of the dam's control.

Wu et al., (2020) provided a reliability-based construction of an earth dam by utilizing the MCS in their work. Taking into consideration the data allowed for the determination of the geographic variation of the soil strength characteristics. The enhancement to the design was examined with regard to its dependability.

Zou et al., (2014) used a probabilistic approach to investigate the state of stability of the "Shuangjiangkou Dam" as shown in Figure (2-6), a 314-meter-high earth dam that is now in the process of being constructed and will be the largest embankment dam in worldwide history once it is finished. First, an essential slip surface was established, and then an MCM was implemented into the calculation in order to calculate the dam reliability factor for a variety of various design conditions.

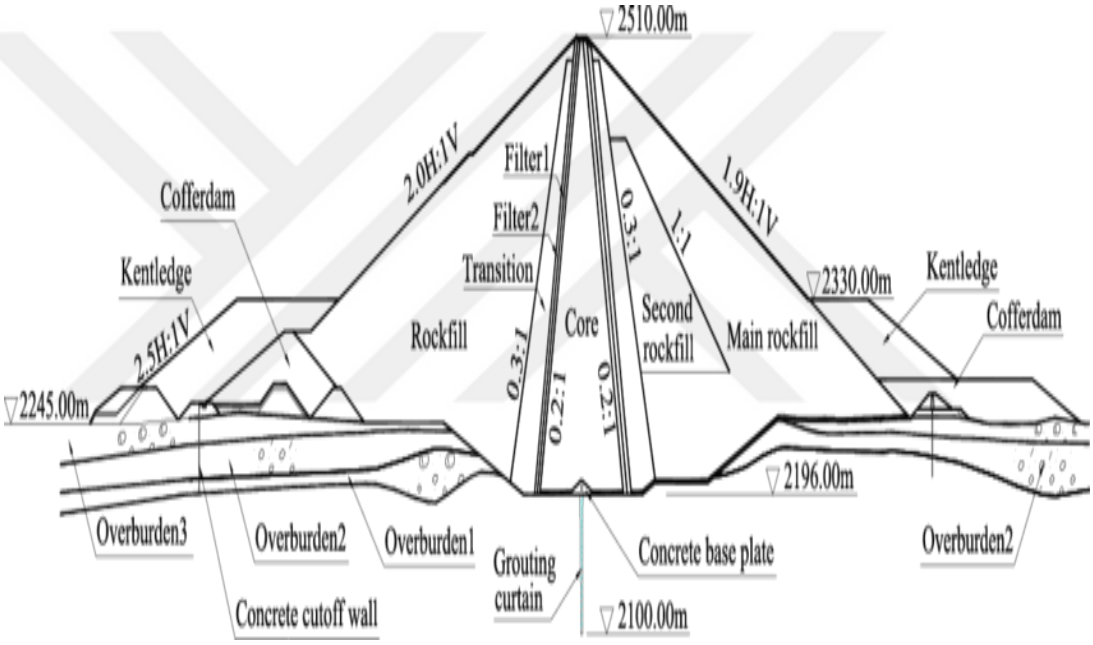

Figure 2.6: The Profile of the "Shuangjiangshou" Dam's Waterway Section

Source: (Zou et al., 2014)

Using data collected in the field, Devi and Anbalagan (2008) conducted a probabilistic evaluation of the durability of an earth dam. They considered three different configurations for the compilation of data in order to determine the dam's safety factor (SF) statistics as their primary objective.

In addition to earth dams, the probability stability evaluation of slopes is the subject of significant research publications that may be found in the relevant literature.

Some examples included those in which the unpredictability of soil shear strength variables, the impacts of rainfall, or earthquake loadings were incorporated. Other examples include those in which earthquake loadings were considered. This research

gave not only valuable information but also helpful findings on the slope issue associated with earth dams.

Figure (2.7) provides an explanation of two failure processes of a slope that have been identified by Fu et al., (2021) using an MCM with randomized shear strength parameters. These collapse processes were found on a slope.

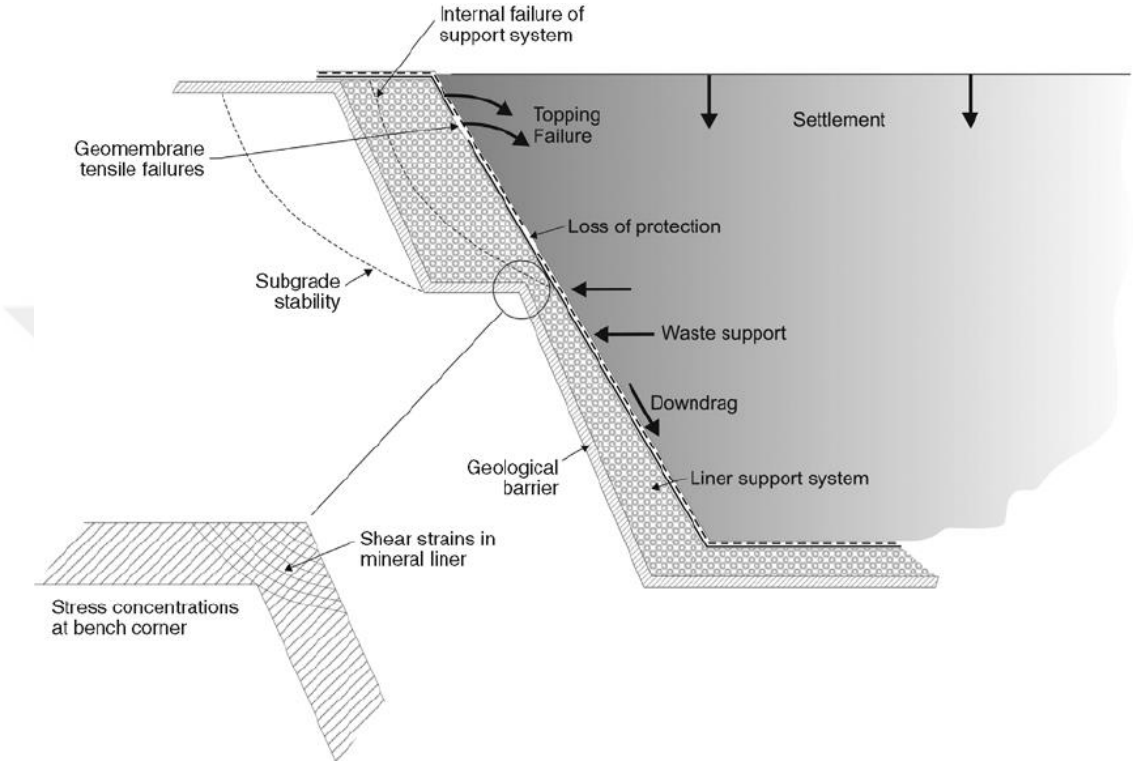

Figure 2.7: Two Failure Processes of the Slope

Source: (Fu et al., 2021)

2.4.3 Interior corrosion

The third category looks into the collapse of the dam as a result of interior corrosion, also known as piping. This term refers to the removal of soil granules brought about by seepage forces. According to Hanson et al., (2010), there are four distinct mechanisms that can be responsible for the process of interior corrosion: concentration leak corrosion, backward corrosion, soil contact corrosion, and suffusion.

At the level of a preliminary evaluation, Chen et al., (2016) presented a methodology that they referred to as "UNSW" for the purpose of evaluating the likelihood of the collapse of earth dams owing to pipes. The "UNSW" was derived by recalculating the historical piping collapse frequency using weighting variables that can be

established depending on the shape, soil conditions, and monitoring information of the dam that was under study.

A rundown of the piping collapses that have recently taken place in embankment dams has been provided. By taking into account a variety of empirical requirements, Goodarzi et al., (2006) evaluated the effectiveness of a filter system as a method for reducing the interior corrosion of dams. By utilizing FFORD, we were able to take into account the variable sizes of both the base material and the filter particles.

The strategy that was proposed by Kanning et al., (2015) for revising the uncertainty modelling of resistance characteristics and the collapse probability estimations due to uplift and piping was described below. The Bayesian inference that was used to execute the update took into consideration the field effectiveness observations made during previous loadings. The essential shear strength and the factor of erosion were the two factors that Ribas et al., (2021) used to create probabilistic simulations for soil corrosion. It was decided to take into account both the cohesive and the non-cohesive involvement. Within a Bayesian structure, the proposed models were given additional calibration through the utilization of data obtained from laboratory experimentation.

An example of possible use for the models was demonstrated using an investigation of the dependability of a conventional earth dam. Estimates were made on the possibilities of the dam experiencing corrosion and not noticing it at all, taking into consideration two erosion factors that were mathematically modelled.

Using the MCM, Gholampoor (2017) carried out a probabilistic evaluation of the pipe while taking into account the spatial fluctuation of three components (the void ratio, Ks, and the amount of the moveable particles). It was planned to construct a risk rating system using an index that would describe the likelihood of seepage instabilities, and then this index would be further expanded.

Probability approaches were proposed by Ribas et al., (2021) for the focused leak corrosion that occurs in earth dams. In order to calibrate the model characteristics utilizing both laboratory and in-situ information, a "Bayesian technique was merged with an SS model and added to the mathematical models. This was done.

In accordance with Vakili et al., (2018), there are primarily three steps involved in a failure that is generated by piping. These stages are the commencement of piping,

backward corrosion, progression and breach process (such as settlement contributing to advisable). These three steps can be seen in an example of a homogeneous dam that is presented in Figure (2.8). As was noted earlier, there are certain extant research that cannot be categorized into any of the three classes that were discussed earlier. As a result, they are gathered together in this article, and a concise explanation of each follows below.

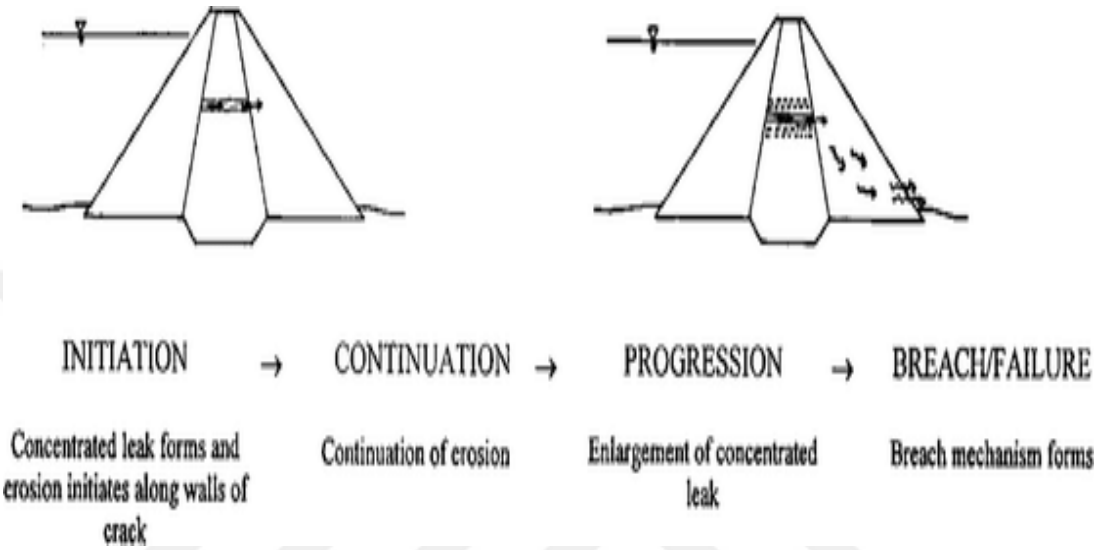

Figure 2.8: There are Three Steps in the Failure of the Piping System

Source: (Vakili et al., 2018)

As was noted earlier, there are certain extant research that cannot be categorized into any of the three classes that were discussed earlier. As a result, they are gathered together in this article, and a concise explanation of each follows below.

An overall statistical analysis of failures that occurred in embankment dams that were built before 1986 was presented by Vakili et al., (2018). According to the findings, the classification of the embankment has a considerable effect on the Probability of piping and slope instabilities. In general, dams made of "homogenous earth-fill", "earth-fill with filter", or "concrete face earth-fill" have suffered more issues linked with the two failure mechanisms that were previously described.

The guidance for dependability investigation and risk evaluation of embankment dams, the many failure mechanisms that are associated with seepage, such as piping and heave, as well as slope instability, were taken into consideration.

A probabilistic approach was suggested by Kanning et al., (2015) for the purpose of modelling the height of the water from floods level in a dam reservoir. It made it

possible to produce many different hydrological scenarios that were relatively near to the reality of actual hydrological events. Additionally, it made it possible to take into account the seasonal variations in the level of the headwaters.

Incorporating the variable hydraulic loadings within a dam's reliability evaluation may require the usage of a model such as this one, which could be valuable to have.

3. STUDY AREA

Khanas dam in Iraq. It is located between coordinates 359513.39 E, 4069863.30 N (Left Abutment) and 359410.61 E, 4069769.00 N (Right Abutment). The lake receives water from numerous small streams that descend from the surrounding mount. The Gomal River is a tributary of the Khazer River. The Dam site is located near Khanas village, 45 km southeast of Dohuk Town; Fig.3.1 shows the location of the proposed Khanas Dam.

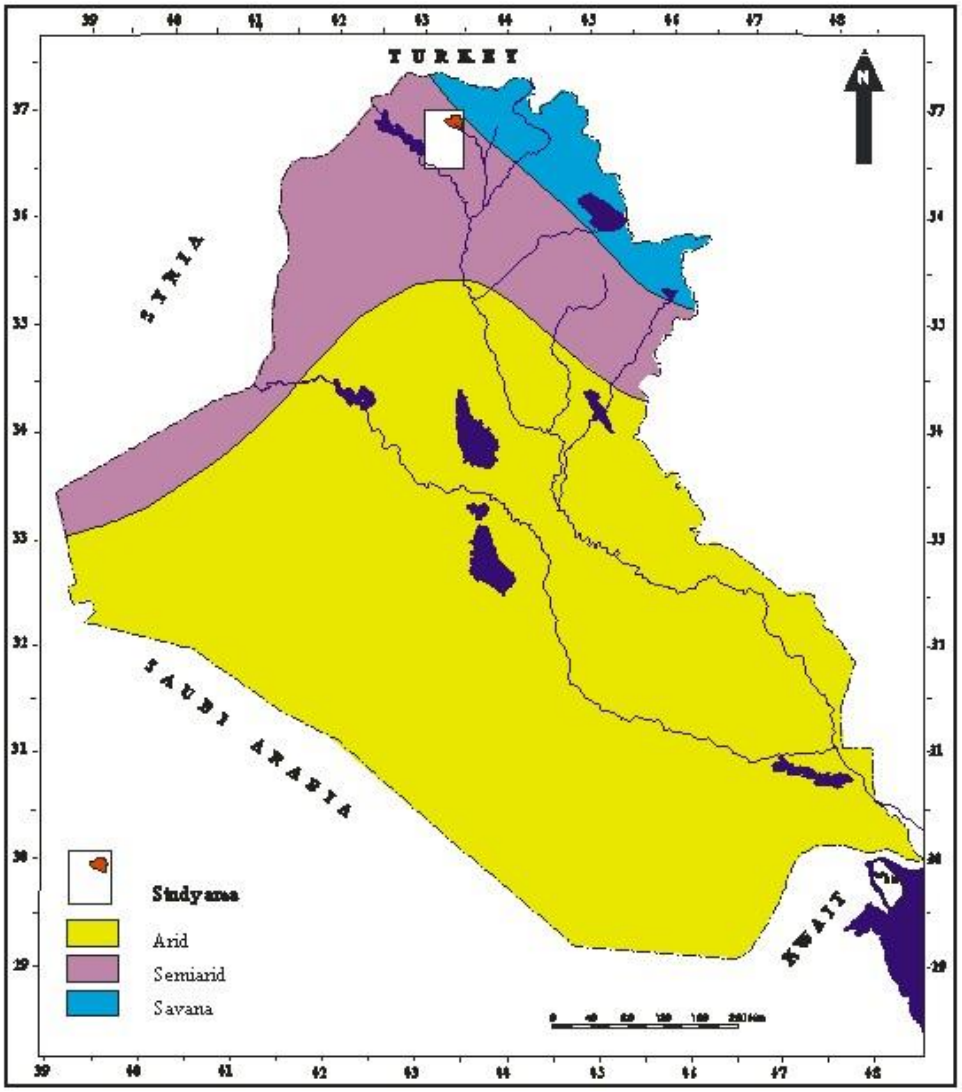

Figure 3.1: Climatic boundaries from (1970-2000)

Source: (Al-Khateeb and Capigian 2007)

3.1 Geology of the study area

Gomel sub-basin belongs to the Great Zab River basin, considered as the largest one within the main basin, and it is drained by two main synclinal valleys which flow towards the east and between Shkira, Kiri-Habakara, Duda Rash and Ain-Sifni mountains, from north to south respectively they have the same direction of the main strike of the bed which is E – W.

The surface runoff is high in the higher parts (northern synclines) due to a lack of vegetation and high gradient, but because the lower parts of the sub-basin have a nearly horizontal gradient with sediments of good permeability, it is believed that the majority of the water is infiltrated and flow as ground water.

The quality of the water in this sub-basin is good due to the absence of dissolved salts which may contaminate the water.

The main sources of water are perennial streams (which flow mainly in the synclinal valleys besides the rainfall and spring, snow covers some of the high mountains, which supply good quantity of water after melting. The main annual precipitation also differs in these mentioned parts.

The areas of limestone outcrops, especially those of Pilaspi and Aqra-Bekhma formations, have good to high infiltration capacity due to high porosity, which is either primary and or secondary due to dolomitization, fracturing and solution cavities, even due to structured aspects of the area.

3.2 Geomorphology

3.2.1 General

The proposed dam area consists of a series of high, wide and comparatively long extended mountains separated by long synclines. The main mountain falls in the high folded zone are Kamaka, Chiya Pang, and Kiri- Rabatki.

The maximum and minimum heights within the map area are 1096 and 500m (a.s.l), respectively. The highest point is located in Chiya Pang Mountain in the eastern part of the area, whereas the lowest point is near the river to the north of Shahia village.

3.2.2 Geomorphologic units

The present morphological feature of the area is controlled mainly by structure. The visible geomorphological units which can be detected are:

A. Units of Structural - Denudational origin:

- Hogbacks and Cuestas: They are structural plains of relatively hard rocks underlain by less resistive rocks and have a perceptibly sloping surface of common regional expression of gently or moderately dipping rocks in the area. The main reason for cuestas is the variation in the lithology; it is common in Injana Formation.
- Strike ridges: These are well-developed in all anticlines present in the area. It is characterized by steep dipping hard rocks; these features are formed due to the resistance of bed rock, controlled by the strike of beds. They are predominant in Pilaspi and Aqra-Bekhma.
- Scarps: It is an escarpment, cliff or steep slope of some extent along a margin of plateau, mesa, terrace or bench. The area consists of several types of scarps related to dip, slope, which they originated by selective erosion of streams, faults, and dipping rocks suites.
- Flat Iron: It is a triangular-shaped sloping-mesa type of Hogback ridge. They are common in Pilaspi Formation, dipping at the flanks of large structures.

B. Units of Denudational Origin

- Slopes: As a result of folding and weathering, different types of slopes as convex, concave and straight slope, where they are related to fault line or high amplitude folds commonly found in Pilaspi, Injana, and Gercus formations.
- Badlands: It is topographically developed in clayey and alluvial sediment as in Gercus formation.
- Pediments: It is well developed along both limbs of anticlines. It is reflecting a break in slope between hilly and mountainous terrain and flat terrain.

A pediment consists of loamy soil with rock fragment (mainly limestone).

C. Units of Fluvial Origin

The most important agent forming the fluvial units is basins of permanent river such as Gomel River and some main valleys.

- Flood Plain Sediments: These are well developed along the banks of Ghomel River and some main valley the width range from few meters up to 300 m in some places. Two levels are distinguished near the dam axis located above the present level of Ghomel River and it is not plotted due to scale limitation of the map, consists mainly of sub-rounded fragments.
- Alluvial fan: Where a stream comes from a relatively high grade to a much gentler slope, as from mountains to plains, its velocity is reduced and for that reason it built up alluvial deposits. It is found on the slopes of some ridges; due to force of eroded load pass throw narrow passage.
- Valley Fill Sediments: These are well developed every where within the area. The sediments on the valley floor are derived during extensive rainfall; the valleys carry their major load from upstream hilly and mountainous terrain which is composed of admixture of silt, clay, gravel and rock fragments.

D. Units of Solution Origin

- Caves: the caves are formed as a result of dynamic effect of the solving water moving on the surface and dissolving the carbonate by passing throw fissures and joint cracks.

All the caves are restricted on Pilaspi Formation., (Generally it is simple chamber).

3.2.3 Geodynamical processes

The following processes are developed in the area:

- Mass Movements

The spontaneous down slope movement of rock debris is controlled to large extend by the degree of water saturation of the rocks, and the amount of precipitation. The most important features are: Rock fall (which are due to gravitational force, seasonal freezing and earth fall by steep cliffs).

Landslides are active during the wet seasons, and they are connected to certain litho morphogenetic conditions; most important features, such as rock slide, a slip of stratum and slumps, are formed mainly in Mukdadiyah, Fatha and Gercus formations

due to the softness of these rocks and underlain by hard rocks formation as Pilaspi, Aqra-Bekhma formations.

Block slide and slump and rock falls are formed especially in areas in where clay sequences are overlain by hard rocks, formed also in Injana, Mukdadiyah and Gercus formations.

Mud flows, earth flows and rock debris flow, take place in wet clayey materials and gravity connected to clastic rock masses.

3.2.4 Drainage pattern

The main valley is structurally controlled where it runs mainly parallel to the main axis of the structures and cuts them perpendicularly in some place like the dam location.

The tributaries of the Ghomel River are also structurally controlled and are mainly of dip valley type.

The following drainage patterns are developed:

- Dendritic and sub dendritic: It is well developed in soft rocks like the rocks of Gercus, Kolosh and Mukdadiyah formations.
- Sub parallel: It is developed especially at the limbs of main structures.

3.3 Stratigraphy

Seven formations ranging in age from Upper Campanian - Late Ma'astrichtian to Late Miocene-Pliocene with Quaternary sediments are exposed in the area. The sequence is described from older to younger as follows:

3.3.1 Aqra – Bekhma formation (Late Campanian – Early Ma'astrichtian)

This formation is exposed in the core of some structures in the area; it forms the bulk of the main mountain in the area steep, irregular slope and rough ridges which are dissected by deep and narrow valleys.

The formation comprises massive, thick-bedded, hard to very hard, well-bedded, scrap-forming limestone and dolomites, in parts dolomitic and bituminous; the

thickness of some beds exceeds 2.5 m, and the rocks are fine-grained, crystalline and highly porous.

The limestone is light grey, grey and greyish brown in colour, and calcite is irregularly interspersed with coarse and fine fragments of coral, shells and other fossils fragments. Petrographically, the formation is characterized by different kinds of carbonates, such as aphano to very finely crystalline, fine – medium and coarse crystalline. These rocks were originally described as reef limestone complexes with massive rudest debris at the upper part. The exposed thickness is about 200 m.

The depositional environment of Aqra – Bekhma Formation is a shallow warm marine.

3.3.2 Kolosh formation (Early Middle Paleocene – Early Eocene)

This formation occurs as a narrow strip striking west – northwest to east – southeast, always forming gentle slopes which are constituents.

This formation consists of soft grey-green and black clastics of sandstone, siltstone, and clayey shale interbedded with cream-colored clayey limestone in the upper part of the sequence and are veined with calcite; no regular distribution was observed vertically or laterally in these mentioned rocks, which is most probably due to structural complication.

- The clayey limestone is rare and not more than 1 – 2 m in thickness, and the clayey shale is soft and fragmentary, highly weathered. They mainly form thick black or grey clayey soil, where the sedimentary structure can hardly be recognized.
- The sandstone is grey – green in color, soft, fairly hard to friable, coarse to medium grained, mainly of dark minerals with large amount of clay cementing materials. Occasionally, they are pebbly; gravel size is not more than a few millimetres. The gravels are rounded and spherical in shape, mainly of silicates and carbonates; the thickness of the sandstone beds ranges from 0.5 m to about 5 m.
- The conglomerates are not more than 1 – 2 m in thickness, and fine pebbles about 0.5 cm in size are mostly of limestone and chert; they are spherical in

shape, sorted and rounded. The conglomerates are poorly cemented with sand and clay.

- The thickness of the formation is variable, reaching a maximum thickness of 200 m in sheet 86/510 scale 1: 20 000. Generally, however, it is roughly around 80 meters' northeast wards decrease to a few meters and sometimes totally missing. The depositional environment of the Kolosh Formation represented as near-shore sediments.

3.3.3 Gercus formation (Middle Eocene)

The rocks of this formation crop out in all the structures of the area; it generally forms as narrow strips, steep slopes of the peripheral ridges surrounding the cores of anticlines present in the area.

The sediments of this formation occur as red, brown and greenish-grey clastic rocks, which are of conglomerates, grindstone, sandstones, siltstones and claystone variation, and claystone prevail over the other rock of the sequence.

- A considerable part of the sequence is occupied by conglomerate and grindstone. They occur as poorly rounded or well-rounded and spherical fragments of siliceous rocks, limestone, basalts, diabase, nummulitic limestone and marls; limestone is white and yellowish in the color of micro granular texture, containing fragments of quartz cemented by clayey and sandy materials which are also red in colour. The thickness of these lenses is not more than 2 m.
- The sandstone is also reddish brown and brown in colour, fairly hard to friable, bedded, medium to coarse-grained cemented by clayey materials. The thickness of the sandstone beds ranges from less than 1.0 m to about 7 m as compared with the claystone, which range in thickness from a few meters up to 20 m; the individual bed is 0.5 m.
- The claystone is reddish brown, rarely violet, greyish brown, grey and green in colour, soft to fairly hard. The claystone is partly silty, and a layer of gypsum is detected in B. H. No.8, B. H. No.3 and B.H. No.2.
- In the upper parts of the formation are interbedded with green marl. The lower contact of this formation with the underlying Kolosh Formation is

gradational; the contact in the field is sharp due to colour change from predominantly green Kolosh Formation to predominantly red Gercus Formation, so the contact based on the first red clastic, occasionally well-marked conglomerate occur in the contact.

- Gercus Formation represents continental classics, probably of the Molasses type.

3.3.4 Pilaspi formation (Late Eocene)

- The rocks of this formation are developed in all the structures of the area. It forms continuous high ridges with very common flat iron morphology. The rocks are mainly white, creamy, yellowish-white, and light grey; these are crystalline dolostone, partly clayey and well bedded, with individual beds ranging from less than 0.3 m to more than 4.0 m; the carbonates are hard to very hard, occasionally splintery with very rough surfaces, partly fossiliferous, cavernous, containing thin veins of fine calcite.
- These rocks can be divided into two parts according to lithologic composition (field recognition). The lower part consisted of white, creamy, yellowish-white, thinly bedded limestone with an interlayer of 1.0 m calcareous red claystone. When it was, a highly weathered appearance was detected along the whole area.
- The upper part is composed of light grey, hard, well-bedded, thin to massive recrystallized limestone and dolomitic limestone; this part is very rich in limonite inscriptions, and the size reaches up to 25 cm in a few localities. `Limestone is often cavernous and contains thin veins of fine calcite.
- The thickness of the formation is highly variable, generally decreasing towards the north; at sheet 86/510 is about 158 m and at sheet 89/510/ near Sulaf is 130 m. The variability in the thickness is due to irregularities in the floor of the sedimentary basin during the deposition of the formation.
- The contact of the formation with the underlying formation is gradational. The formation is deposited in the lagoon (back reef environment), the age of the formation is supposed to be Late Eocene.

3.3.5 Fat'ha formation (Lower Fars) (Middle Miocene)

The rocks of the formation form a continuous belt bordering all structures. Morphologically the formation forms a hilly area with some continuous high ridges of this limestone beds. The formation consists of claystone, sandy claystone, limestone and gypsum.

The claystone is the main constituent of the formation, formed mainly by montmorillonite, Kaolinite, mica and illite clay minerals with other minerals like calcite. The claystone is sometimes with silty texture at the base, passing upwards gradually into marl, and marly limestone of conchoidal fracturing is common in the claystone; occasionally, it is silty or gypsiferous. The main colour is greenish, greyish green and reddish brown colours also occur in the lower parts of the formation:

- The gypsum is finely crystalline and dissected by veins filled with coarse gypsum crystals forming light interlocking crystals of anhedral to subhedral shapes.
- The gypsum is light grey or greyish white and white. There is a green or red band of clay is also present.
- Some secondary gypsum occurs within the claystone, either as thin veins filling the fractures, joints and other cavities.
- The siltstone is light green to grey in colour, thinly bedded, fairly hard, frequently in the upper parts of the formation, and grade to very fine sandstone. The silty and sandy grains within the siltstones are of quartz and chlorite, crystals with few chert, feldspars and muscovite, and the finely crystalline calcite and clay admixture form the matrix.
- Limestone has been encountered in a few horizons and has better development in the middle part of the formation, and they are also generally thinner, hard, well bedded; limestone occurs as fossiliferous, dolomitized sandy fossiliferous, silty dolomite and oolitic near the top, occasionally sandy limestone is common more towards the north and also changes upwards from marl to marly limestone and sandy limestone, hence ripple marks and cross-bedding is clearly developed.

- The limestone is intercalated with thick claystone; the thickness of these limestone beds increases upwards from 0.5 – 5 m, the thickness decreases towards the northern part.
- Sandstone horizons may occur in the uppermost part of the formation; they are fine-grained, hard, cemented by clayey and calcareous materials, greyish brown in colour and occur as thin horizons.
- The thickness of the formation is variable depending on the shape of the basin.
- The lower contact of this formation with the underlying Pilaspi Formation is unconformable. The contact is sharp and very clear, marked by the presence of conglomerate and also, morphologically, it is very clear due to the difference in the degree of resistance to erosion between the formations.
- The thickness of the conglomerate is about 3.0 m; the pebbles are mainly of limestone cemented by red and green clayey and calcareous materials.
- At areas where conglomerate is absent, the contact was based at the presence of first red or grey claystone, which overlies the limestone beds of the Pilaspi Formation.
- The depositional environment of the formation shows a gradual change from shallow marine to freshwater nature with the presence of some isolated lagoons, which caused the deposition of the evaporite, but these lagoons are not prevailing, oolitic, ripple marks and cross-bedding gives the indication of shallow water condition, these represent the close of the evaporite sediments of Fat'ha Formation as well as the close of Middle Miocene cycle.
- The age of the formation is Middle Miocene.

3.3.6 Injana formation (Upper Fars) (Upper Miocene)

The rocks of the formation are developed in the flanks of all structures; the slight dip is largely responsible for this vast area.

Morphologically, the formation forms a hilly area with continuous strike ridges and valleys, due to the alternation of hard and soft rocks, the total red succession of the formation gives a monotonous appearance in the field.

The formation is divided into two members, based on the predominance of the lithotypes i., e., claystone member (lower part) and sandstone member (upper part), and the contact between the two members is arbitrary and diachronous.

A. Lower claystone member:

This member occur as mainly grey-brown, brown, reddish brown, green and violet calcareous claystone, sandstone and siltstone, soft to fairly hard, conchoidally fractured, having a spheroid shape with some black staining of probable iron oxides occur, secondary gypsum filling the fractures and palygorskite have been observed with thick sandstone beds. The claystone is usually alternated with thin horizons of siltstone; the percentage of the claystone in the whole bulk of the member is more than half, and the beds range in thickness from a few meters up to a few tens of meters.

The thickness of this member shows some variations depending on the palaeogeography of the depositional basin, it becomes thicker towards the south.

B. Upper sandstone member:

It forms a monotonous sequence in comparison to the lower member, characterized by thick sandstone beds, fine medium and coarse-grained, generally greyish or brownish in colour, sometimes calcareous interbedded with reddish brown, calcareous, silty, conchoidal fractured claystone. Load casts, groove casts, ripple marks and cross-bedding are common sedimentary structures throughout the formation.

The thickness of the formation attains 440 m, where the lower claystone member has 120 – 60 m, and the upper sandstone member attains 320 – 180 m.

The lower contact of the formation with the underlying Fat'ha Formation is conformable; the contact in many localities is covered, however; it was based in the field, on the last grey olive green silty claystone bed of the underlying Fat'ha Formation and the base of the first sandstone of Injana Formation.

The depositional environment of the formation is brackish to fresh water (fluvial).

3.3.7 Mukdadiyah formation (Lower Bakhtiari) (Late Miocene – Pliocene)

These sediments are exposed in some synclines, like Ain- Sifni and Shaikan synclines Kani Qalan syncline. Morphologically, they form continuous low-strike ridges and valleys due to the alternation of hard and soft rocks. The formation is composed of cyclic deposits of clastic materials, sandstone, claystone and an admixture of both. Siltstone occurs either as thin beds or as silty materials within the claystone. The formation generally is a monotonous sequence and showing extensive development.

- The sandstone is usually light grey to grey in colour, but some of them are greyish brown, medium to coarse-grained, friable to fairly compacted occasionally fine-grained pebbly, pebbles are either disseminated along belts and lenses. Sedimentary structures are common in the sandstone, such as cross-bedding, graded bedding, mud balls, ripple marks, groove casts and load casts, sandstone composed of quartz, feldspar, carbonate grains, chert, igneous rock fragments, metamorphic rock fragment, iron oxides and others.
- The sandstone bed of this formation showing smooth and rounded edges giving boundary shapes to them due to weathering.
- The upper parts of the formation contain lenses of conglomerates with small lateral extensions, with a thickness of 1.0 m; the average thickness of the sandstone beds ranges from 1-15m.
- Claystones are dominantly light brown, dark brown to reddish, and partly greenish in colour.
- Soft to fairly hard, depending on the presence or abundance of silty materials, the claystone shows common conchoidal fracture; they are fragmented into small pieces
- Mudstone is usually calcareous, containing silt and sand-size detritus fragments, which are composed of calcite, quartz and feldspars grains.
- The thickness of the claystone bed is more than that of the sandstone beds. It reaches up to 40 m, which forms more than half the thickness of the formation.

Lateral and vertical variation from sandstone to claystone is common in the formation.

- The thickness of the formation attains its maximum at Amadiya anticline sheet No. 89/520 about 1500 m, but occasionally it becomes tectonically reduced towards the eastern part, towards the south, the exposed part is not more than 500 m sheet No. 86/550 at Miraba area, the thickness ranges of the formation as measured from the cross sections.
- The lower contact of this formation with the underlying Injana Formation is diachronous. Lithologically, it was based on the first occurrence of the pebbly sandstone horizon. The pebbles may laterally disappear in the distance, so the contact might be missed easily at the field.
- Field observation of the formation shows that the sediments are fining upward sequences, which indicates of fluviatile environment.

3.3.8 Quaternary sediments

3.3.8.1 Slope Sediments (Pleistocene – Holocene)

These sediments occupy the lower, gentler reaches of the slope curves; accordingly, they are composed of fine fractions in comparison to the colluvial slope sediments. These sediments are brought mainly by the seasonal rain wash.

The main constituents of the slope are clay which is loamy, silty, brown, ochre, and compacted structure less, and it is not aggregated; in the upper part of the slopes, there is an admixture of pebbles, gravels and brown clayey materials representing the transitional character of the boundary between the two zones.

3.3.8.2 Flood Plain (Holocene)

Floodplain sediments in the area are poorly represented; they are not mapped because of scale limitations. It represents a discontinuous strip adjoining the river course. It consists of sandy, clayey silt containing organic materials.

3.3.8.3 Valley Fills Sediments (Holocene)

The valley-filling sediments are comparatively recent in age. The sediments on the valley floor are derived during extensive rainfall; the valley carries its major load from upstream mountainous terrain, which is composed of erodable material.

The materials that filled the valley consisted of sand, silt and rock fragments derived from the surrounding formations

3.3.8.4 Alluvial Fan (Holocene)

A major alluvial fan is developed on the northern limb of the Shaikan anticline. It consists mainly of limestone fragments derived from Pilaspi Formation.

3.4 Structural Geology

The area lies in the northern part of the northern thrust zone, whilst the Shaikan and Al-Qush Anticlines represents the separating line of High Folded Zone from Foot Hill Zone (Dunnington, 1958).

The area occupies Amadiya block and partly of Shaqlawa block which belongs to Amadiya – Shaqlawa Sub Zone (Buday, 1973), these structures zones belongs to the Unstable Shelf of Nubio – Arabian Platform.The area is generally comprised of several anticline and synclines and the anticlines which have nearly parallel axis represent high mountain range i. e. Aqra and Shaikan anticlines.

The anticlinal structures encountered at the area described below:

1. Aqra Anticline:

This anticline is relatively very long and broad with highest topography about (1572 m).a.s.l It is double plunging anticline, the eastern plunge is out of the area, while the western plunge is traced NE of Atrush Village.

- The axis of this anticline is trend E – W with Aqra – Bekhma Formation being the rock unit which crop out in the core.
- Generally, the anticline is complex, highly disturbed structure show asymmetrical with southern limb as the steepest limb (10º – 65º) dip and even overturned thrusted, for which Kolosh Formation is missed. The northern

limb is gentler and has (10º – 35º) dip, the axis, after its western local plunging near Atrush village continuous toward (N 70º W) direction.

2. Kiri- Rabatki Structure:

It forms the second one in order of length, reaching about 30 km, treading E-W direction, with Aqra-Bekhma formation as the oldest rock unit in its core.

Two turning was observed in the axis towards W-NW, the first and second flexuring are at its eastern limit both are in Gercus Formation, first one at Rabatki at the east and second one Ghalhoki towards west.

These turning might be related to some basement block movement at the time of folding stress. The structure is built up of 2 anticlines which are from east to west, these are:

a. Rabatki anticline

The length of this anticline is about 8 km with Gercus Formation as the oldest rock unit in its core. The anticline is relatively symmetrical type with average dip for both flanks (5 – 25º), it is double plunging type. The southern limb is faulted by strike normal fault, trending E-W direction, traced on along Pilaspi Formation., near Shilis village. Another minor folding is traced of very short axis, about 3 km in length with southern limb (45º) being steeper than the northern one (15 º).

b. Ghalhoki anticline

It is relatively the longest anticline within the whole structure with Aqra – Bekhma Formation as the oldest rock unit. The axis trend E-W dissected by a set of block normal faults, striking NE – SW direction and truncating the axis transversally with proximate horizontal shift about 0.3 km in distance, traced along the contact of Gercus and Khurmala (outside the catchments area).

The anticline is a symmetrical type, the steepest is the southern limb reaches (80 º) and even overturned. The southern limb is affected by long strike reverse fault (thrust) which brings Fatha, Injana, Mukdadiyah formation structurally in contact with Pilaspi Formation, in addition it affects the axis causes a horizontal shift in the axis. This fault is traced near the eastern plunge at Kanbirk village.

3. Shaikan Anticline:

This structure is built up of two anticlines (major and minor), axis being in enechelon position with Aqra-Bekhma Formation as the oldest rock unit. The major one is relatively long and wide double plunging anticline trending E-W direction, a small part of the eastern part is outside the mapped area. The remaining part shows symmetrical type with average dip of both limbs, (25-40 º).

The northern limb is transversally faulted (Graben type) with average shift (200m.) traced on the contact of Avanah and Pilaspi formations south west of Rakawa village about 2 km.

The axis at the western part near Ishkft, Handur and Maghara, striking NW-SE and NE – SW directions respectively, in addition, a strike normal fault was traced on contact of Injana and Mukdadiyah Formation in the southern limbs near eastern part of the axis of the anticline about 0.5 km. NW of Qob village.

The minor one is relatively shorter, with double plunging anticline, trending NW – SE direction, a symmetrical type with the southern limb steep than northern due to major reverse fault.

4. Shaikan syncline:

It is relatively narrow and long, with total length 50 km. a small sector about 10 km in eastern part is out of the mapped area. The axis trend W-E with, the axis changes it's direction at Asas village to (N 40 º W), this finally changes to its original trend W-E direction.

This flexuring is coinciding with basement block movement at the time of folding. The syncline in two places forming hanging syncline topographical. The syncline is a symmetrical type with (10-35 º) for both limbs.

3.5 Seismicity

3.5.1 Historical seismicity of Iraq

According to time-space distribution of seismic activity the recent events in Iraq and surrounding areas was grouped into three time zones as follow:

- Seismicity for 1900-1930

The rate of seismicity for this period is equal (2.6) events/year, the area during this interval are subjected to 80 events with magnitude between (7.4-4.0) degree.

The seismic activity in this period was scattered than trended, but it was concentrated in some small places (outside the area).

- Seismicity for 1930-1960

The area during this period showed a high seismic rate (5.16) events/year; the area was subjected to 155 events with a magnitude range between (7.3-4.0).

- Seismicity for 1960-1980

The area was subjected to 415 events of magnitude range between (6.0-3.0) degree, and the rate of seismicity are (20.75) events/year, which is higher than the past two periods.

Inside Iraq, most of the events are concentrated in the north and northeastern part.

- Al-Sinawi and Ghalib, 1974, concluded that:

The geographic distribution of seismicity is regular in the north and northeastern part of Iraq.

The activity of low focal depth seism is bigger than the seism of intermediate and high focal depth, and all the seism are of (5-50) km focal depth.

- The direction of distribution is Northwest –South East

Most of the seism are (≥ 5) of seismic magnitude occur within the coordinates:

N 30◦ - 38◦

E 40◦ - 48◦

The proposed dam site is located in the northeastern part of Iraq, which represents part of Western Asia Seismic Zone carrying number: (346- Iraq Iran borders) region and the number and the seismic name: (29- West Asia) and these places are characterized by its low quake sensitivity frequency and low seismic activity, S76= 0.15-0.35

- Seismic intensity

The number of seismic intensity N ($1 \geq 3$) is 21, within the coordinates:

N 36◦ - 37◦

E 43◦ - 44◦

While the number of seismic intensity N (1≥4) is 7, the number of seismic intensity N (1≥5) is 3, and the number of seismic intensity N (1≥6) is 2 within the same coordinate.

3.5.2 Engineering seismic risks

Engineering seismic risks mean the probability of happening of critical seism during the limited time of design, and the critical seism is called the design seism, which depends upon the seismic magnitude.

Figure (3.2) shows the homogeneity of seismic risks in the areas of high seismic frequency, which are located in the northern and northeastern parts of Iraq. Contour represents the probability % of occurrences of an earthquake of minimum acceleration of 0.05(Safety factor is IS 0.01g) during a design period of 50 years.

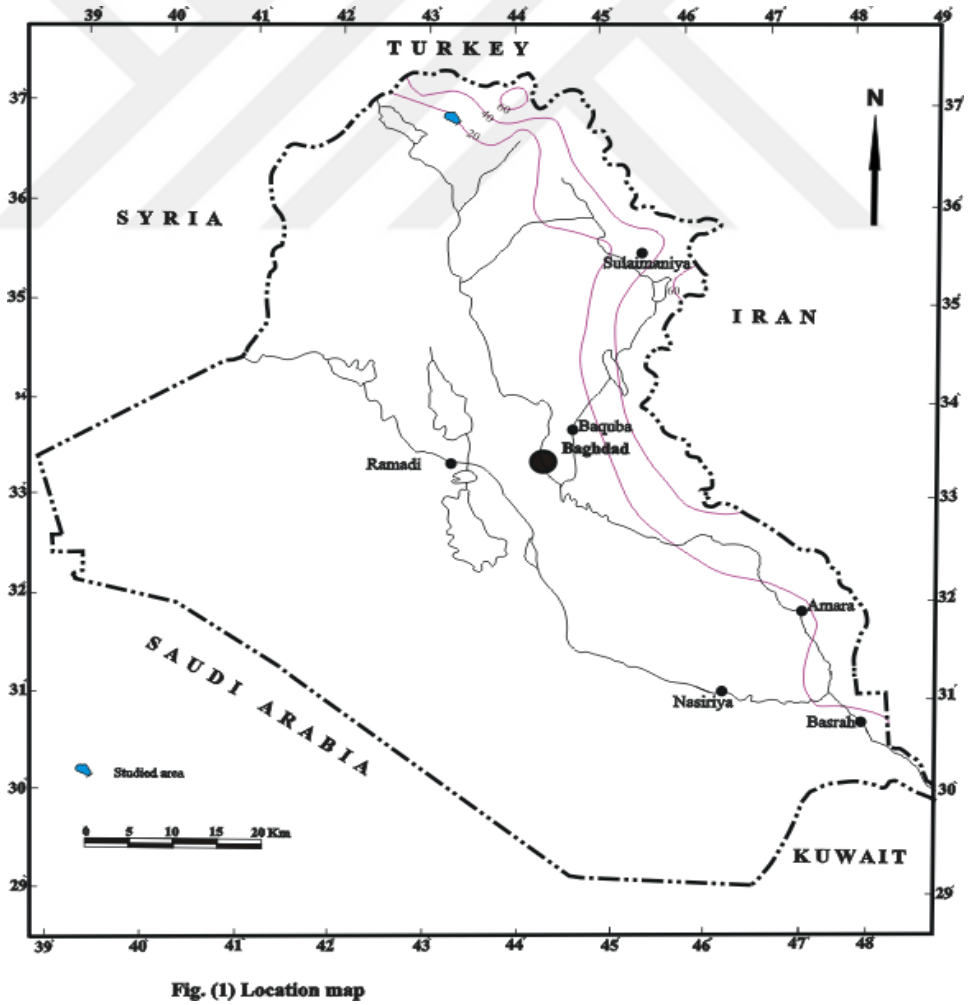

Figure 3.2: Earthquake Risk Map of the Area

Source: (Al-Sinawi and Ghalib, 1974)

The areas located within the coordinates;

N 36.5 E 44

N 37 E 44

Have a 15% probability of occurrences of an earthquake with a minimum acceleration of 0.05 (safety factor IS 0.01g) during a design period of 50 years.

3.6 The catchment area of Khanas dam

The catchment area has been defined using Digital Elevation Model (DEM) (12.5). As shown in figure (3.3). The catchment area of the Khanas dam site covers an area of about 530.3 km2.

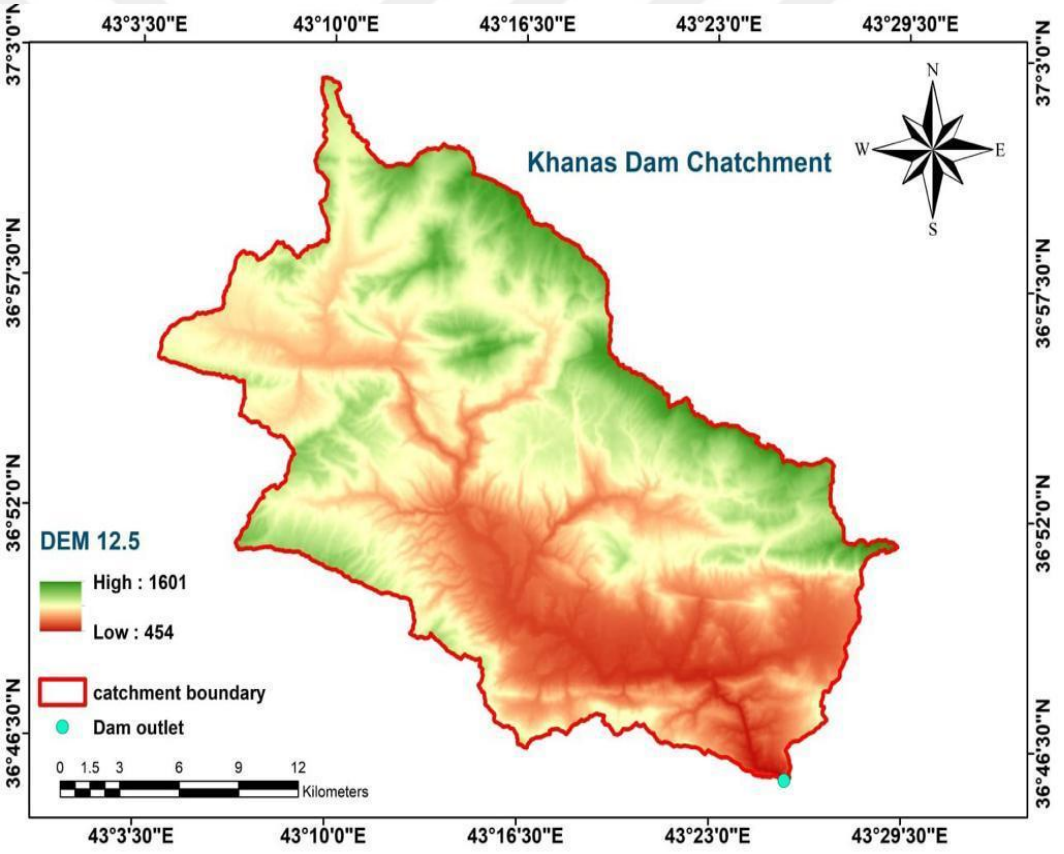

Figure 3.3: The Catchment Area of Khanas Dam

Source: (Hussain, 2023)

3.7 Hydrology and meteorology of the study area

3.7.1 Climate

Khanas reservoir area is located in the semi-arid zone of Iraq, with hot summer and cold winter.

Rainfall events may occur from October to May.

In this study, one meteorological station (Duhok) is chosen for analyzing data.

The climate of the area under consideration, according to the Climatic Atlas of Iraq (1961-1991), is characterized by the following data:

Mean annual temperature < 18º.

Mean annual amount of rainfall is > 500.

Mean annual amount of humidity < 48%.

Mean annual amount of evaporation ranges from (2100 – 2200) mm.

Mean annual number of days with frost, fog range from (4-3), and (10) days, respectively.

Mean annual number of days with dust and thunderstorm ranges from (10) and (18 – 20) days, respectively.

From reviewing the aforementioned data, it could be concluded that the area is under the influence of semi-arid climatic conditions, and the influence of the climate on the chemical and mechanical weathering of rocks is moderate and absent or insignificance respectively (Figs (3.4) and (3.5), Peltier's, 1950, in Fookes, et al., 1971).

Figure (3.4) shows the position of the area within the climatic provinces of Iraq, as mentioned by Al-Khateeb and Capigian, 2007.

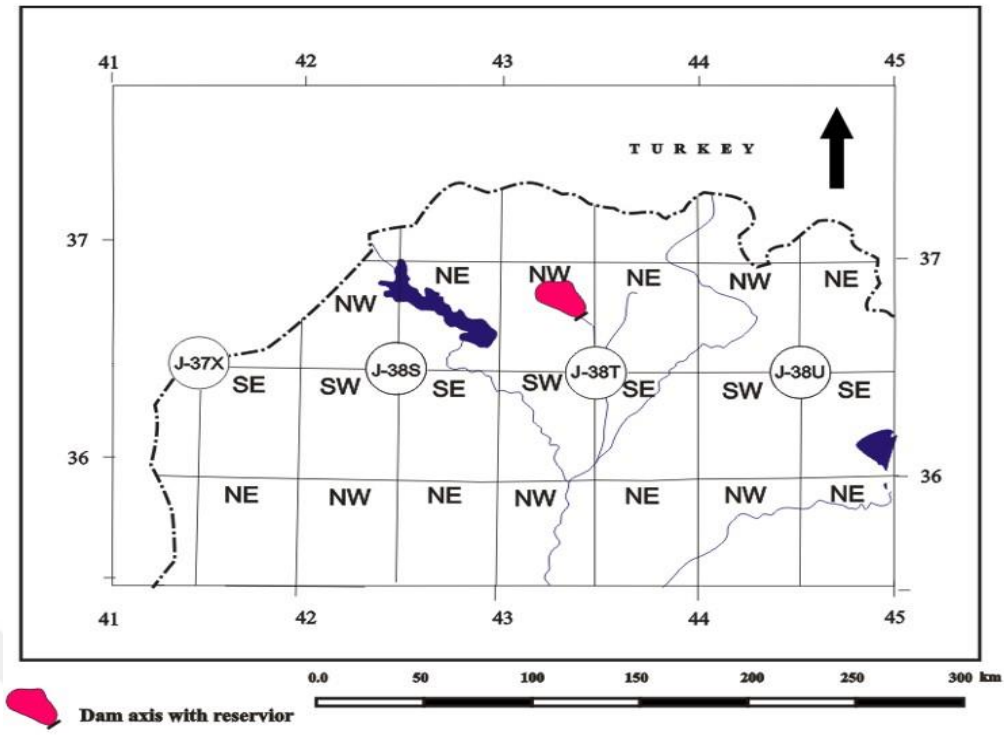

Duhok Station Maximum (24 hours) Rainfull (1991-2022)	
Year	Maximum (24)hr Rainfall
1991-1992	55.5
1992-1993	150
1993-1994	120.9
1994-1995	58.5
1995-1996	33.6
1996-1997	47
1997-1998	60
1998-1999	37
1999-2000	67.4
2000-2001	45
2001-2002	53
2002-2003	60
2003-2004	65
2004-2005	64
2005-2006	71.6
2006-2007	54
2007-2008	34
2008-2009	38.5
2009-2010	57.5
2010-2011	62.7
2011-2012	35.2
2012-2013	70.4
2013-2014	101.5
2014-2015	48.4
2015-2016	44.1
2016-2017	39.3
2017-2018	65.2
2018-2019	75.4
2019-2020	109
2020-2021	82
2021-2022	33

Figure 3.4: Position of the area within the climatic provinces of Iraq

Source: (Al-Khateeb and Capigian, 2007)

3.7.2 Rainfall

Maximum daily rainfall depth data are available for the period of (1991-2022) for Duhok meteorological station.

3.7.3 Evaporation

The North part of Iraq is characterized by moderate evaporation rates; monthly evaporation data available in Dohuk station for the years of (1989-2008) were utilized to estimate the annual evaporation losses from the reservoir of Khanas Dam.

The total average annual evaporation in Dohuk station was 1439 mm, while the max. The value was 1695 mm. These values represent the evaporation from class A land pan. The values can be multiplied by a coefficient of 0.70, K Subramanya, 1999, to get the evaporation from the free water surface. Therefore the average annual evaporation from Khanas reservoir is 1008 mm.

3.7.4 Khanas Dam (Elevation-Area Storage) curve

According to figure (3-5) of Khanas dam original design, the capacity is about (7) million cubic meters, and the surface area of the lake is about 600,000 m2 at normal water level at elevation 478.25 m.a.s.l.

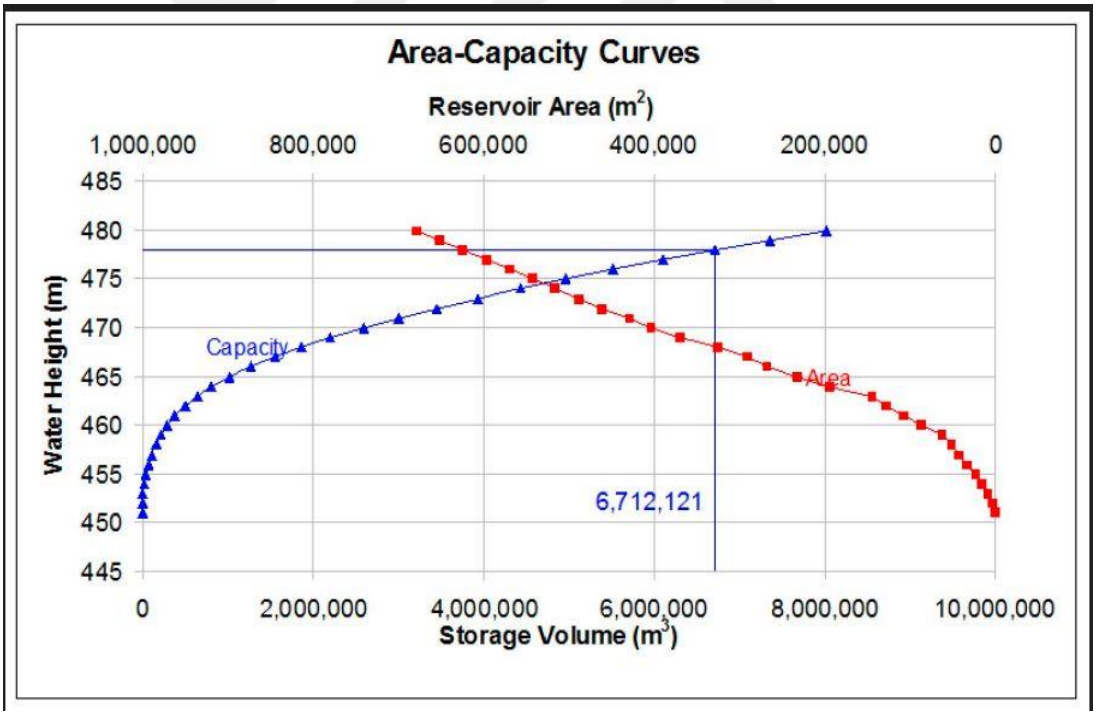

Figure 3.5: Khanas Dam Original Design the Capacity

Source: (Al-Khateeb and Capigian, 2007)

4. RESEARCH METHODOLOGY

4.1 Introduction

Hydrologic occurrences are unpredictable and have a varied character. So hydrologic variables have both deterministic and stochastic (or random) components. On the other hand, their future projections are crucial for the development of hydraulic infrastructure. In this regard, statistical and stochastic methods are particularly beneficial. They are employed in analysing historical data on hydrologic variables to ascertain their properties in order to predict their future values or to use the knowledge gathered for one place to establish the value at another location when no observations are available. Practitioners in a variety of industries are increasingly using extreme-value techniques. In environmental science, where severe events may be used as a barometer for climate change, the significance of effectively modelling extreme occurrences has grown. These investigations call for tools that must be easy to use but yet execute intricate statistical models and provide the results that follow. The software that is now accessible to scientists for the statistical modelling of severe occurrences is reviewed in this publication. We describe every piece of software that the authors are aware of—proprietary and open source—that targets various kinds of data and application domains.

4.2 Software used for Analyzing the Data

Frequency analysis is used to assess historical data on hydrologic events as a basis for estimating the likelihood that they will occur again in the future. The method entails selecting a subset of the available data, "fitting" that subset to a theoretical probability distribution, and "extracting" the rule that will be used to generate predictions from that distribution.

A programme used to fit statistical distributions is called HYFRAN-PLUS (Hydrological Frequency Analysis PLUS). For the statistical analysis of severe occurrences, it comprises a variety of strong, adaptable, and user-friendly

mathematical tools. Independent and identically distributed (IID) time series data may also be analyzed fundamentally using this tool.

INRS-Eau developed this program in collaboration with Hydro-Québec Hydraulic Service (Department Hydrology) as portion of Hydro-Québec's quantitative hydrology architecture.

Adapting a quantitative distribution to a sample at random is made easier with the help of the Windows application HYFRAN-PLUS. Two categories can be used to classify these tasks:

1. Collecting information and analyzing a random sample's statistical features.
2. Analysis of data in light of one or more statistical rules.

At each task corresponds a different tab box with adapted options. HYFRAN- PLUS help is organized around these two tasks and also contains two groups of documents, named “Sample” and “Fitting”.

Multiple statistical probability distributions:

- Exponent Generalised Pareto, Weibull (2 parameters), Gumbel (EV1), Generalised Extreme Value (GEV: EV2, EV3),
- Type A (HA), Type B (HB), and Type Inverse B (HIB) are all Halphen subtypes.
- Regular
- Lognormal 2 (LN2) and 3 (LN3) Parameters Compound Poisson exponential; Gamma (G); Generalised Gamma (GG); Inverse Gamma (IG); Pearson type 3 (P3); Log Pearson type 3 (LP3);

Details about the software can be obtained from the Ling Below (www.wrpllc.com):

4.3 The Criteria for Selecting the Best Fit Are

- AIC: Akaika information criterion
  AIC= 2k-2ln (L)

L is the maximum value of the likelihood function for the estimated model, and k is the total number of variables in the mathematical framework.

- BIC: Bayesian information criterion
  BIC= -2ln (L) + kln (n)

Where n is the number of data points (sample size)

4.4 Fitting Distribution

The to fit a variety of theoretical distributions to the observed data and then choosing the most suited distribution using statistical tests. Weibull, Gumbel, Pearson Type-III, lognormal distribution, etc., are among the recommended distributions for the estimation of the maximum design flood. The occurrence of zero values is one of the major problems that the majority of LFFA and distribution fitting studies deal with.

The bottom bound for hydrological datasets, including streamflow and precipitation, is frequently zero. Neglecting zero values could result in an inaccurate estimation of the relevant variable. However, distributions that are fitted to zero values give a positive probability to the variable's negative values. In certain circumstances, the distributions may be limited to have a lower limit, which could produce physically meaningless results and test the distribution's flexibility (Smakhtin, 2001).

Hann (1977) employed a conditional probability technique in a different strategy to 18 accounts for zero values of low flows. Utilising the total probability theory. By analysing all non-zero observations first and multiplying the resulting probabilities by the percentage of non-zero values in the data, it is possible to account for the proportion of values that equal zero, which is Where is the chance that all values will exceed, c is the likelihood that x is not zero and is the likelihood that the non-zero values will surpass. The parameters of probability distributions define them.

The sample data series must be used to determine the true parameter values of the distribution in order to fit it to the dataset.

Two dominant parameter estimation techniques exist:

1. Method of maximum likelihood
2. Method of Moments.

Method of maximum likelihood Considers a sample of N random variables with independent and symmetric distributions, where the parameters are the probability density function. The independent and identical distributions that make up the

likelihood function are defined. Finding the values of that make the data (most probable) is the goal of maximising the likelihood function (L). Where j=1, 2, N, the maximum of the likelihood function is given by it.

Method of Moments, by comparing sample moments to theoretical moments, the moment's approach is used. The method of maximum likelihood is utilised in this report for parameter estimation for a section of N observations. For a section of N annotations, is the rh theoretical moment about the origin, is the rth theoretical moment about the mean, is the rth sample moment about the sample mean, and so on.

Once the variables have been determined, the selected distributions are analyzed to see if they truly represent the probability distribution that best accounts for the observed data. Common statistical methods include the Chi-square and Kolmogorov-Smirnov tests (Huang et al., 2008; McCuen, 2003).

Hann (1977) asserts that the goodness of fit tests should not be used when fitting distributions to streamflow data because they are insensitive to the distribution's tails and produce inaccurate results when the sample size is small, increasing the likelihood that the distribution fits when it does not actually. However, these tests are useful in assessing the relative merits of various distributions.

Common Hydrologic Probability Distributions

1. Standard Spreading:

Concentration Measure of Probabilities is:

$$P(X)= \frac{1}{\sigma\sqrt{2\pi}} e^{-\frac{(x-\mu)^2}{2\sigma^2}}$$

Parameters:

μ is the population Mean

σ is the standard deviation

2. Log – Standard Spreading

The probability Density Function is:

$$p(x) = \frac{1}{x\sigma_y\sqrt{2\pi}} e^{-\frac{(\ln x - \mu_y)^2}{2\sigma_y^2}}$$

Parameters:

μy is the average of x's natural logarithms

y is the natural logarithms of x's mean and standard deviation.

3. Log – Normal III

The probability Density Function is:

$$p(x) = \frac{1}{(x-a)\sigma_y\sqrt{2\pi}} e^{-\frac{(\ln(x-a) - \mu_y)^2}{2\sigma_y^2}}$$

Parameters:

The Logical logarithmic equation of (x) have values (μy) and (σy), where they are the standard deviation, and the lower limit is denoted by (a).

4. Pearson Type III

The probability Density Function is:

$$p(x) = \frac{a^{\lambda}}{\Gamma(\lambda)}(x-m)^{\lambda-1} e^{-a(x-m)}$$

Parameters:

Γ(λ) is the Gamma function and α, λ and m are the scale parameters for form and position estimated via one of many techniques.

5. Log – Pearson Type III

The probability Density Function is:

$$p(x) = \frac{a^{\lambda}}{x\Gamma(\lambda)}(\ln x - m)^{\lambda-1} e^{-a(\ln x - m)}$$

Parameters:

Γ(λ) is the Gamma function, and α, λ and m are the measurement parameters for form and position estimated via one of many techniques.

6. Generalized Extreme Value

The probability Density Function is:

$$p(x) = \frac{1}{a}\left(1 - \frac{k}{a}(x-u)\right)^{\frac{1}{k}-1} e^{-\left(1-\frac{k}{a}(x-u)\right)^{\frac{1}{k}}}$$

Parameters:

u is the position bound, α is the measure bound, and k is the shape parameter.

7. Gumbel (EV II)

The probability Density Function is:

$$p(x) = \frac{1}{a} e^{\left(-\frac{x-u}{a} - e^{-\frac{x-u}{a}}\right)}$$

Parameters:

u is the position bound, and α is the measure bound.

8. Weibull (EV III)

The probability Density Function is:

$$p(x) = \frac{c}{a}\left(\frac{x}{a}\right)^{c-1} e^{-\left(\frac{x}{a}\right)^{c}}$$

Parameters:

c is the shape parameter, and α is the measure bound.

9. Gamma

The probability Density Function is:

$$p(x) = \frac{a^{\lambda}}{\Gamma(\lambda)} x^{\lambda-1} e^{-ax}$$

Parameters:

Where Γ(λ) is the gamma function, α is the measure bound, and λ is the shape parameters for form and position estimated via one of many techniques.

10. Exponential

The probability Density Function is:

$$p(x) = \frac{a^{\lambda}}{\Gamma(\lambda)} x^{\lambda-1} e^{-ax}$$

Parameters:

α is the position bound, whereas is the measure bound.

4.5 Peak Discharge Calculation by SCS (Soil Conservation Service)

Surface runoff calculation:

The SCS model (soil conservation service) is best suited for this purpose, and it has been used to create the maximum runoff volume, based on the following equation, at the watershed site during the maximum daily rainfall:

$Q= (P-0.2S)^2 / (P+0.8S)$

Where:

Q: is the daily runoff in (mm).

P: is the daily rainfall in (mm).

S: is called detention, which can be calculated from to get the monthly amount of losses (mm):

S= (25400/ CN) -254

CN: Is a number representing a runoff curve that depends on three variables (soil type, cover type, and initial moisture level).

Using a dataset compiled by the Soil Conservation Service, we approximated the CN for each basin based on the relative complexity of its mountainous and agricultural land uses. We then used this data to determine the CN for each reservoir catchment.

According to the highest 24-hour rainfall totals in the table above, the highest potential Flood discharge is

Q peak = 0.0208 * A* Q / Tp

In which Qpeak is in m3/s

A is catchment area in hectares

Q is in (cm)

And Tp in an hour

The time to peak (Tp) in hour can be computed by using the following formula

$Tp= 0.6Tc + \sqrt{Tc}$

Tc: Time of Concentration in hr

Tc in minutes = 0.01947 L0.77 S-0.385

L in meter

S = Slope $\Delta h/L$

5. RESULTS AND DISCUSSION

5.1 Introduction

Khanas Dam was hydrologically studied using the maximum 24-hour rainfall data of Duhok Station for the period (1991-2022) as shown in Table (5.1):

Table 5.1: Hydrologically Studied using Maximum Khanas Dam

Duhok Station Maximum (24 hours) Rainfull (1991-2022)	
Year	Maximum (24)hr Rainfall
1991-1992	55.5
1992-1993	150
1993-1994	120.9
1994-1995	58.5
1995-1996	33.6
1996-1997	47
1997-1998	60
1998-1999	37
1999-2000	67.4
2000-2001	45
2001-2002	53
2002-2003	60
2003-2004	65
2004-2005	64
2005-2006	71.6
2006-2007	54
2007-2008	34
2008-2009	38.5
2009-2010	57.5
2010-2011	62.7
2011-2012	35.2
2012-2013	70.4
2013-2014	101.5
2014-2015	48.4
2015-2016	44.1
2016-2017	39.3
2017-2018	65.2
2018-2019	75.4
2019-2020	109
2020-2021	82
2021-2022	33

HYFRAN – PLUS software was used for estimating maximum daily rainfall (mm/day) values at different return periods for 5, 10, 15, 20, 25, 50, 100, 200, 1000, and 2000 years by (11) Methods as shown below:

1. Duhok Meteorological Station Observation data (Maximum 24 hrs. rainfall) for the period (1991-2022) analyzed by HYFRAN software as shown in figures (5.1), (5.2), and (5.3). And data shows a maximum of 24 hrs. rainfall in the water year (1992-1993), and the amount is

(150) mm. First, the observation data interred to the program and will be ordered automatically from the largest to the smallest.

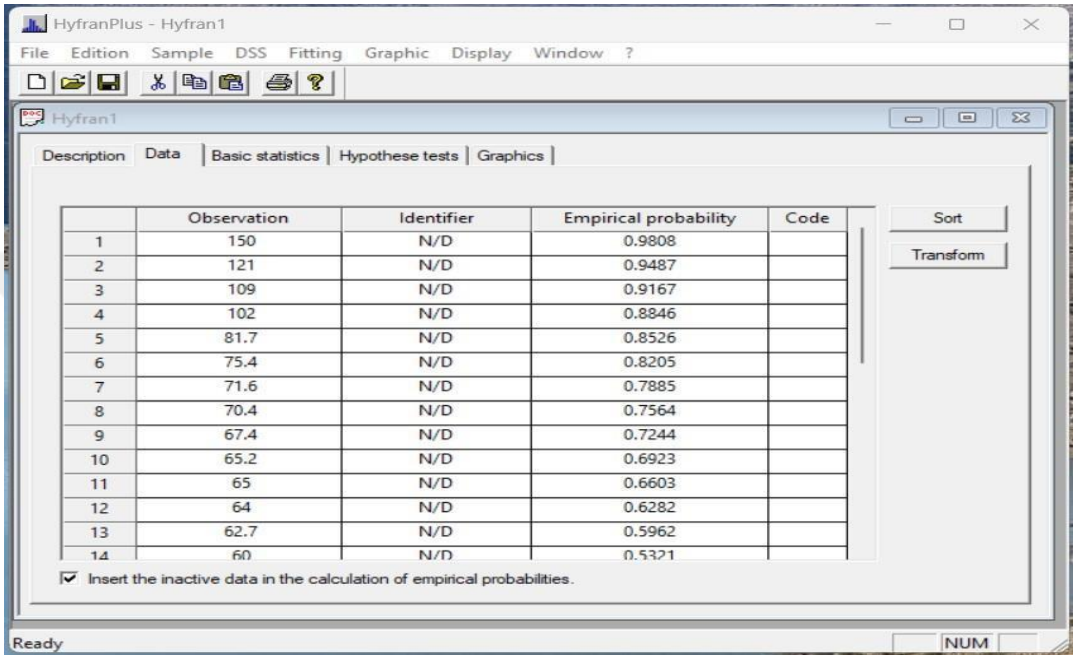

	Observation	Identifier	Empirical probability	Code
1	150	N/D	0.9808	
2	121	N/D	0.9487	
3	109	N/D	0.9167	
4	102	N/D	0.8846	
5	81.7	N/D	0.8526	
6	75.4	N/D	0.8205	
7	71.6	N/D	0.7885	
8	70.4	N/D	0.7564	
9	67.4	N/D	0.7244	
10	65.2	N/D	0.6923	
11	65	N/D	0.6603	
12	64	N/D	0.6282	
13	62.7	N/D	0.5962	
14	60	N/D	0.5321	

Figure 5.1: Duhok Meteorological Station Observation Data (1)

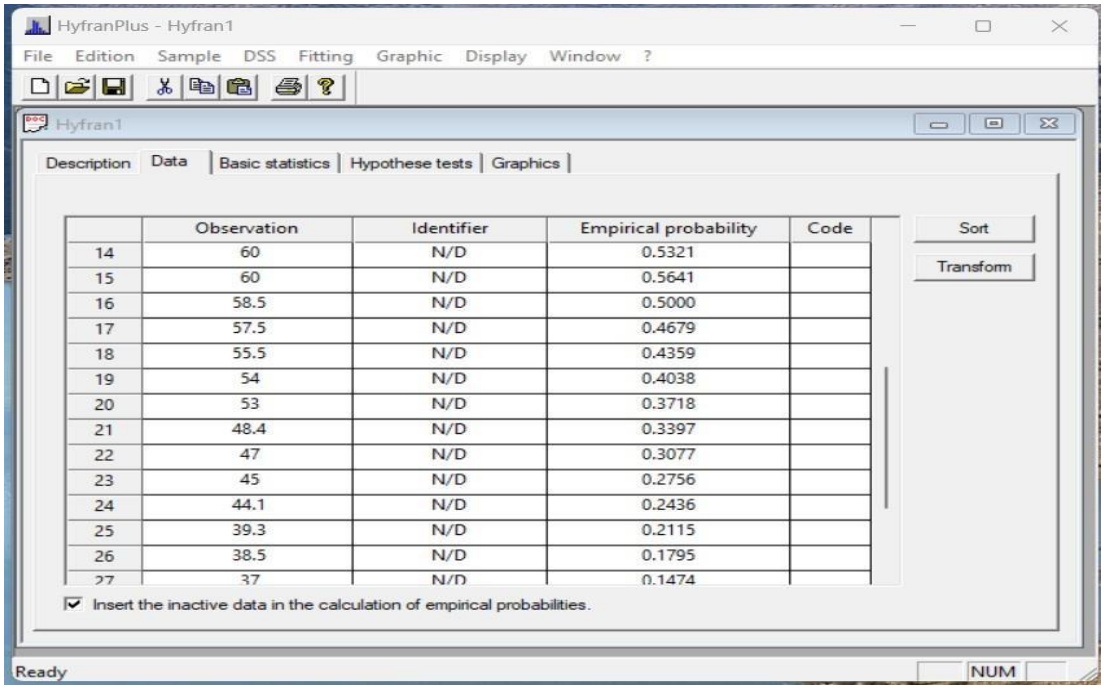

	Observation	Identifier	Empirical probability	Code
14	60	N/D	0.5321	
15	60	N/D	0.5641	
16	58.5	N/D	0.5000	
17	57.5	N/D	0.4679	
18	55.5	N/D	0.4359	
19	54	N/D	0.4038	
20	53	N/D	0.3718	
21	48.4	N/D	0.3397	
22	47	N/D	0.3077	
23	45	N/D	0.2756	
24	44.1	N/D	0.2436	
25	39.3	N/D	0.2115	
26	38.5	N/D	0.1795	
27	37	N/D	0.1474	

Figure 5.2: Duhok Meteorological Station Observation Data (2)

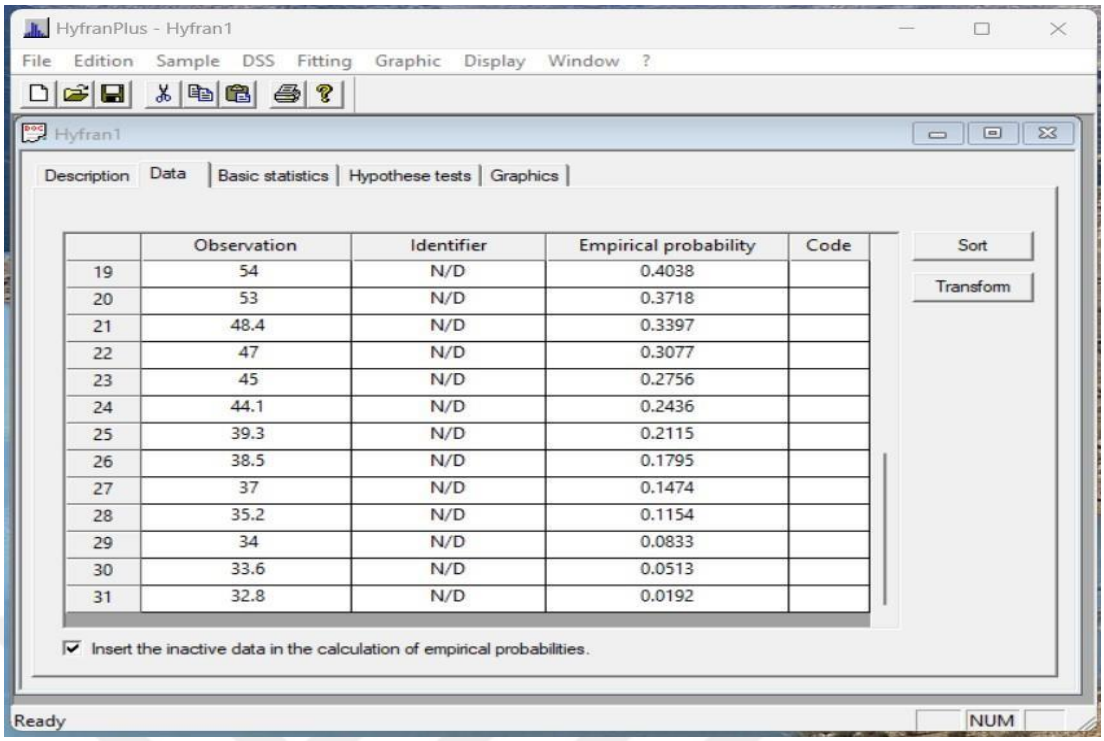

Figure 5.3: Duhok Meteorological Station Observation Data (3)

In Figure (5.4) basic statistics shown used for estimation of maximum 24 hrs. rainfall

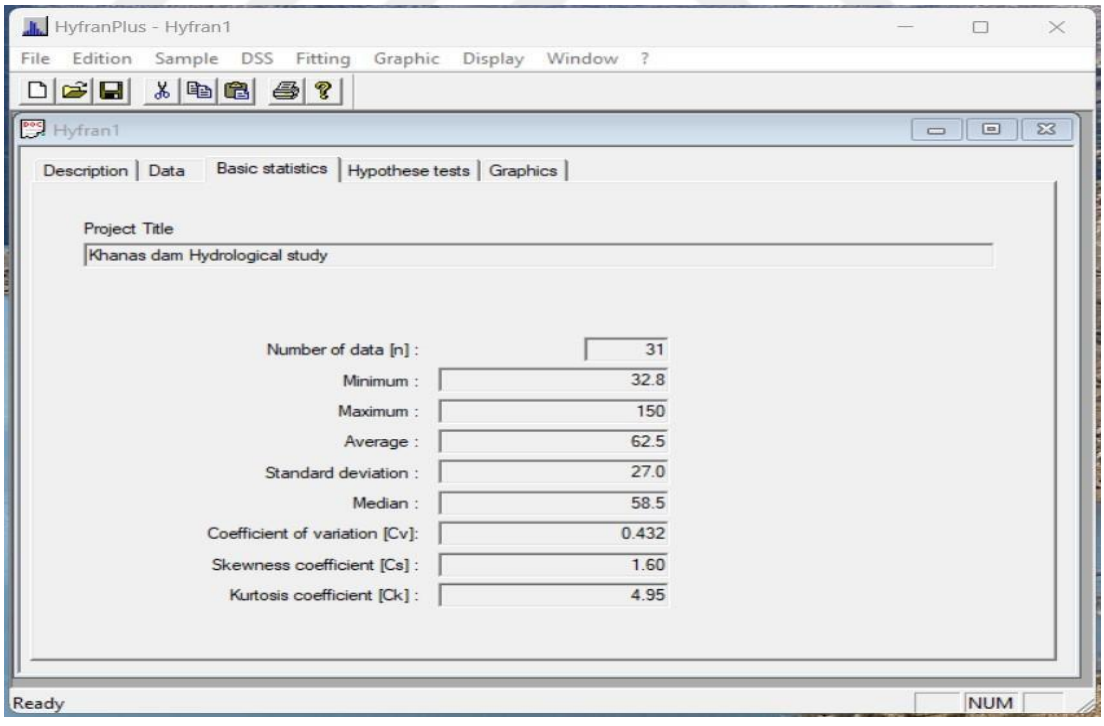

Figure 5.4: Basic Statistics Shown Used For Estimation of Maximum 24 Hrs. Rainfall

Figures (5.5) and (5.6) illustrate hypotheses tests and graphics of the data, respectively.

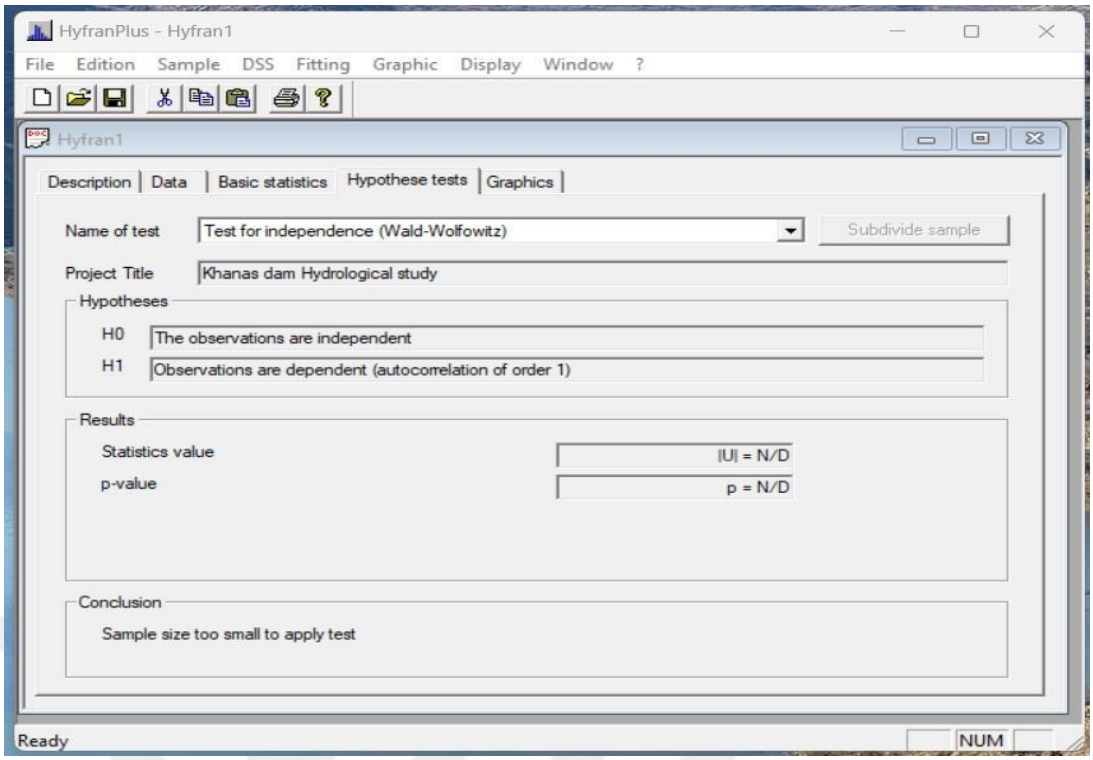

Figure 5.5: Illustrate Hypotheses Tests, and, Graphics of the Data(1)

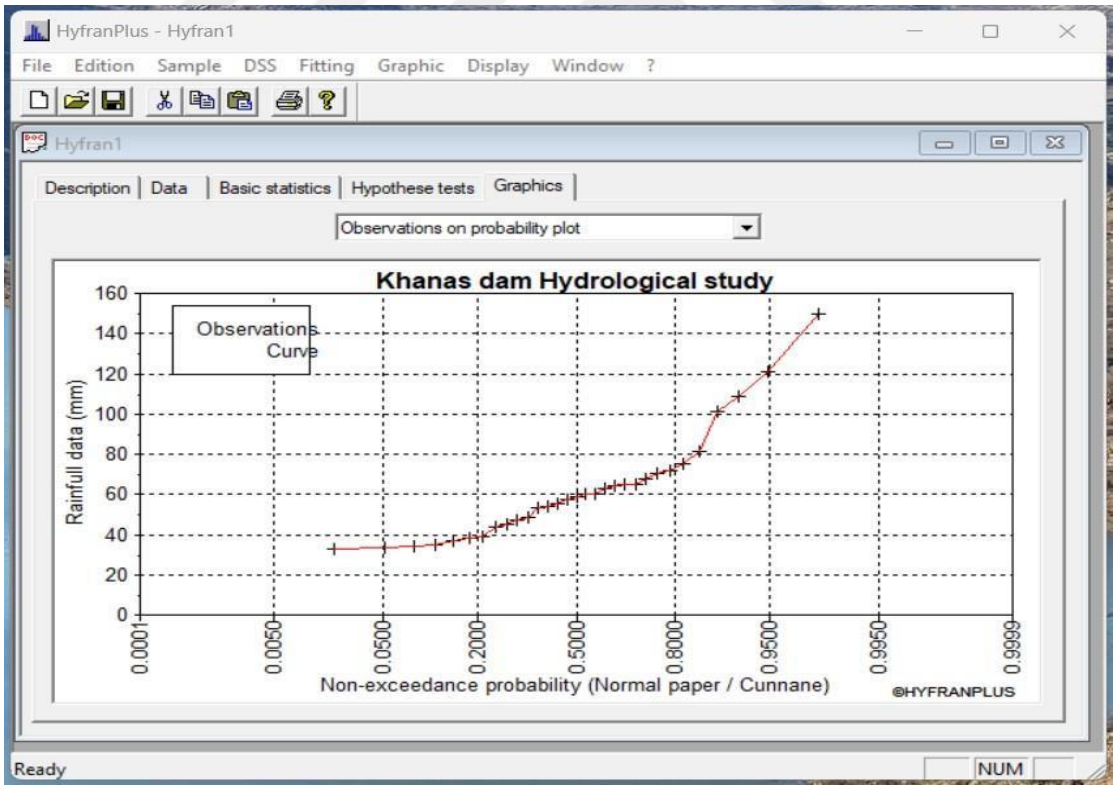

Figure 5.6: Illustrate Hypotheses Tests and Graphics of the Data(2)

2. Figure (5.7) explain the results of the estimated maximum 24 hrs. rainfall by the Exponential (Maximum Likelihood) method for many return periods.

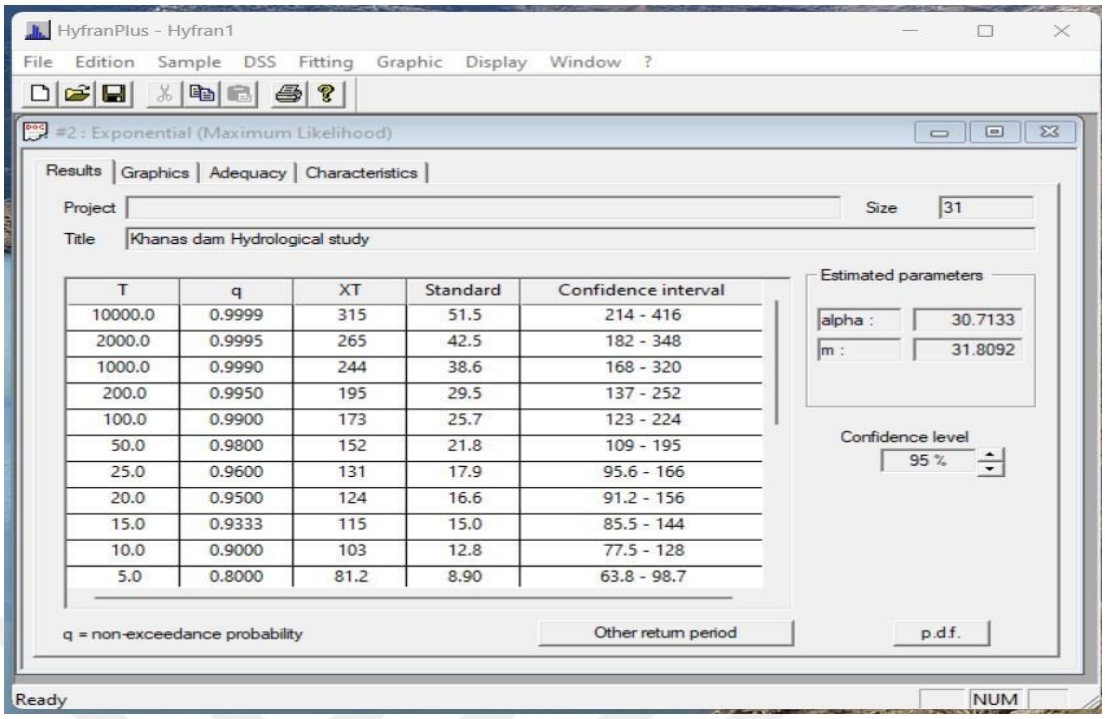

T	q	XT	Standard	Confidence interval
10000.0	0.9999	315	51.5	214 - 416
2000.0	0.9995	265	42.5	182 - 348
1000.0	0.9990	244	38.6	168 - 320
200.0	0.9950	195	29.5	137 - 252
100.0	0.9900	173	25.7	123 - 224
50.0	0.9800	152	21.8	109 - 195
25.0	0.9600	131	17.9	95.6 - 166
20.0	0.9500	124	16.6	91.2 - 156
15.0	0.9333	115	15.0	85.5 - 144
10.0	0.9000	103	12.8	77.5 - 128
5.0	0.8000	81.2	8.90	63.8 - 98.7

Figure 5.7: Results of Estimated Maximum 24 Hrs. Rainfall By Exponential (Maximum Likelihood) Method

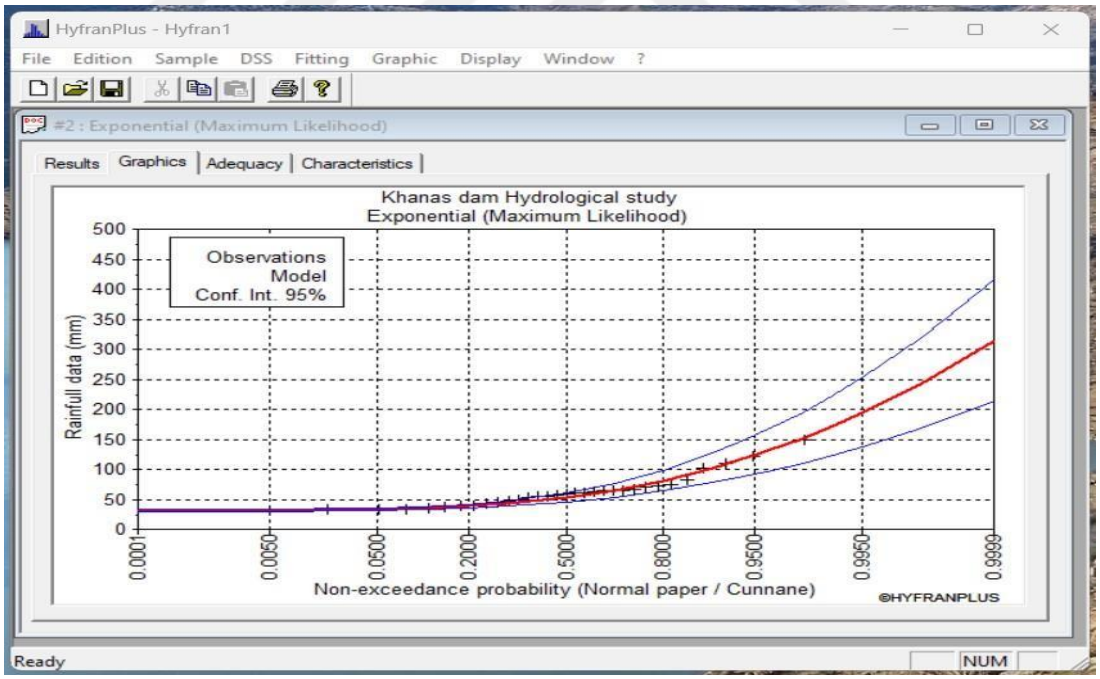

Figure 5.8: Graphic, Adequacy, and Characteristics Exponential (Maximum Likelihood) Method (1)

Figures (5.8) , (5.9), and (5.10) represent graphics, Adequacy, and characteristics by the same method.

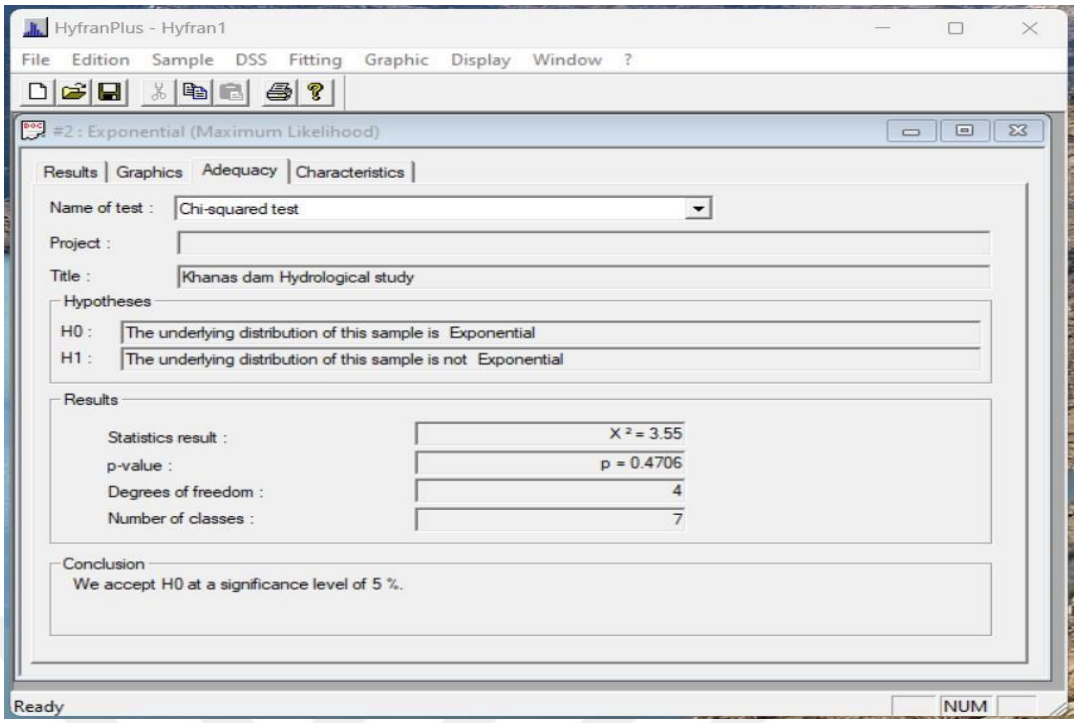

Figure 5.9: Graphic, Adequacy, and Characteristics Exponential (Maximum Likelihood) Method(2)

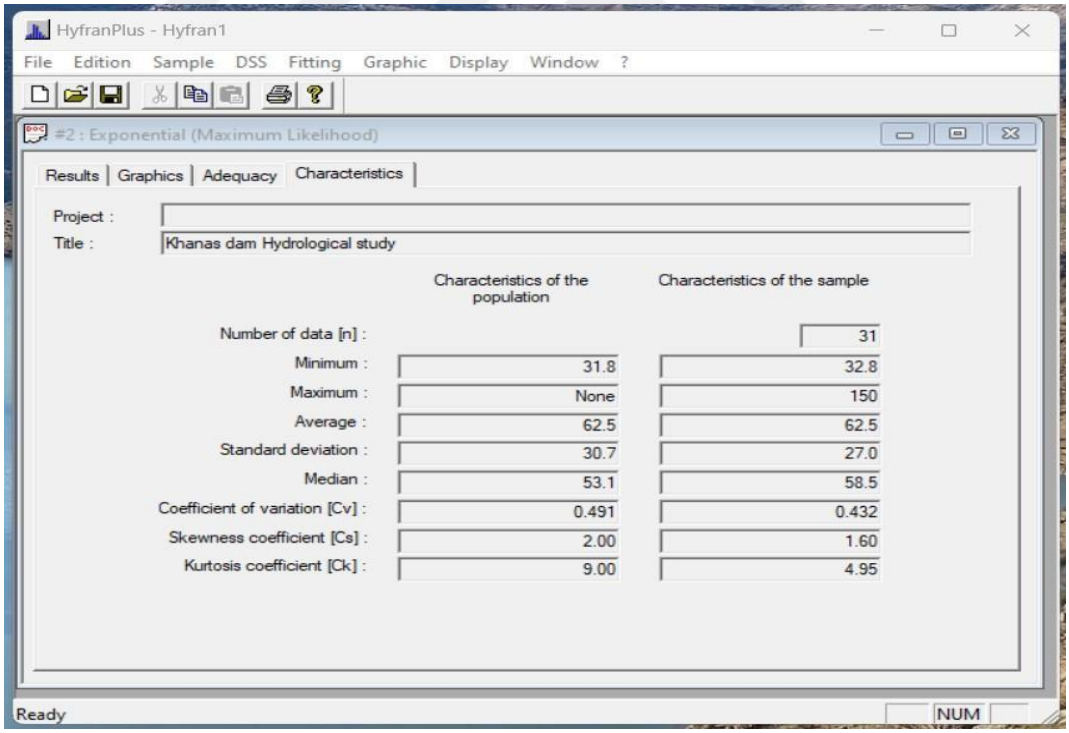

Figure 5.10: Results of Estimated Maximum 24 Hrs. Rainfall By Exponential (Maximum Likelihood) Method (3)

3. Figures (5.11), (5.12), (5.13), and (5.14) explain the results of estimated maximum 24 hrs. rainfall by GEV (Maximum Likelihood) method, for many return periods, graphics, adequacy, and characteristics, respectively by this method.

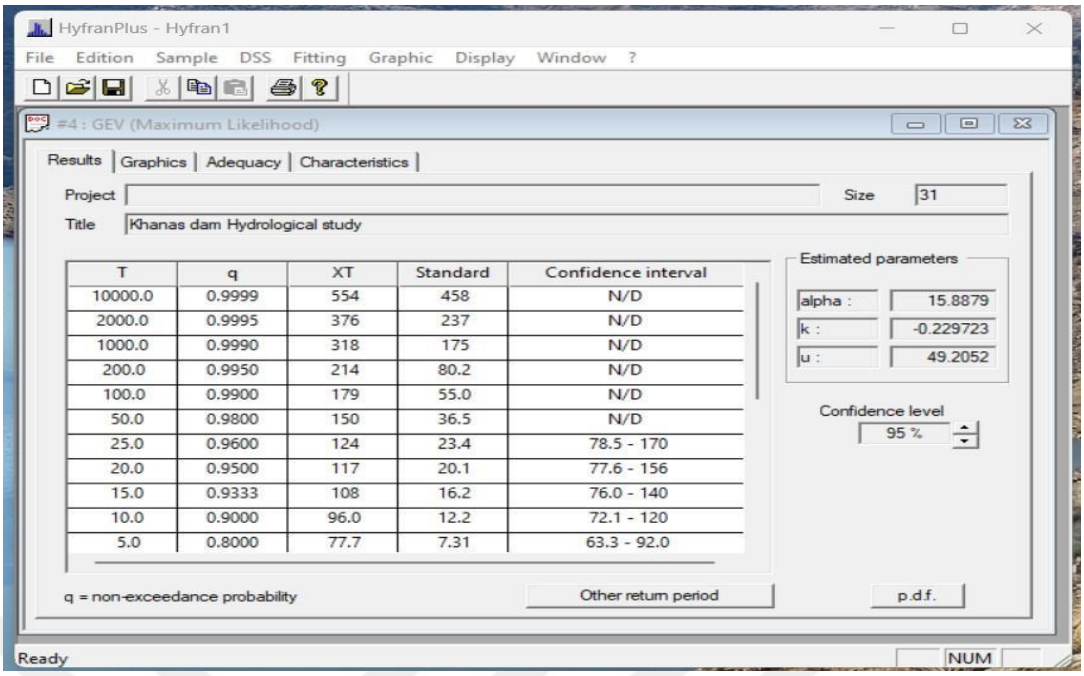

Figure 5.11: Explaining the Results of Estimated Maximum 24 Hrs. Rainfall By GEV (Maximum Likelihood) Method (1)

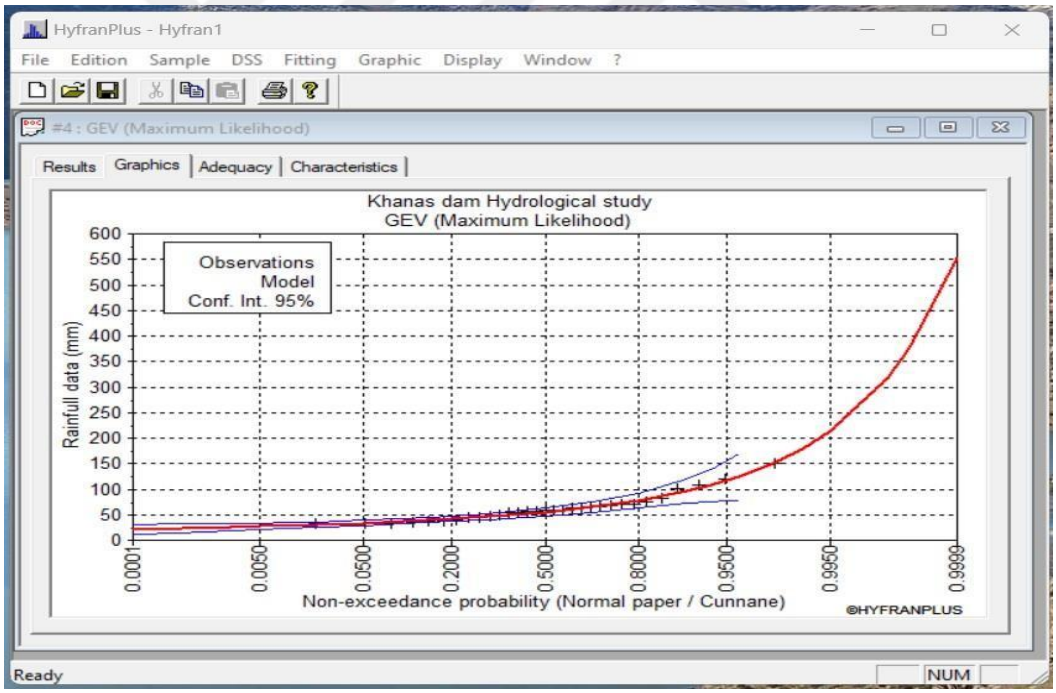

Figure 5.12: Explaining the Results of Estimated Maximum 24 Hrs. Rainfall By GEV (Maximum Likelihood) Method

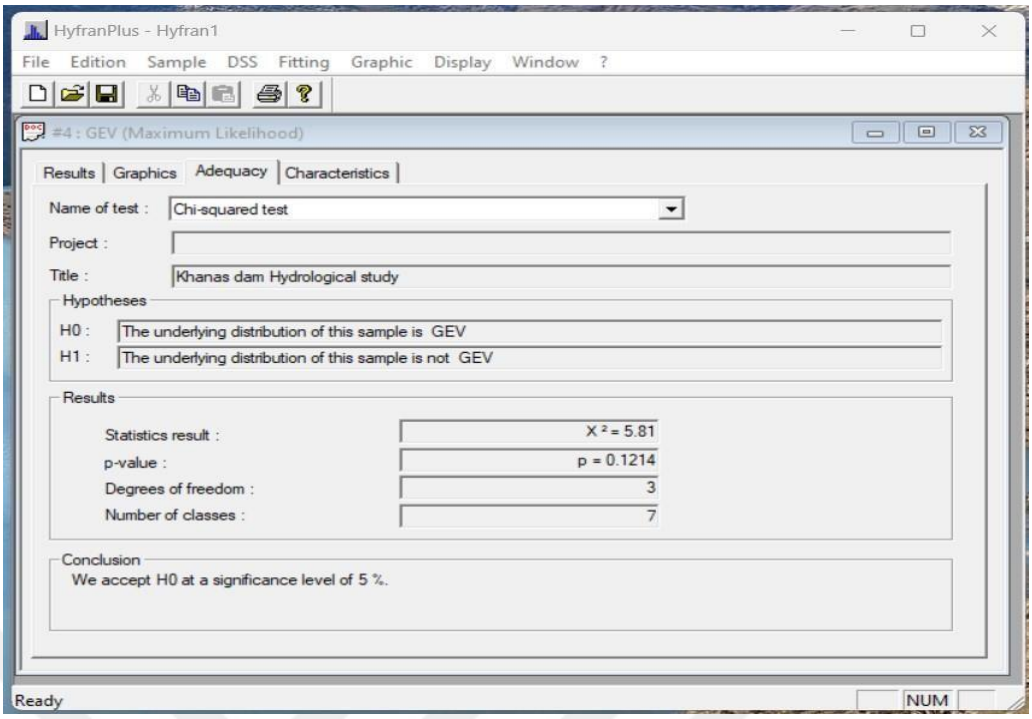

Figure 5.13: Explaining the Results of Estimated Maximum 24 Hrs. Rainfall By GEV (Maximum Likelihood) Method (3)

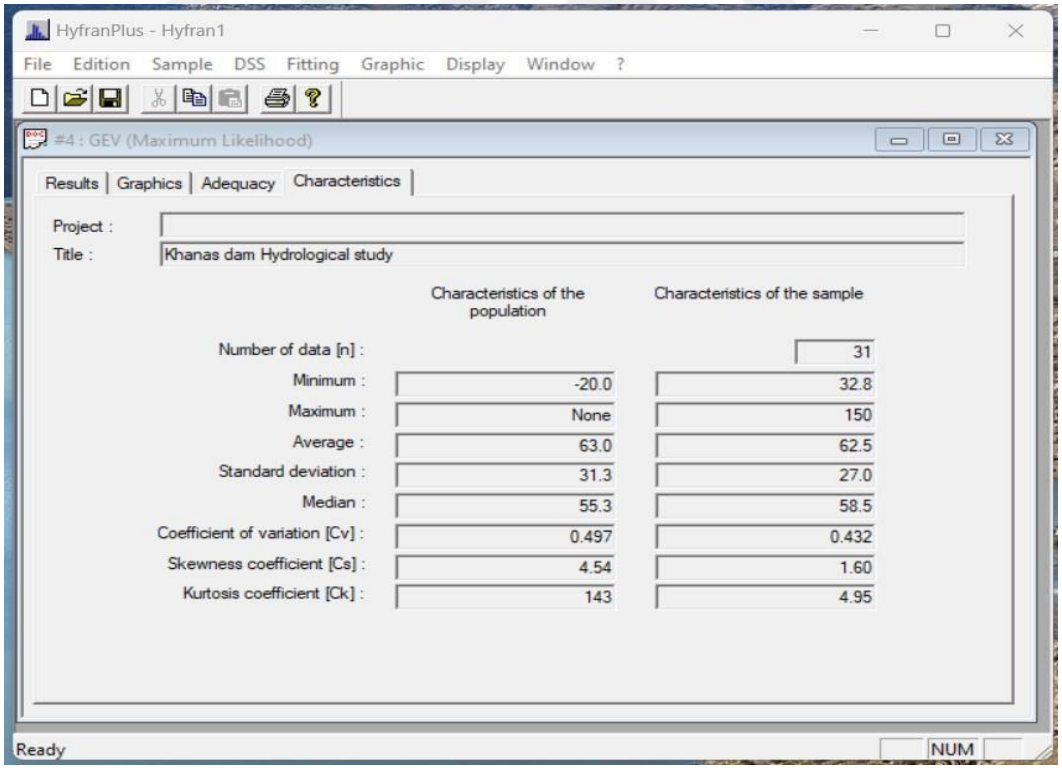

Figure 5.14: Explaining the Results of Estimated Maximum 24 Hrs. Rainfall By GEV (Maximum Likelihood) Method(4)

4. Figures (5.15), (5.16), (5.17), and (5.18) show the results of estimated maximum 24 hrs. rainfall by Gumbel (Maximum Likelihood) method, for many return periods, graphics, adequacy, and characteristics, respectively by this method.

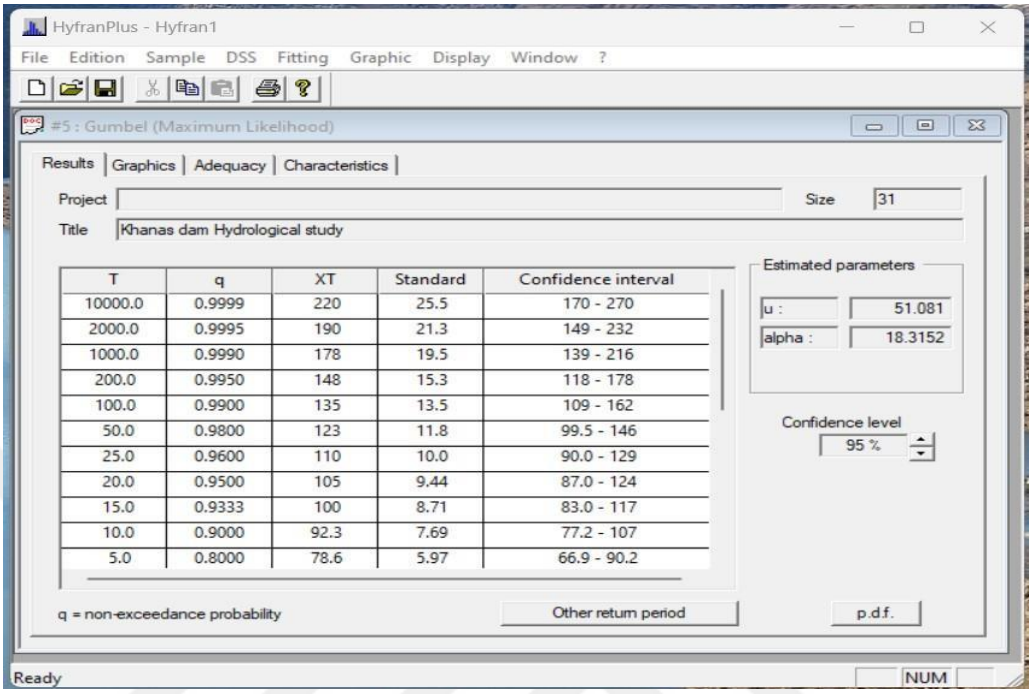

T	q	XT	Standard	Confidence interval
10000.0	0.9999	220	25.5	170 - 270
2000.0	0.9995	190	21.3	149 - 232
1000.0	0.9990	178	19.5	139 - 216
200.0	0.9950	148	15.3	118 - 178
100.0	0.9900	135	13.5	109 - 162
50.0	0.9800	123	11.8	99.5 - 146
25.0	0.9600	110	10.0	90.0 - 129
20.0	0.9500	105	9.44	87.0 - 124
15.0	0.9333	100	8.71	83.0 - 117
10.0	0.9000	92.3	7.69	77.2 - 107
5.0	0.8000	78.6	5.97	66.9 - 90.2

Figure 5.15: Results of Estimated Maximum 24 Hrs. Rainfall By Gumbel (Maximum Likelihood) Method (1)

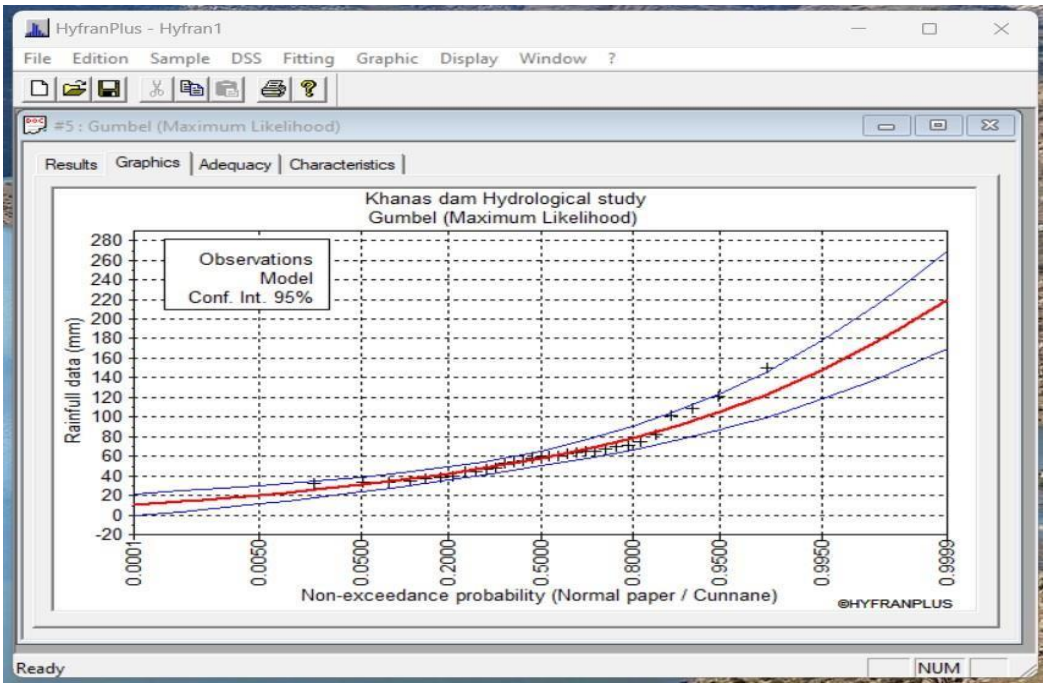

Figure 5.16: Results of Estimated Maximum 24 Hrs. Rainfall By Gumbel (Maximum Likelihood) Method (2)

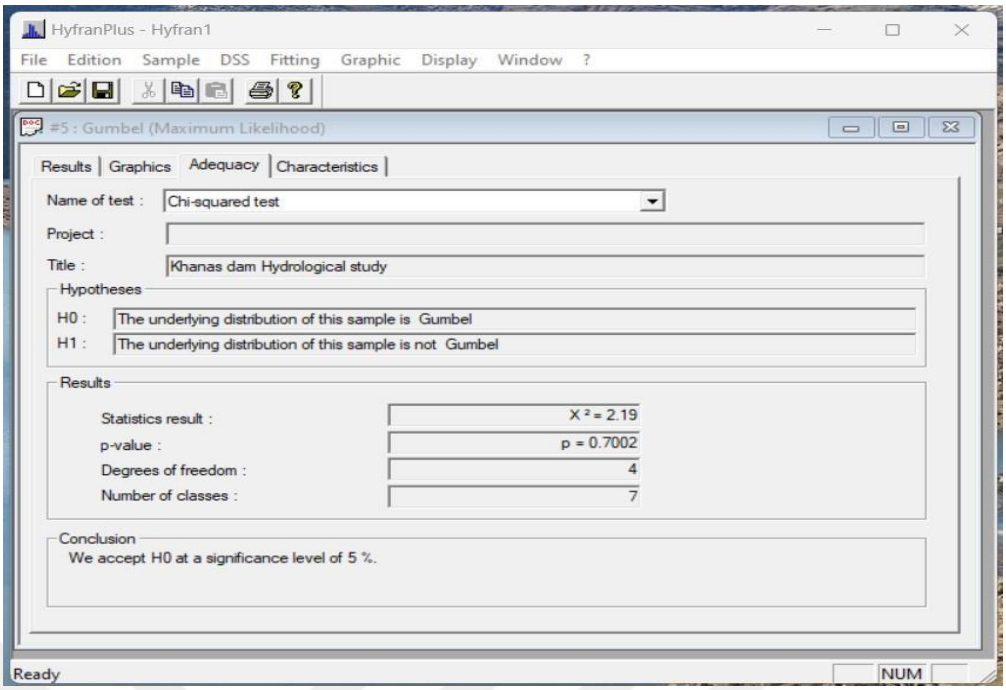

Figure 5.17: Results of Estimated Maximum 24 Hrs. Rainfall By Gumbel (Maximum Likelihood) Method (3)

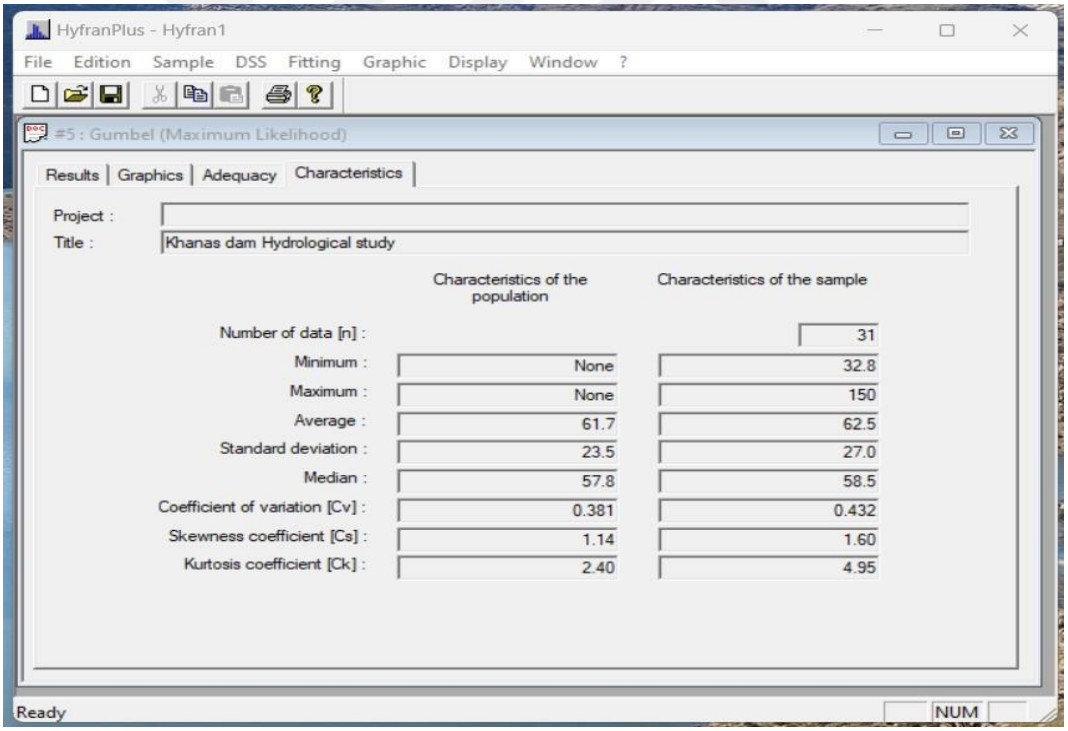

Figure 5.18: Results of Estimated Maximum 24 Hrs. Rainfall By Gumbel (Maximum Likelihood) Method (4)

5. Figures (5.19), (5.20), (5.21), and (5.22) show the results of estimated maximum 24 hrs. rainfall by Weibull (Maximum Likelihood) method, for many return periods, graphics, adequacy, and characteristics, respectively by Weibull method.

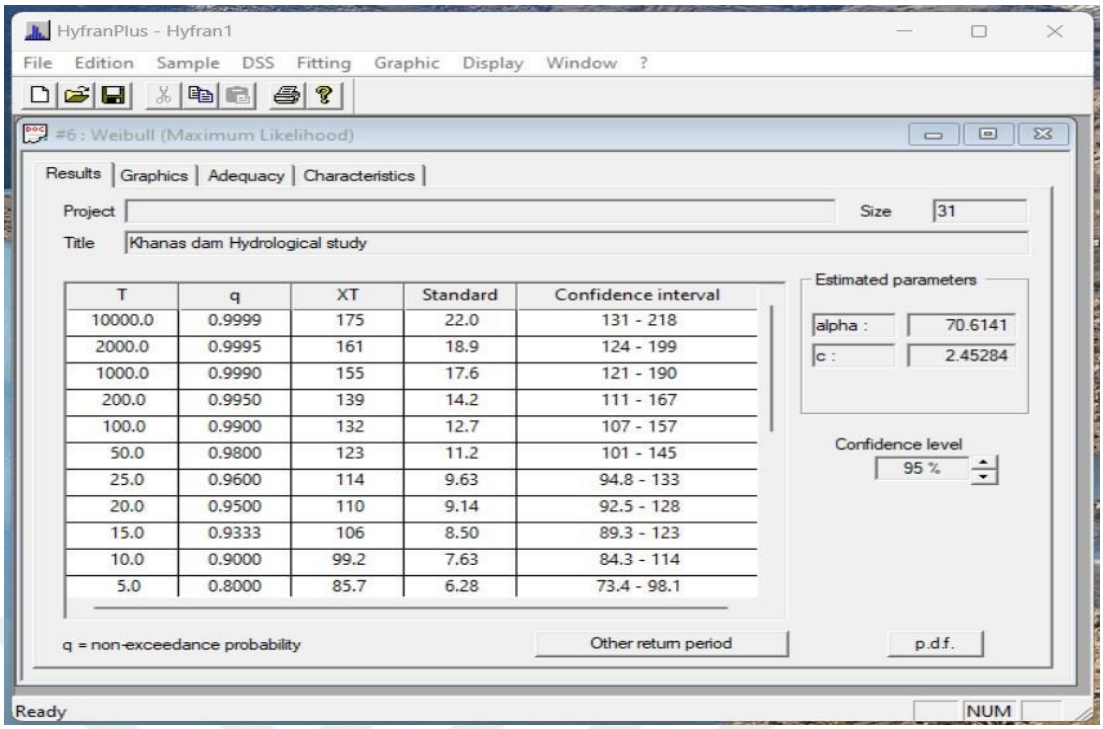

T	q	XT	Standard	Confidence interval
10000.0	0.9999	175	22.0	131 - 218
2000.0	0.9995	161	18.9	124 - 199
1000.0	0.9990	155	17.6	121 - 190
200.0	0.9950	139	14.2	111 - 167
100.0	0.9900	132	12.7	107 - 157
50.0	0.9800	123	11.2	101 - 145
25.0	0.9600	114	9.63	94.8 - 133
20.0	0.9500	110	9.14	92.5 - 128
15.0	0.9333	106	8.50	89.3 - 123
10.0	0.9000	99.2	7.63	84.3 - 114
5.0	0.8000	85.7	6.28	73.4 - 98.1

Figure 5.19: Results of Estimated Maximum 24 Hrs. Rainfall Weibull (Maximum Likelihood) Method (1)

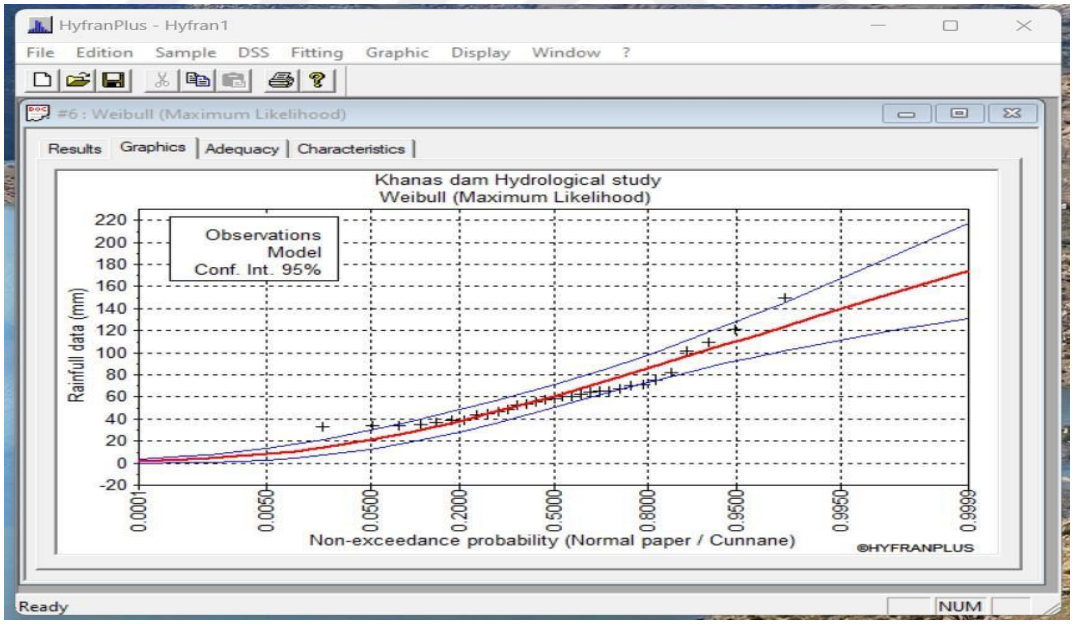

Figure 5.20: Results of Estimated Maximum 24 Hrs. Rainfall Weibull (Maximum Likelihood) Method (2)

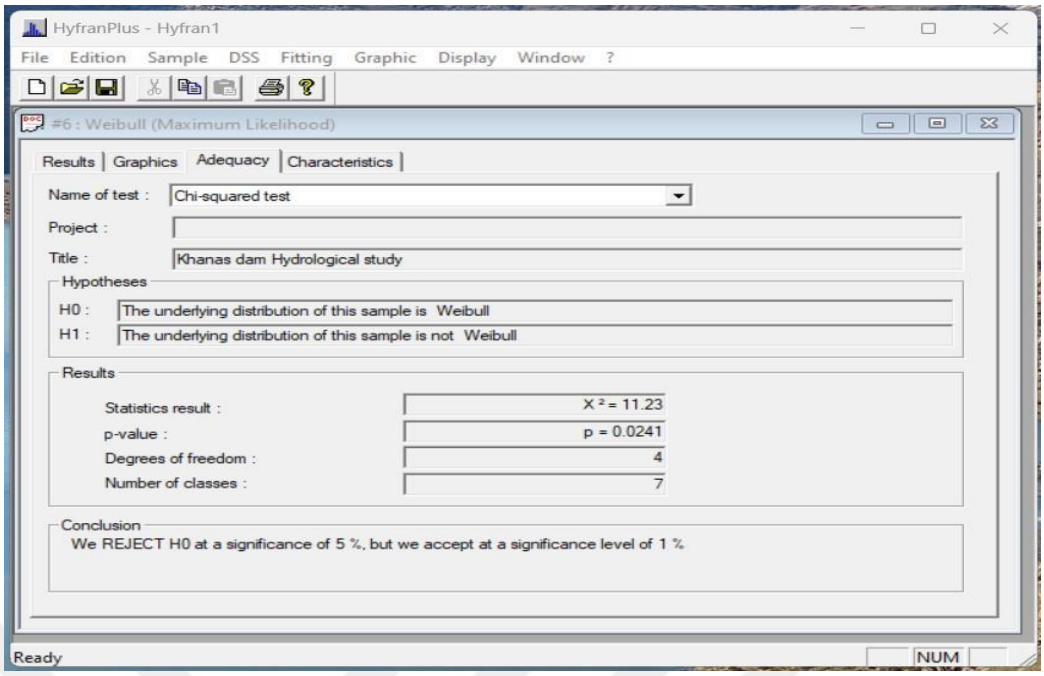

Figure 5.21: Results of Estimated Maximum 24 Hrs. Rainfall Weibull (Maximum Likelihood) Method (3)

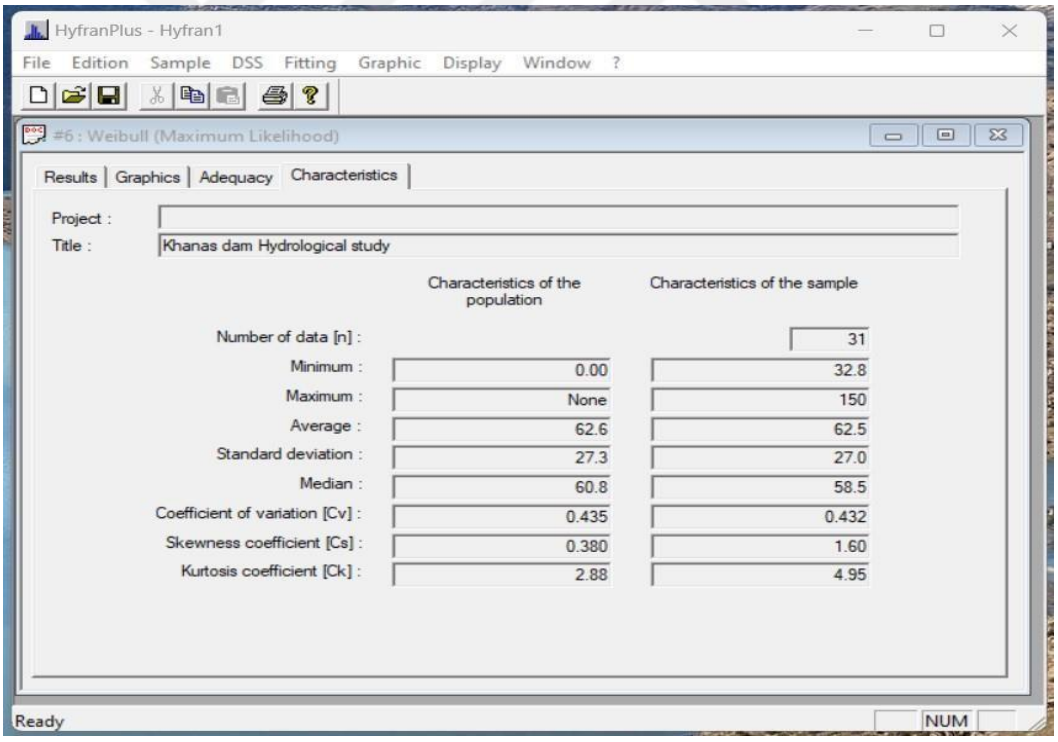

Figure 5.22: Results of Estimated Maximum 24 Hrs. Rainfall Weibull (Maximum Likelihood) Method (4)

6. Figures (5.23), (5.24), (5.25), and (5.26) show the results of estimated maximum 24 hrs. rainfall by Halphen of type b inverse (Maximum Likelihood) method for many return periods, graphics, adequacy, and characteristics respectively by this method.

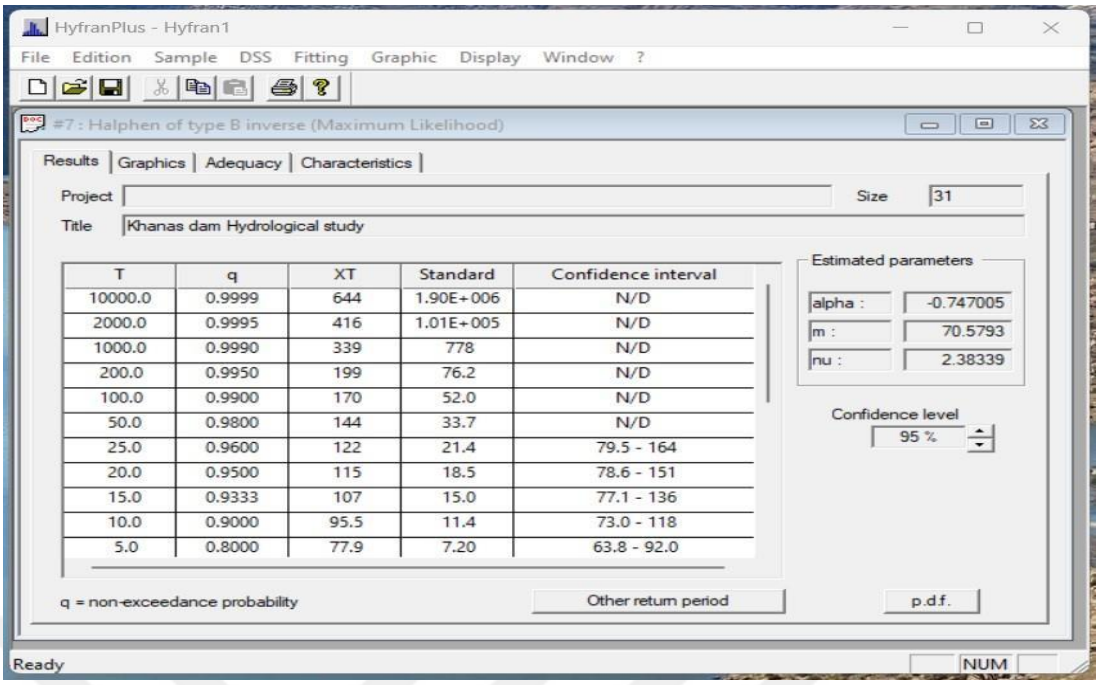

T	q	XT	Standard	Confidence interval
10000.0	0.9999	644	1.90E+006	N/D
2000.0	0.9995	416	1.01E+005	N/D
1000.0	0.9990	339	778	N/D
200.0	0.9950	199	76.2	N/D
100.0	0.9900	170	52.0	N/D
50.0	0.9800	144	33.7	N/D
25.0	0.9600	122	21.4	79.5 - 164
20.0	0.9500	115	18.5	78.6 - 151
15.0	0.9333	107	15.0	77.1 - 136
10.0	0.9000	95.5	11.4	73.0 - 118
5.0	0.8000	77.9	7.20	63.8 - 92.0

Figure 5.23: Results of Estimated Maximum 24 Hrs. Rainfall Halphen of Type B Inverse (Maximum Likelihood) Method (1)

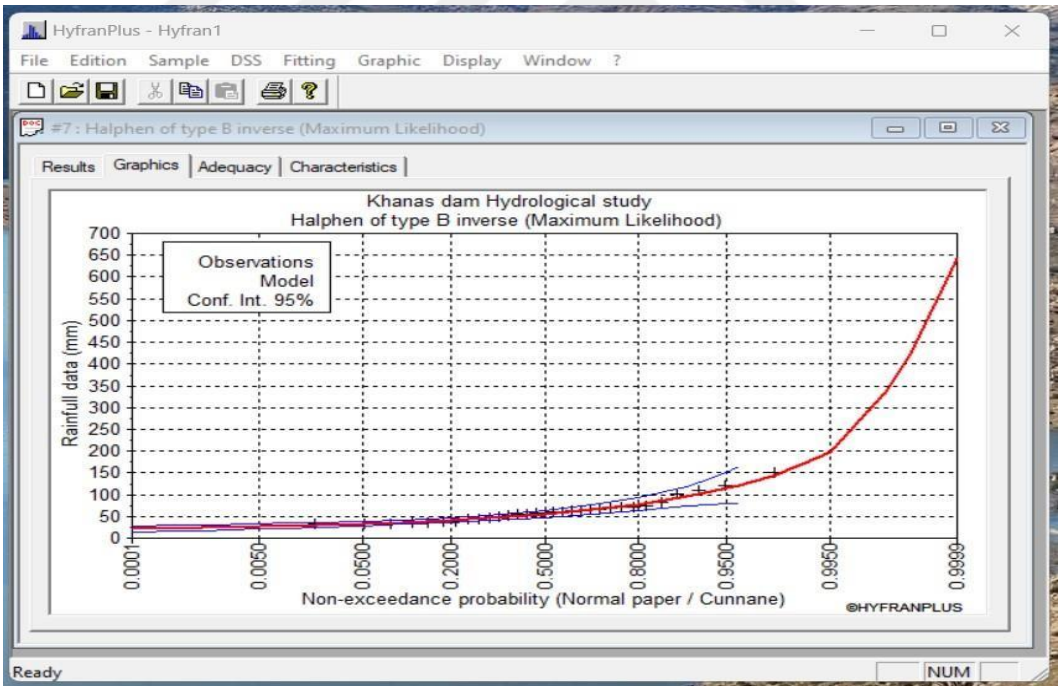

Figure 5.24: Results of Estimated Maximum 24 Hrs. Rainfall Halphen of Type B Inverse (Maximum Likelihood) Method (2)

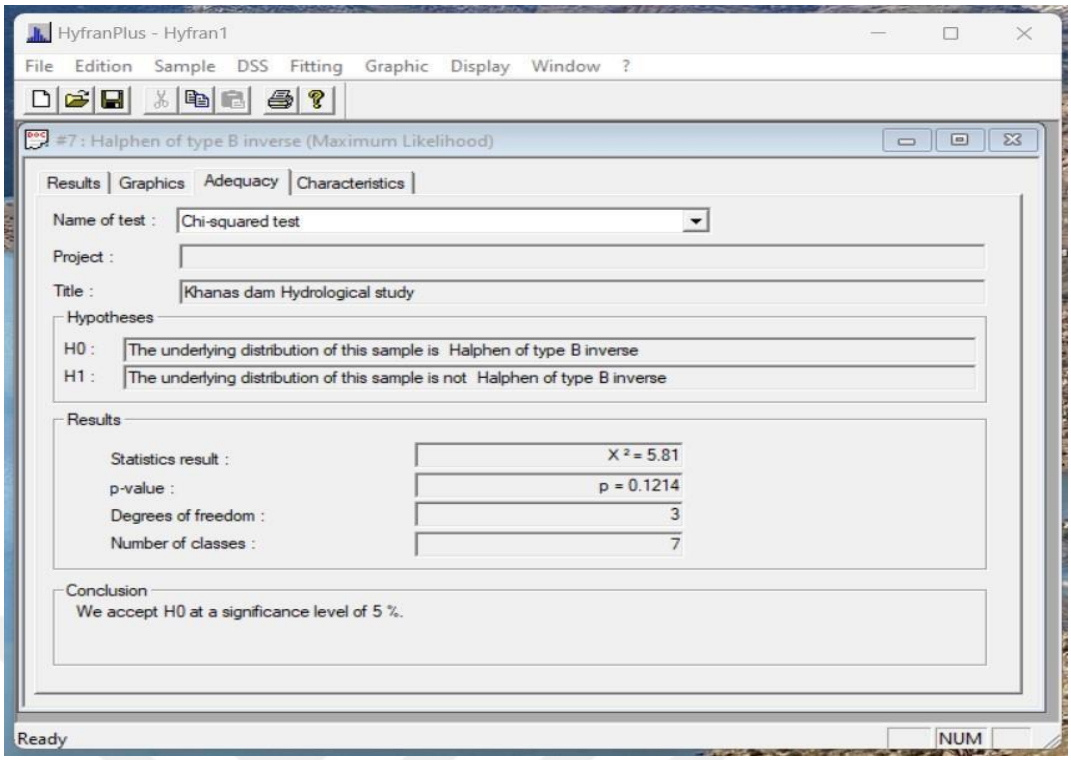

Figure 5.25: Results of Estimated Maximum 24 Hrs. Rainfall Halphen of Type B Inverse (Maximum Likelihood) Method (3)

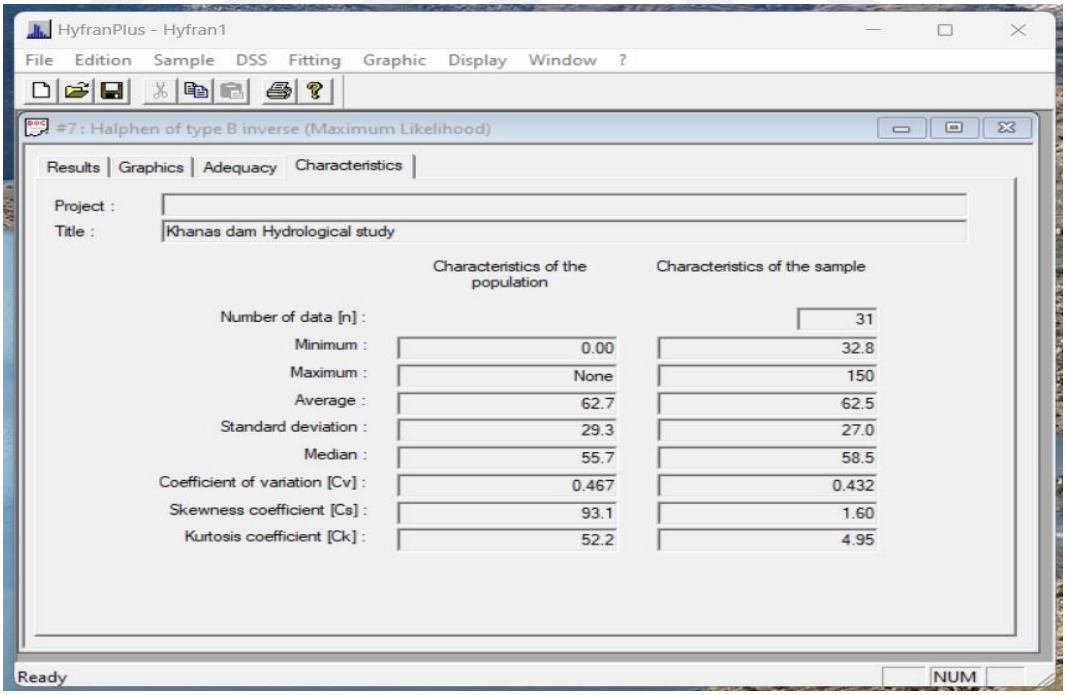

Figure 5.26: Results of Estimated Maximum 24 Hrs. Rainfall Halphen of Type B Inverse (Maximum Likelihood) Method (4)

7. Figures (5.27), (5.28), (5.29), (5.30) and (5.31) explain the results of estimated maximum 24 hrs. rainfall by Normal (Maximum Likelihood) method for many return periods, graphics, adequacy, and characteristics respectively by Normal method.

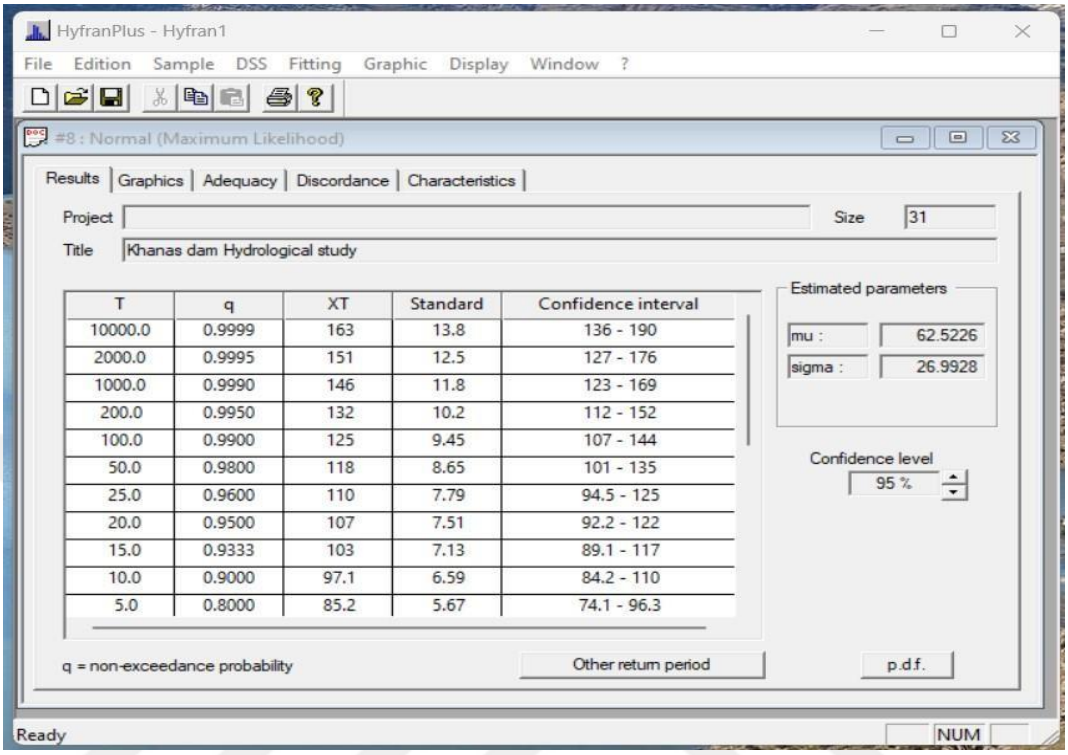

T	q	XT	Standard	Confidence interval
10000.0	0.9999	163	13.8	136 - 190
2000.0	0.9995	151	12.5	127 - 176
1000.0	0.9990	146	11.8	123 - 169
200.0	0.9950	132	10.2	112 - 152
100.0	0.9900	125	9.45	107 - 144
50.0	0.9800	118	8.65	101 - 135
25.0	0.9600	110	7.79	94.5 - 125
20.0	0.9500	107	7.51	92.2 - 122
15.0	0.9333	103	7.13	89.1 - 117
10.0	0.9000	97.1	6.59	84.2 - 110
5.0	0.8000	85.2	5.67	74.1 - 96.3

Figure 5.27: Results of Estimated Maximum 24 Hrs. Rainfall By Normal (Maximum Likelihood) Method (1)

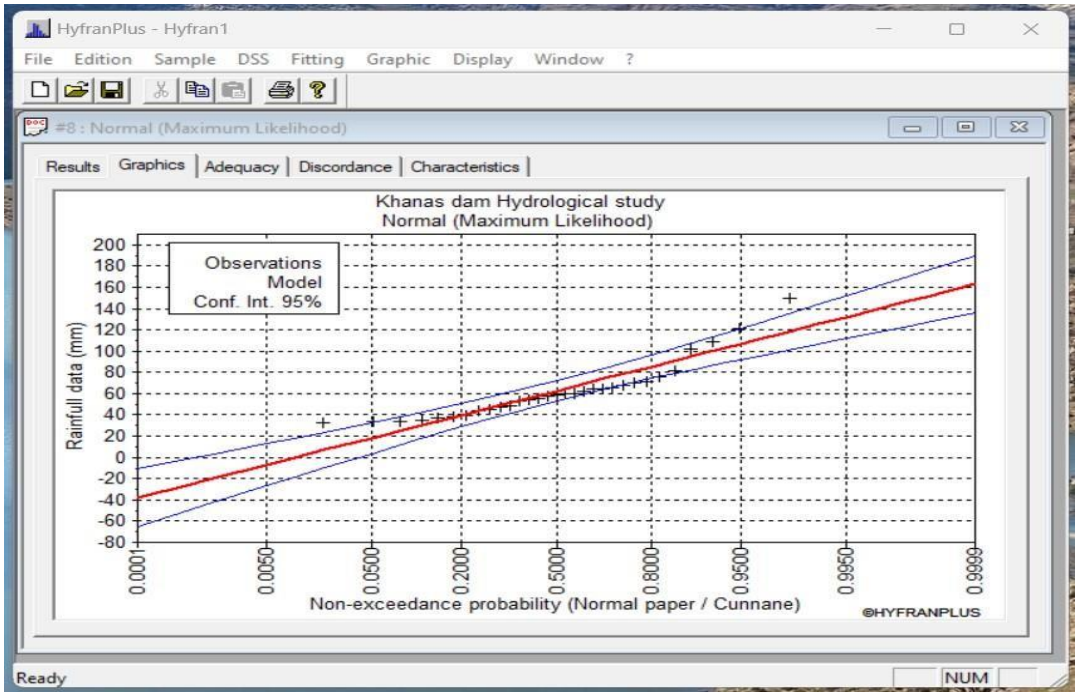

Figure 5.28: Results of Estimated Maximum 24 Hrs. Rainfall By Normal (Maximum Likelihood) Method (2)

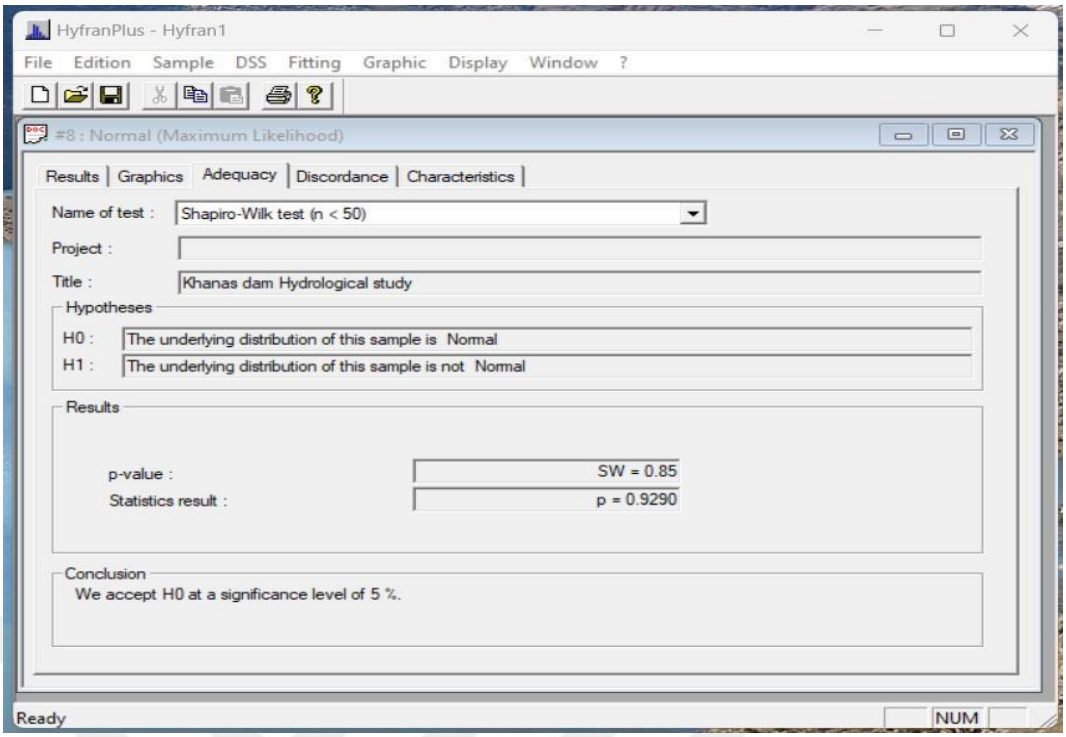

Figure 5.29: Results of Estimated Maximum 24 Hrs. Rainfall By Normal (Maximum Likelihood) Method (3)

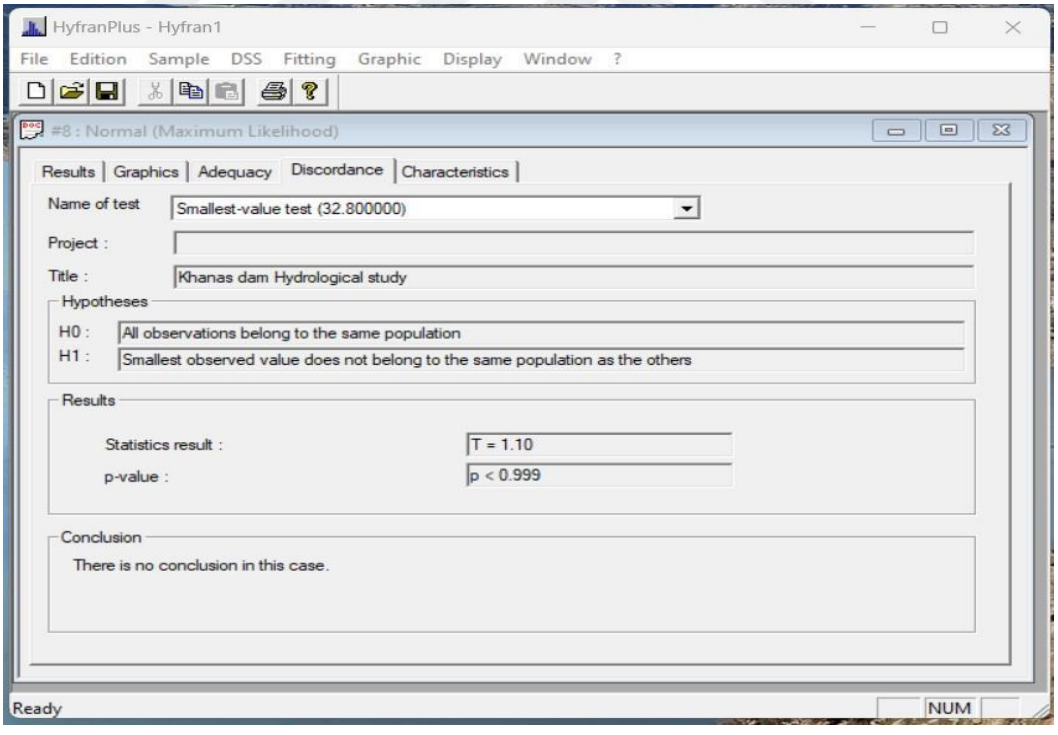

Figure 5.30: Results of Estimated Maximum 24 Hrs. Rainfall By Normal (Maximum Likelihood) Method (4)

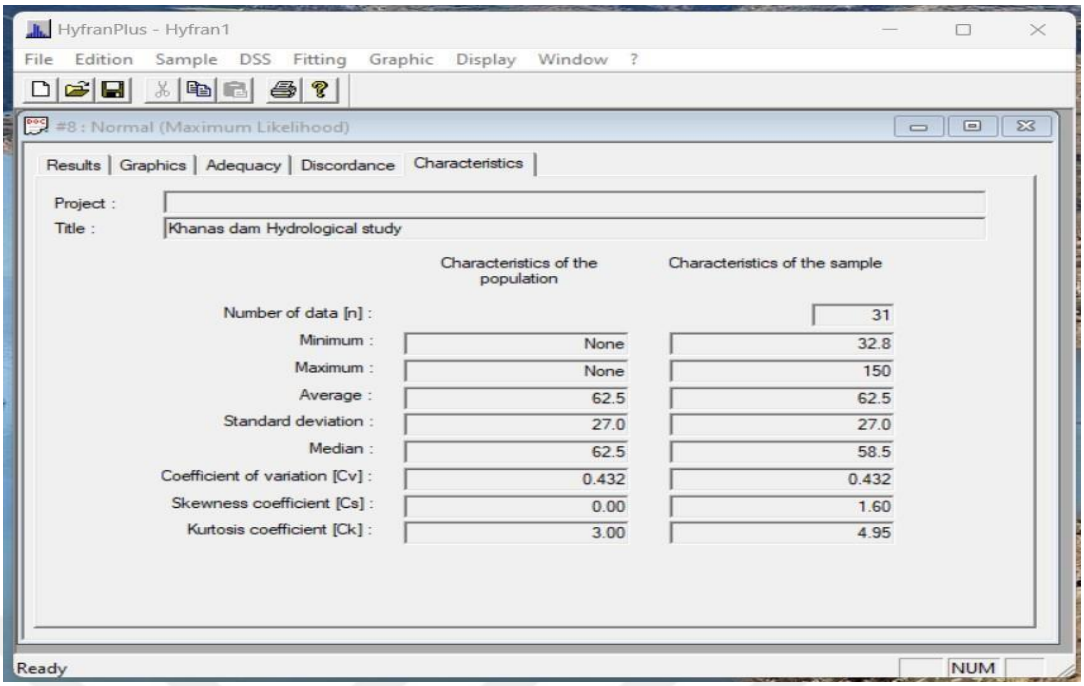

Figure 5.31: Results of Estimated Maximum 24 Hrs. Rainfall By Normal (Maximum Likelihood) Method (5)

8. Figures (5.32), (5.33), (5.34), (5.35) and (5.36) representing the results of estimated maximum 24 hrs. rainfall by Lognormal (Maximum Likelihood) method for many return periods, graphics, adequacy, and characteristics respectively by this method.

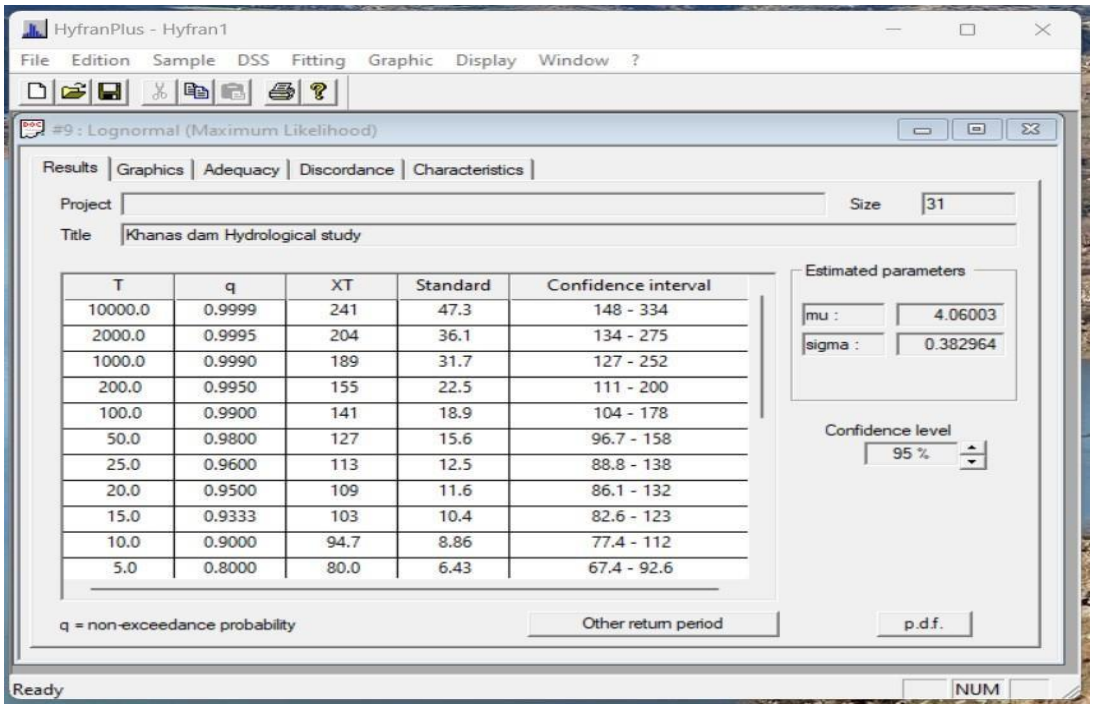

Figure 5.32: Results of Estimated Maximum 24 Hrs. Rainfall By Lognormal (Maximum Likelihood) Method (1)

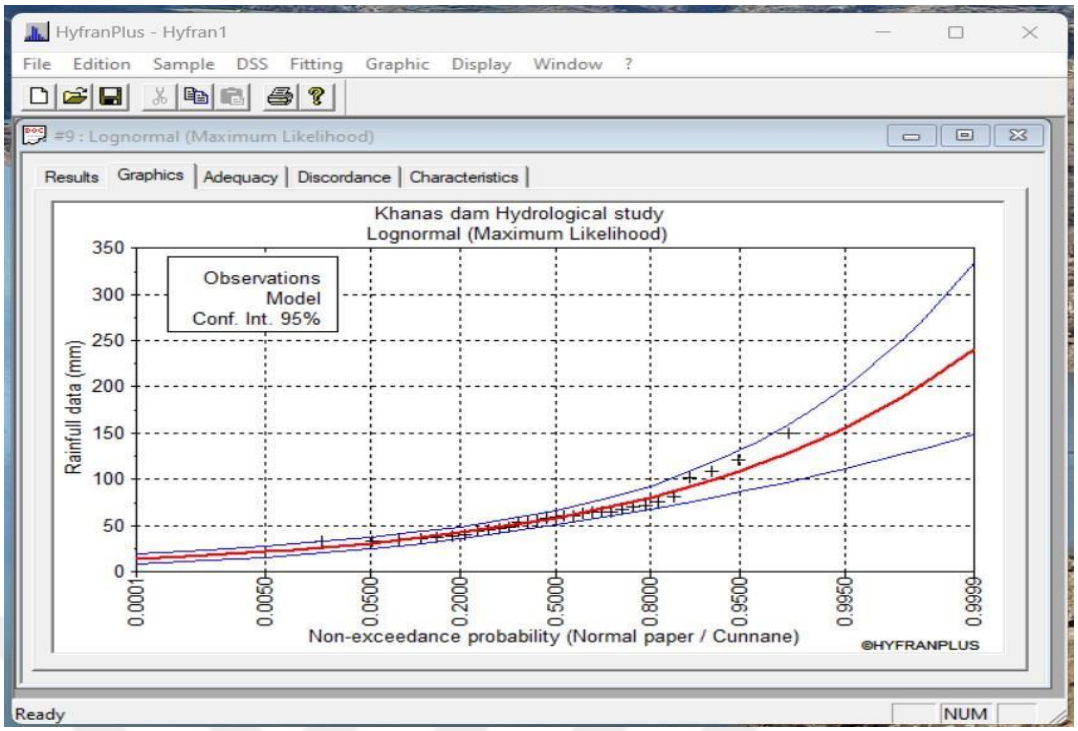

Figure 5.33: Results of Estimated Maximum 24 Hrs. Rainfall By Lognormal (Maximum Likelihood) Method (2)

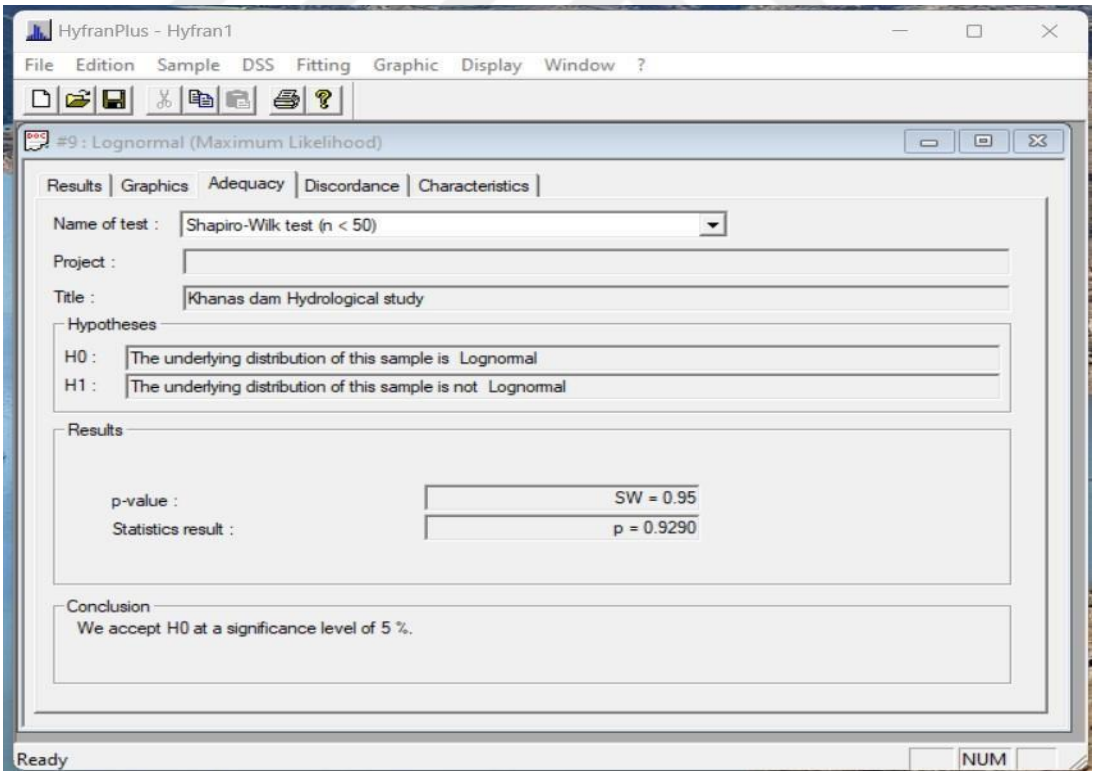

Figure 5.34: Results of Estimated Maximum 24 Hrs. Rainfall By Lognormal (Maximum Likelihood) Method (3)

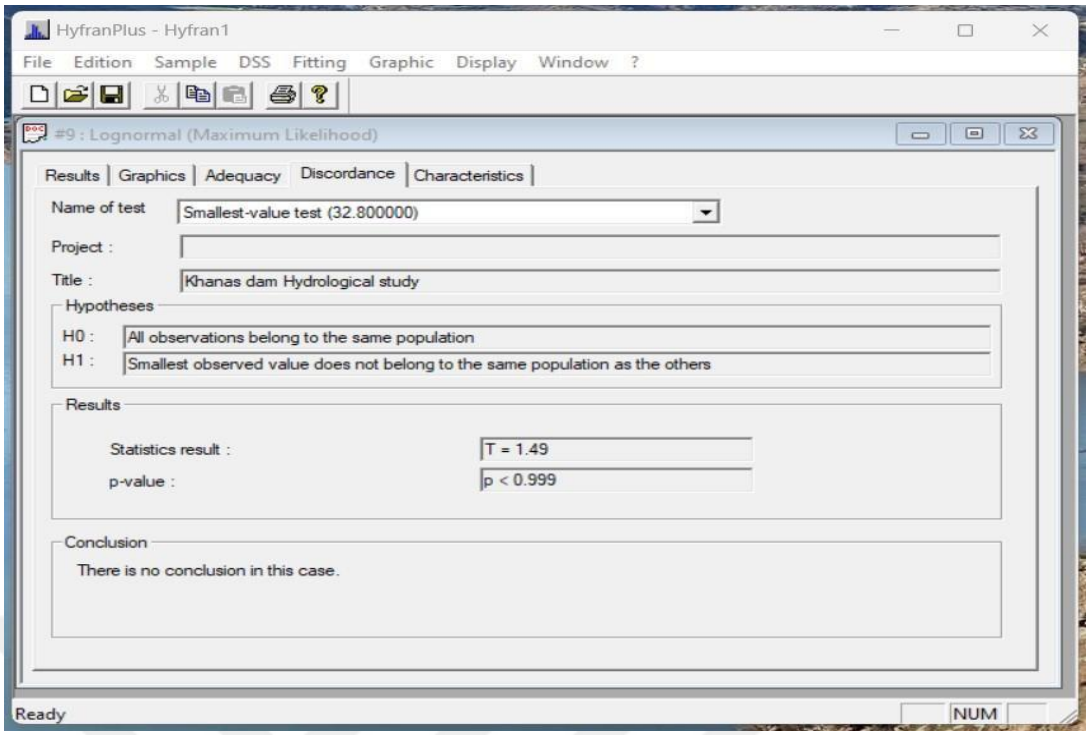

Figure 5.35: Results of Estimated Maximum 24 Hrs. Rainfall By Lognormal (Maximum Likelihood) Method (4)

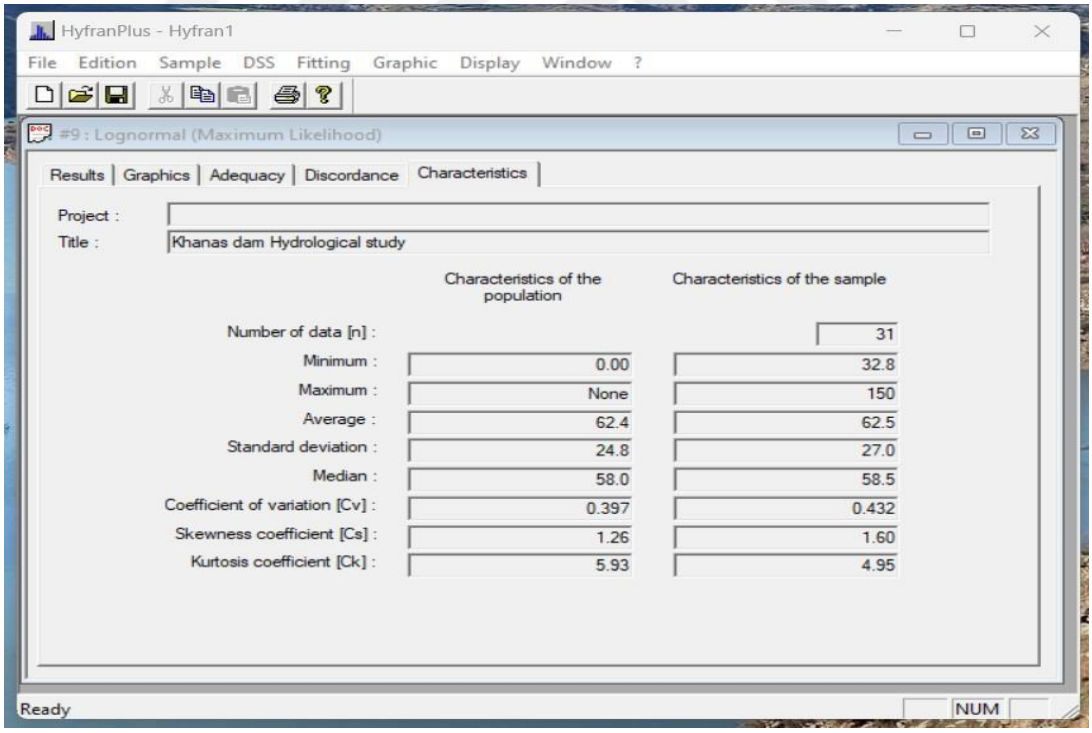

Figure 5. 36: Results of Estimated Maximum 24 Hrs. Rainfall By Lognormal (Maximum Likelihood) Method (5)

9. Figures (5.37), (5.38), (5.39), and (5.40) show the results of estimated maximum 24 hrs. rainfall by 3- parameter lognormal (Maximum Likelihood) method for many return periods, graphics, adequacy, and characteristics respectively by this method.

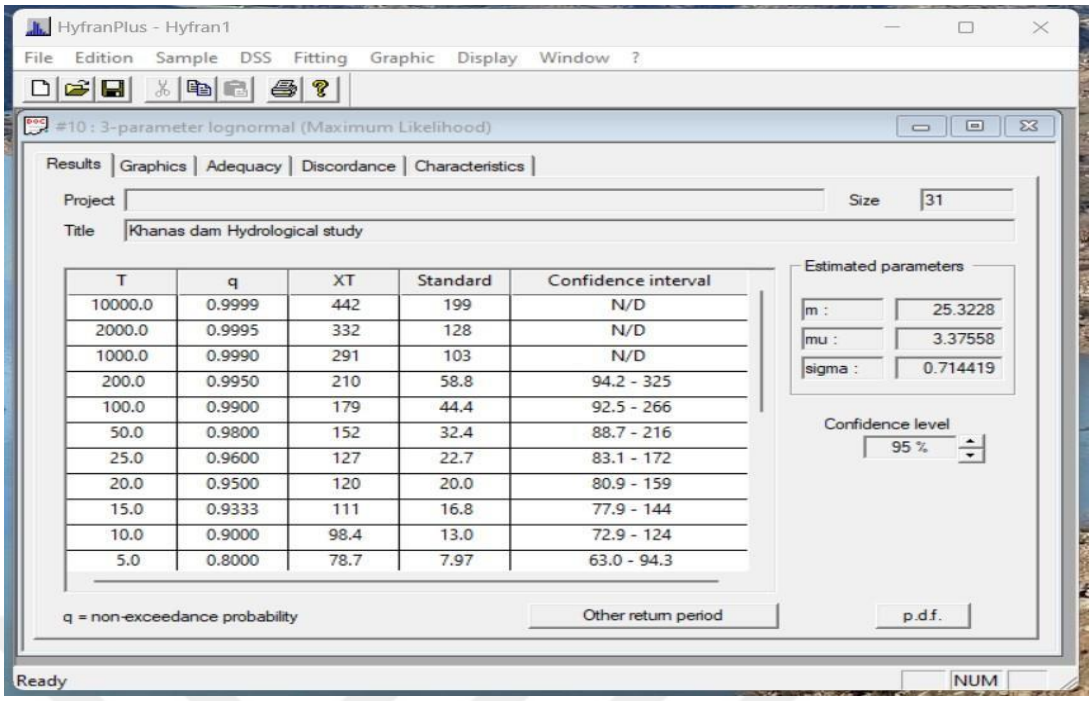

Figure 5.37: Results of Estimated Maximum 24 Hrs. Rainfall By 3- Parameter Lognormal (Maximum Likelihood) Method (1)

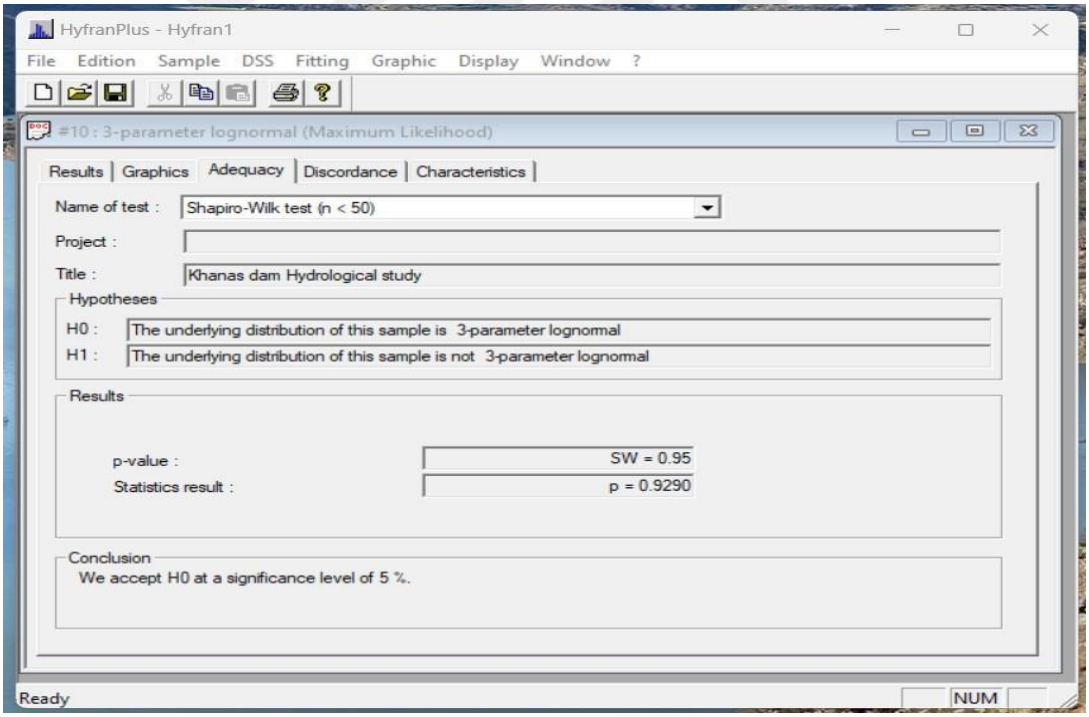

Figure 5.38: Results of Estimated Maximum 24 Hrs. Rainfall By 3- Parameter Lognormal (Maximum Likelihood) Method (2)

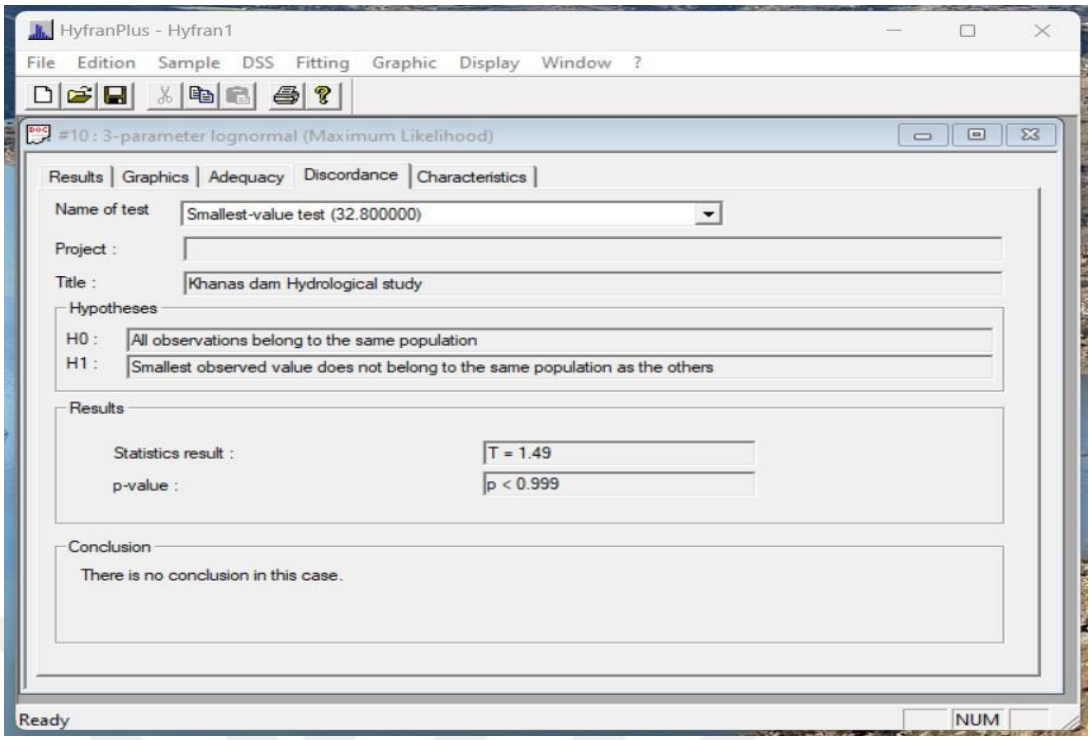

Figure 5.39: Results of Estimated Maximum 24 Hrs. Rainfall By 3- Parameter Lognormal (Maximum Likelihood) Method (3)

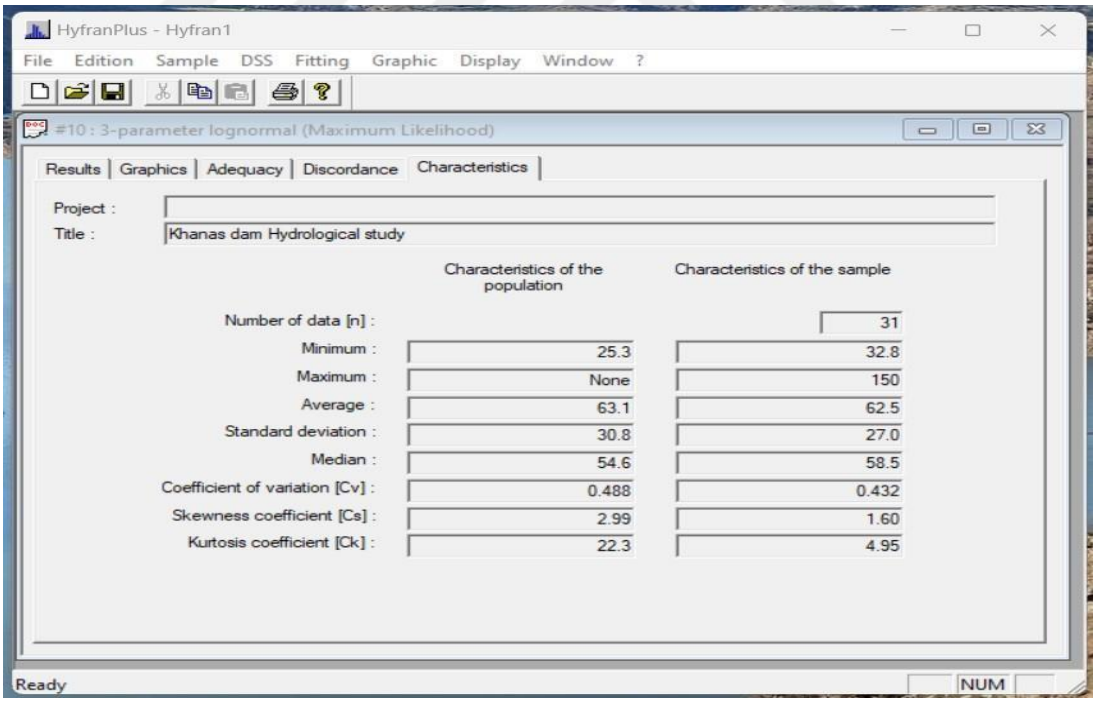

Figure 5.40: Results of Estimated Maximum 24 Hrs. Rainfall By 3- Parameter Lognormal (Maximum Likelihood) Method (4)

10. Figures (5.41), (5.42), (5.43), and (5.44) show the results of estimated maximum 24 hrs. rainfall by Gamma (Maximum Likelihood) method, for many return periods, graphics, adequacy, and characteristics, respectively by Gamma method.

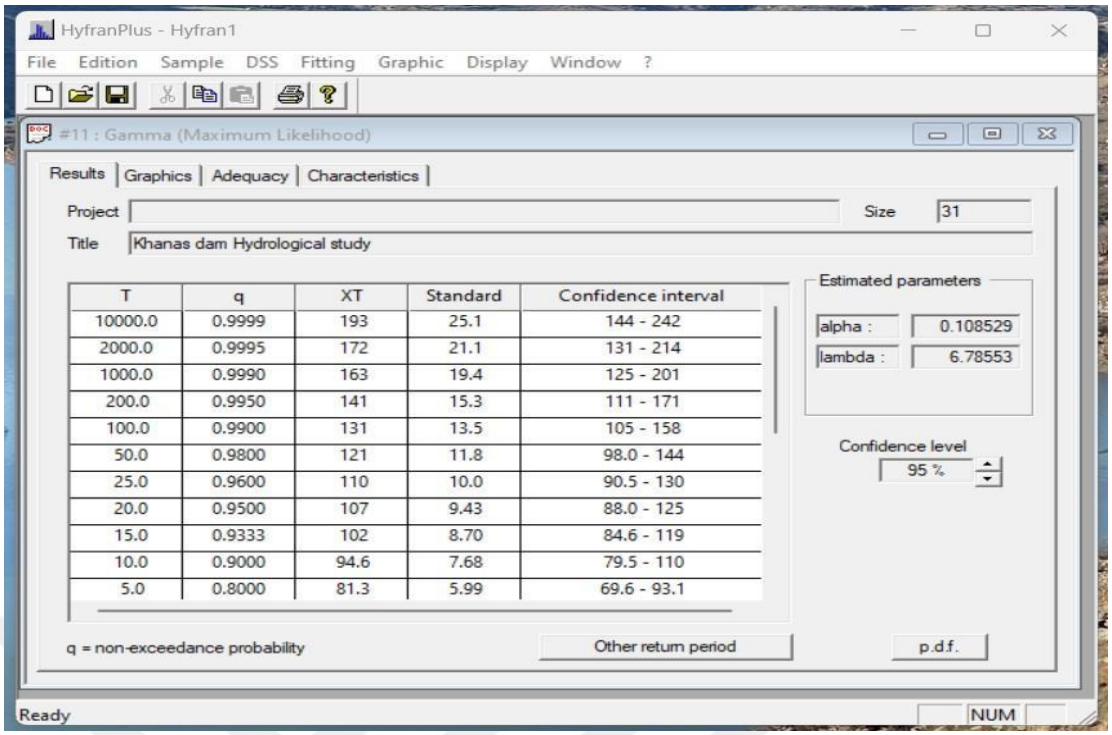

T	q	XT	Standard	Confidence interval
10000.0	0.9999	193	25.1	144 - 242
2000.0	0.9995	172	21.1	131 - 214
1000.0	0.9990	163	19.4	125 - 201
200.0	0.9950	141	15.3	111 - 171
100.0	0.9900	131	13.5	105 - 158
50.0	0.9800	121	11.8	98.0 - 144
25.0	0.9600	110	10.0	90.5 - 130
20.0	0.9500	107	9.43	88.0 - 125
15.0	0.9333	102	8.70	84.6 - 119
10.0	0.9000	94.6	7.68	79.5 - 110
5.0	0.8000	81.3	5.99	69.6 - 93.1

Figure 5.41: Results of Estimated Maximum 24 Hrs. Rainfall By Gamma (Maximum Likelihood) Method (1)

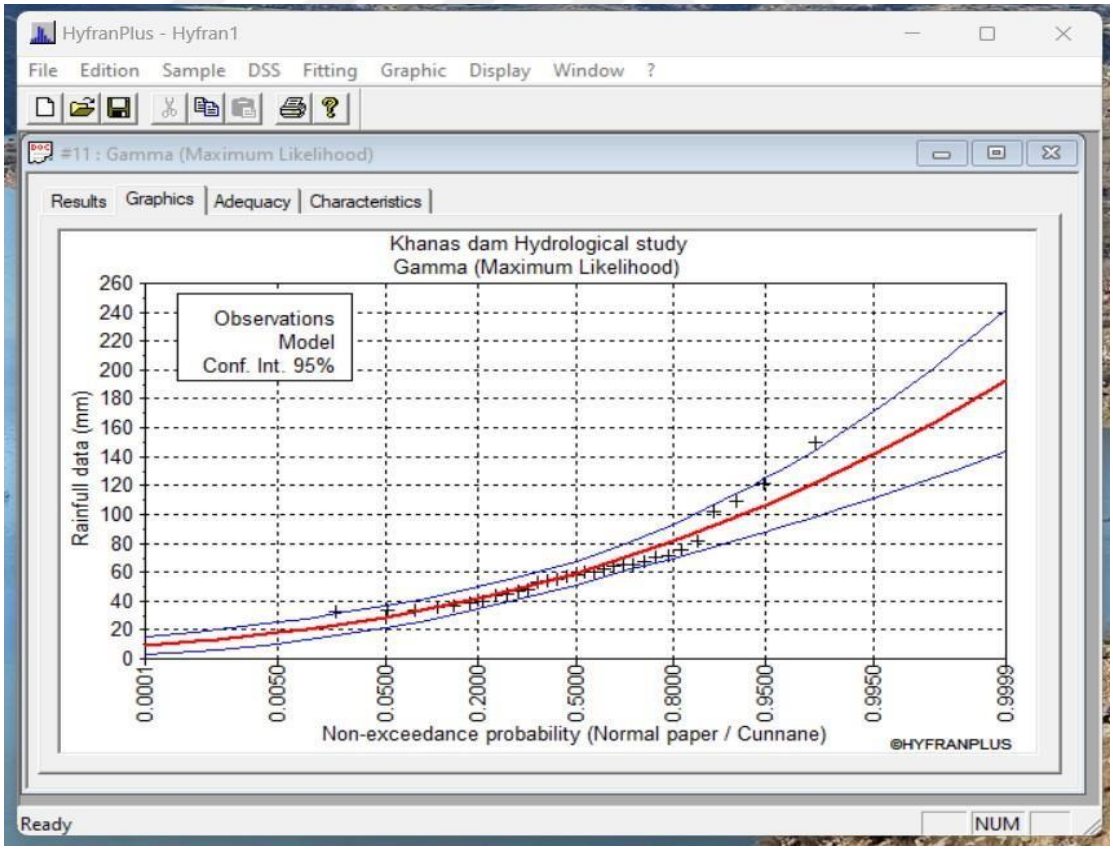

Figure 5.42: Results of Estimated Maximum 24 Hrs. Rainfall By Gamma (Maximum Likelihood) Method (2)

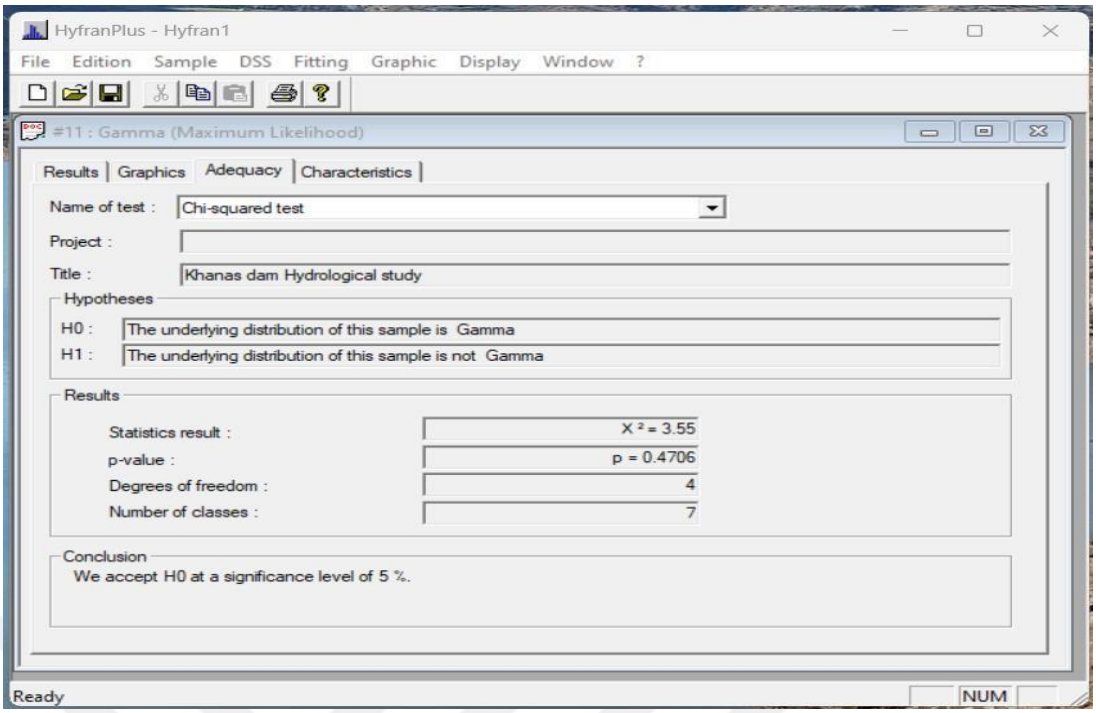

Figure 5.43: Results of Estimated Maximum 24 Hrs. Rainfall By Gamma (Maximum Likelihood) Method (3)

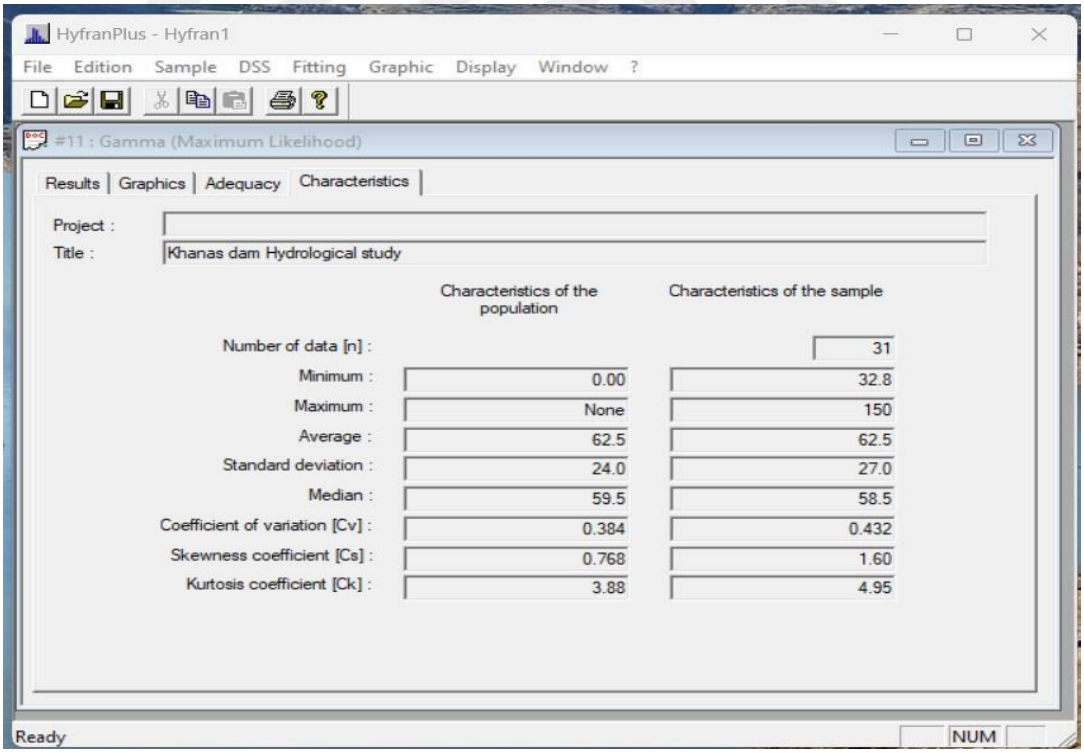

Figure 5.44: Results of Estimated Maximum 24 Hrs. Rainfall By Gamma (Maximum Likelihood) Method (4)

11. Figures (5.45), (5.46), (5.47), and (5.48) show the results of estimated maximum 24 hrs. rainfall by Invers Gamma (Maxmum Likelihood) method for many return periods, graphics, adequacy, and characteristics respectively by this method.

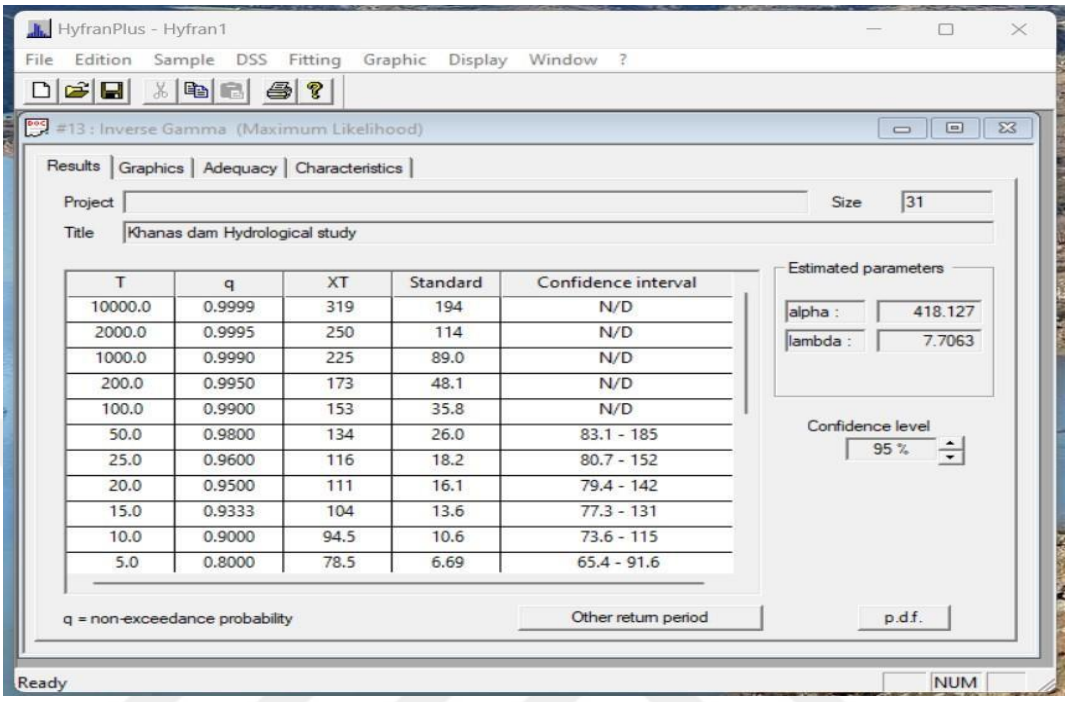

T	q	XT	Standard	Confidence interval
10000.0	0.9999	319	194	N/D
2000.0	0.9995	250	114	N/D
1000.0	0.9990	225	89.0	N/D
200.0	0.9950	173	48.1	N/D
100.0	0.9900	153	35.8	N/D
50.0	0.9800	134	26.0	83.1 - 185
25.0	0.9600	116	18.2	80.7 - 152
20.0	0.9500	111	16.1	79.4 - 142
15.0	0.9333	104	13.6	77.3 - 131
10.0	0.9000	94.5	10.6	73.6 - 115
5.0	0.8000	78.5	6.69	65.4 - 91.6

Figure 5.45: Results of Estimated Maximum 24 Hrs. Rainfall By Gamma (Maximum Likelihood) Method (1)

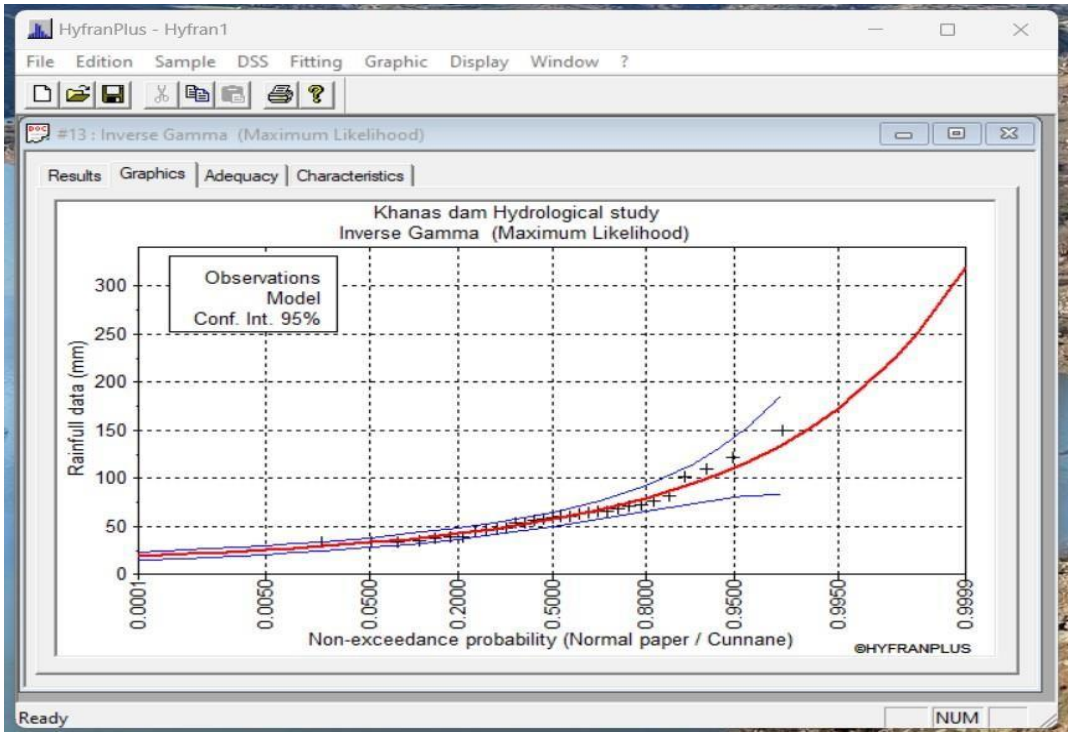

Figure 5.46: Results of Estimated Maximum 24 Hrs. Rainfall By Gamma (Maximum Likelihood) Method (2)

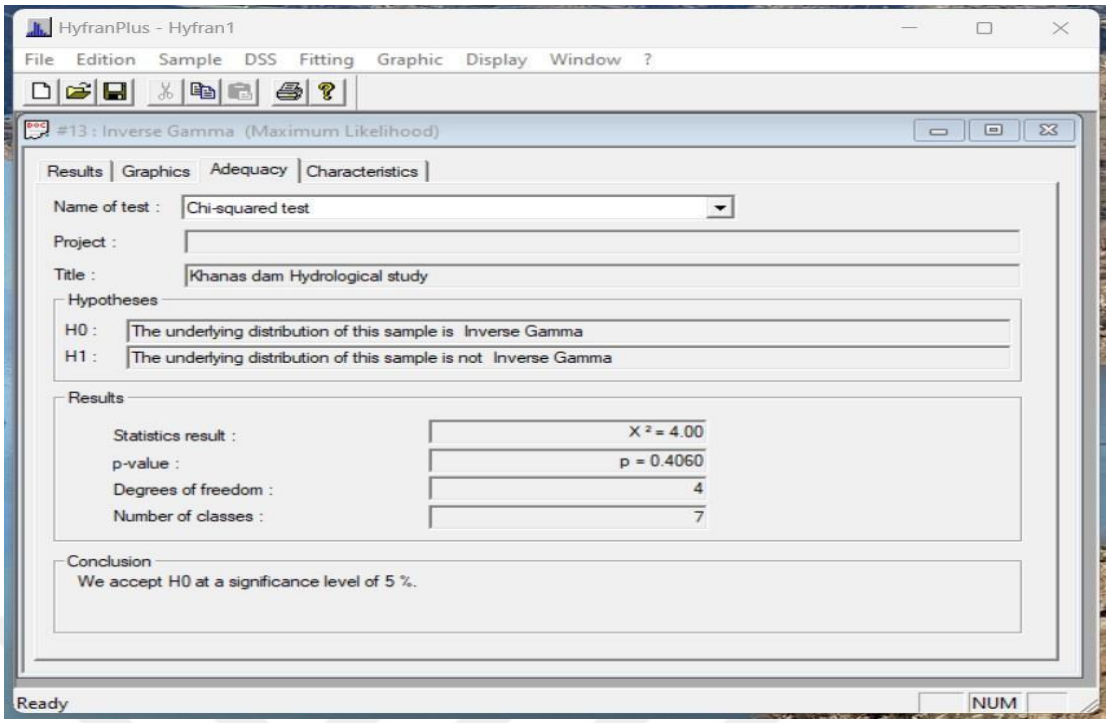

Figure 5.47: Results of Estimated Maximum 24 Hrs. Rainfall By Gamma (Maximum Likelihood) Method (3)

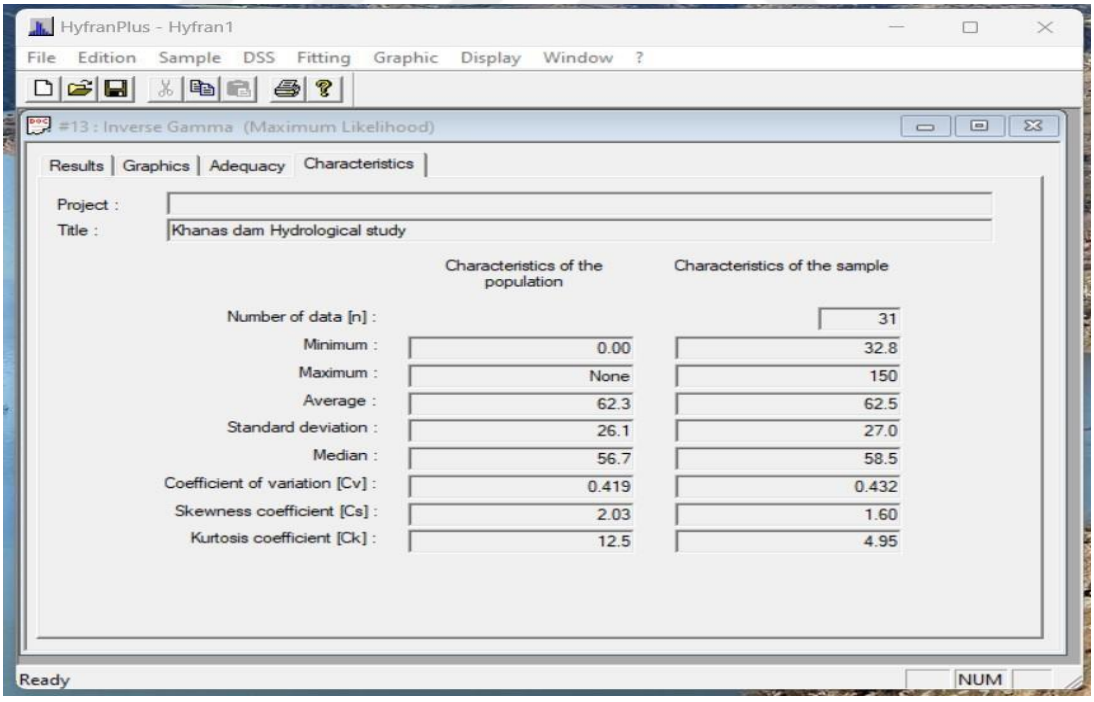

Figure 5.48: Results of Estimated Maximum 24 Hrs. Rainfall By Gamma (Maximum Likelihood) Method (4)

12. Figures (5.49), (5.50), (5.51), and (5.52) show the results of estimated maximum 24 hrs. rainfall by Log – Pearson type 3 (Maximum Likelihood) method for many return periods, graphics, adequacy, and characteristics respectively by this method.

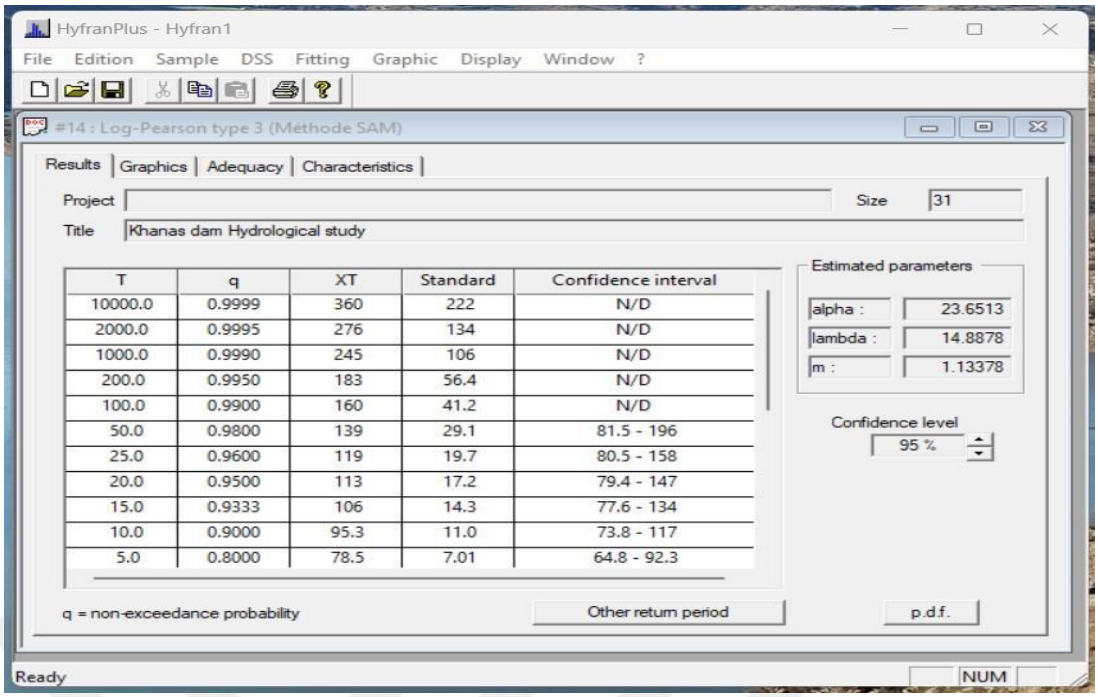

T	q	XT	Standard	Confidence interval
10000.0	0.9999	360	222	N/D
2000.0	0.9995	276	134	N/D
1000.0	0.9990	245	106	N/D
200.0	0.9950	183	56.4	N/D
100.0	0.9900	160	41.2	N/D
50.0	0.9800	139	29.1	81.5 - 196
25.0	0.9600	119	19.7	80.5 - 158
20.0	0.9500	113	17.2	79.4 - 147
15.0	0.9333	106	14.3	77.6 - 134
10.0	0.9000	95.3	11.0	73.8 - 117
5.0	0.8000	78.5	7.01	64.8 - 92.3

Figure 5.49: Results of Estimated Maximum 24 Hrs. Rainfall By Log – Pearson Type 3 (Maximum Likelihood) Method (1)

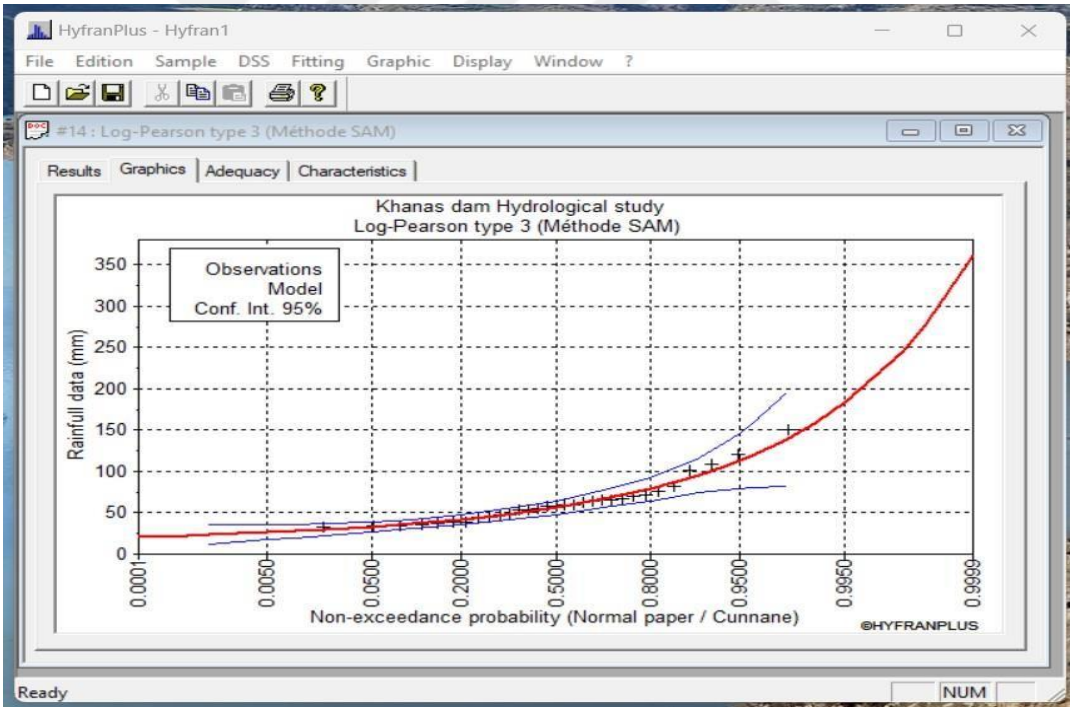

Figure 5.50: Results of Estimated Maximum 24 Hrs. Rainfall By Log – Pearson Type 3 (Maximum Likelihood) Method (2)

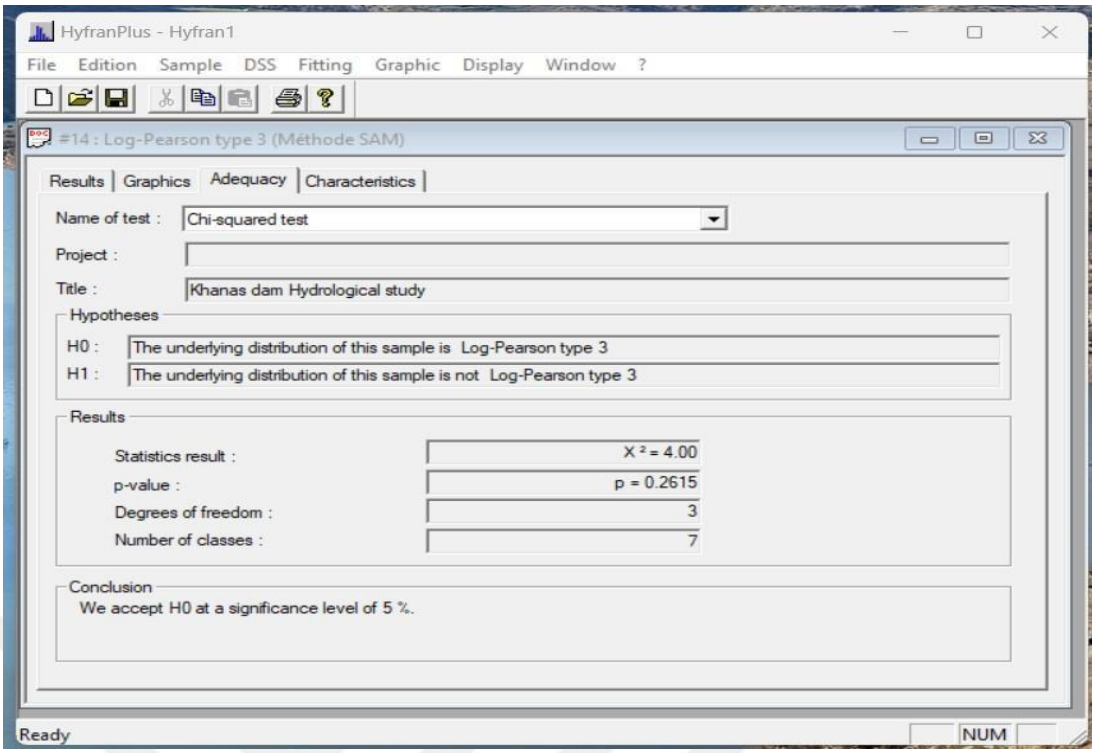

Figure 5.51: Results of Estimated Maximum 24 Hrs. Rainfall By Log – Pearson Type 3 (Maximum Likelihood) Method (3)

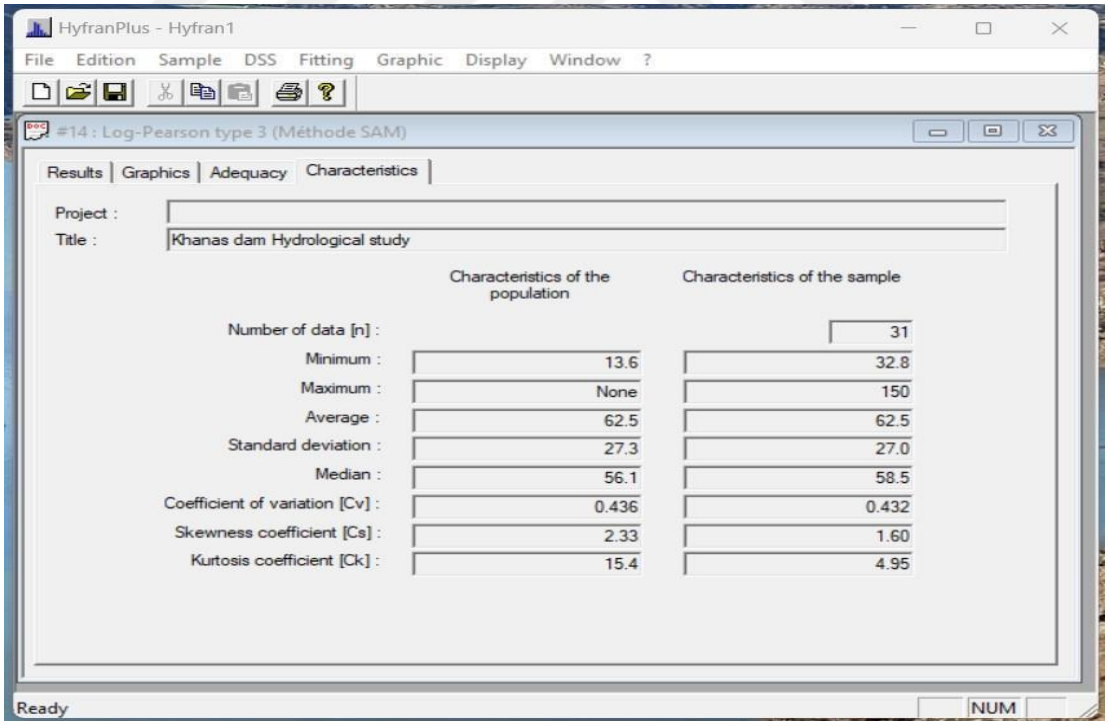

Figure 5.52: Results of Estimated Maximum 24 Hrs. Rainfall By Log – Pearson Type 3 (Maximum Likelihood) Method (4)

5.3 Comparison between Methods

1. Figures (5.53) and (5.54) explain BIC and AIC between Exponential (maximum Likelihood) and Gumbel (Maximum Likelihood), and Gumbel (maximum of moments) and the best one is Exponential (maximum Likelihood) because they have the lower values of BIC and AIC, and the maximum estimated 24 hrs. rainfall is (265.26) mm for the (2000) years return Periods.

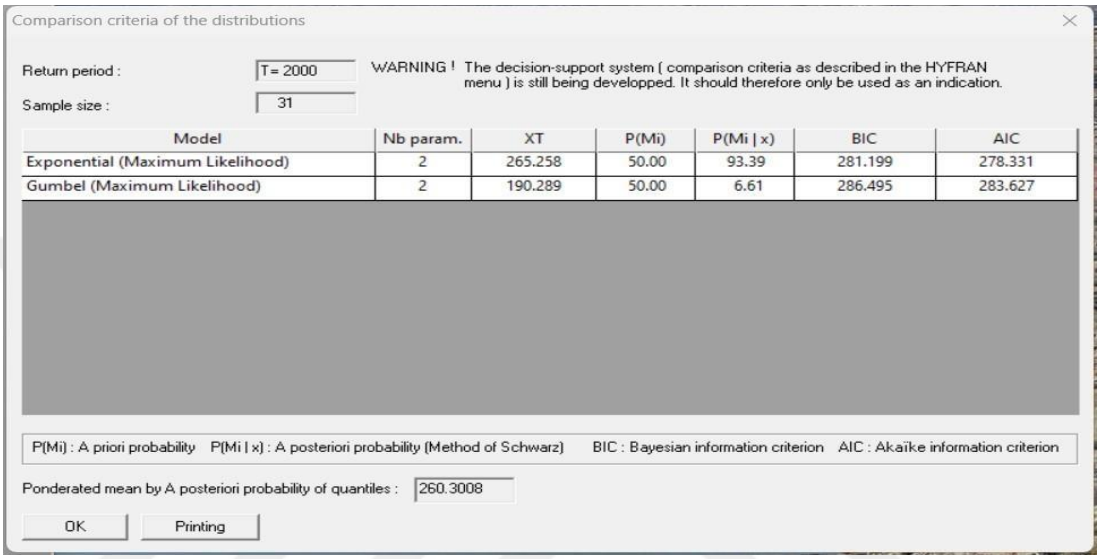

Figure 5.53: BIC and AIC Between Exponential (Maximum Likelihood) and Gumbel (Maximum Likelihood), and Gumbel (Maximum of Moments) and the Best One Is Exponential (Maximum Likelihood) (1)

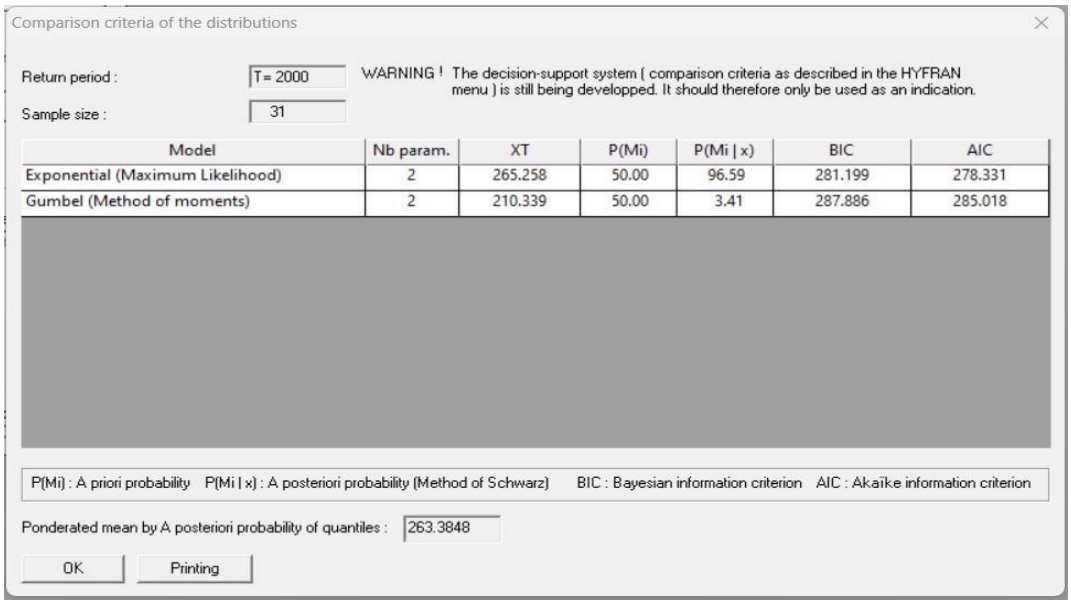

Figure 5.54: BIC and AIC Between Exponential (Maximum Likelihood) and Gumbel (Maximum Likelihood), and Gumbel (Maximum of Moments) and the Best One Is Exponential (Maximum Likelihood) (2)

2. Figure (5. 55) to Figure (5.84) represent a comparison of BIC and AIC between all other methods and also showing the Exponential (maximum Likelihood) is the best method results showing lower values of BIC and AIC and the maximum estimated 24 hrs. rainfall as shown below:

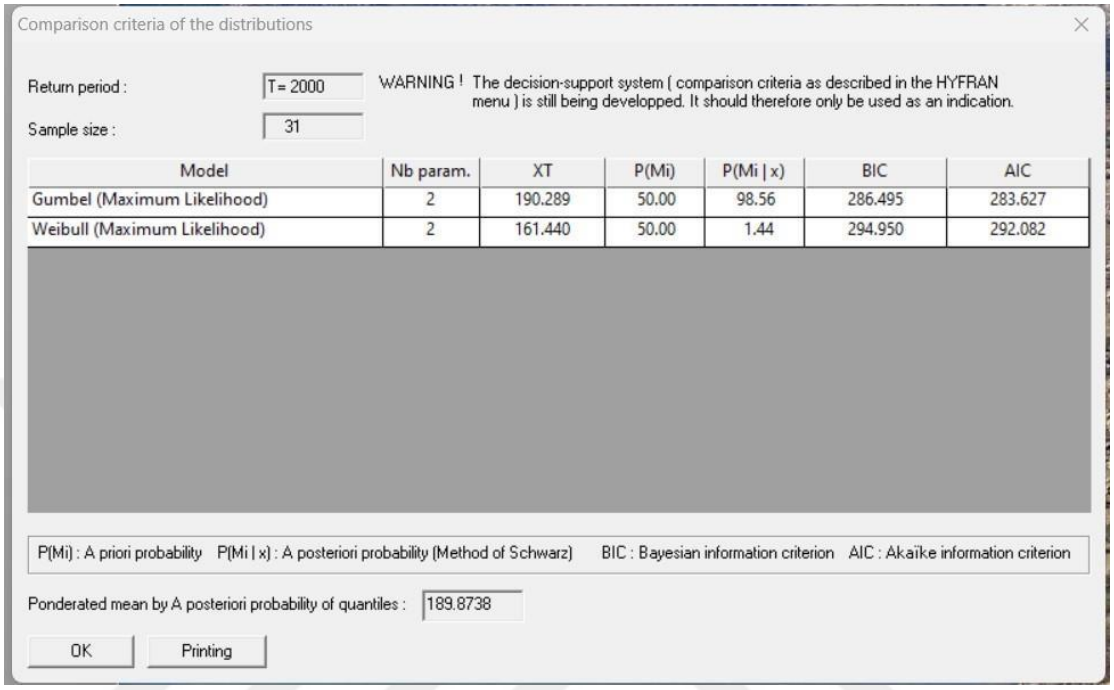

Figure 5.55: BIC and AIC, and the Maximum Estimated 24 Hrs. Rainfall (1)

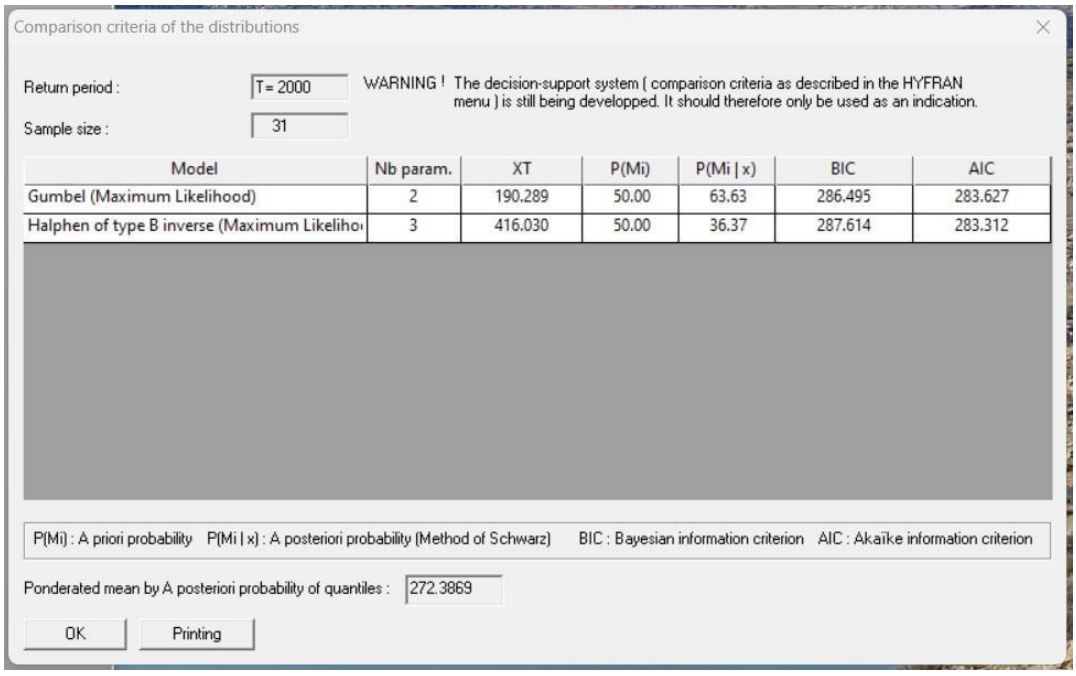

Figure 5.56: BIC and AIC, and the Maximum Estimated 24 Hrs. Rainfall (2)

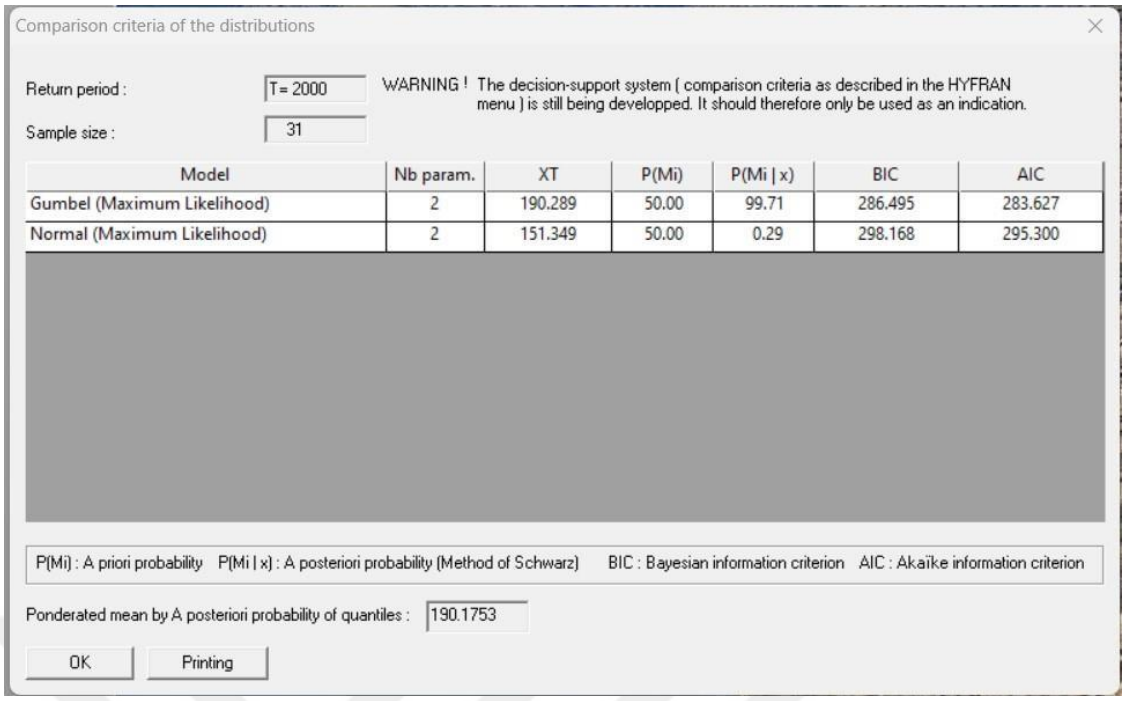

Figure 5.57: BIC and AIC, and the Maximum Estimated 24 Hrs. Rainfall(2)

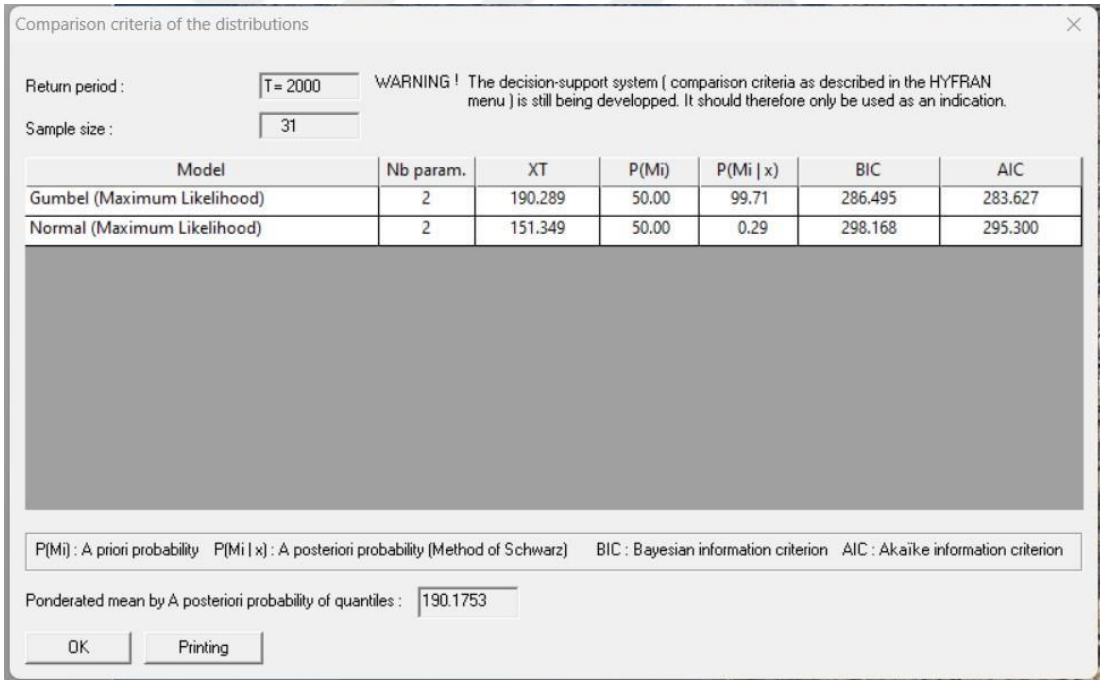

Figure 5.58: BIC and AIC, and the Maximum Estimated 24 Hrs. Rainfall (3)

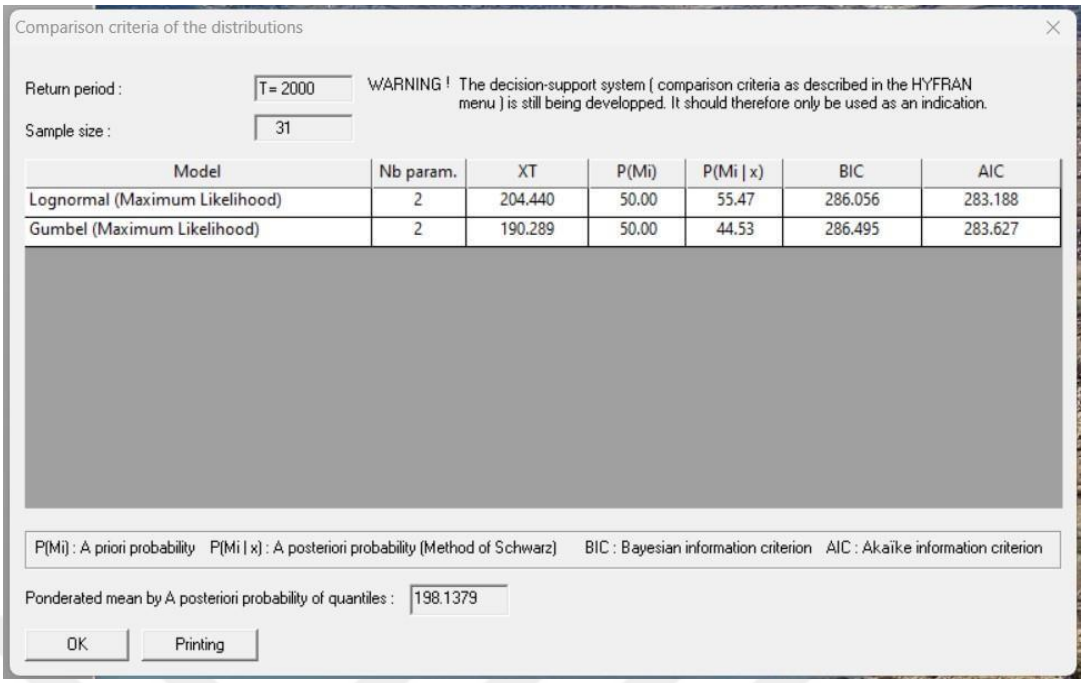

Figure 5.59: BIC and AIC, and the Maximum Estimated 24 Hrs. Rainfall (3)

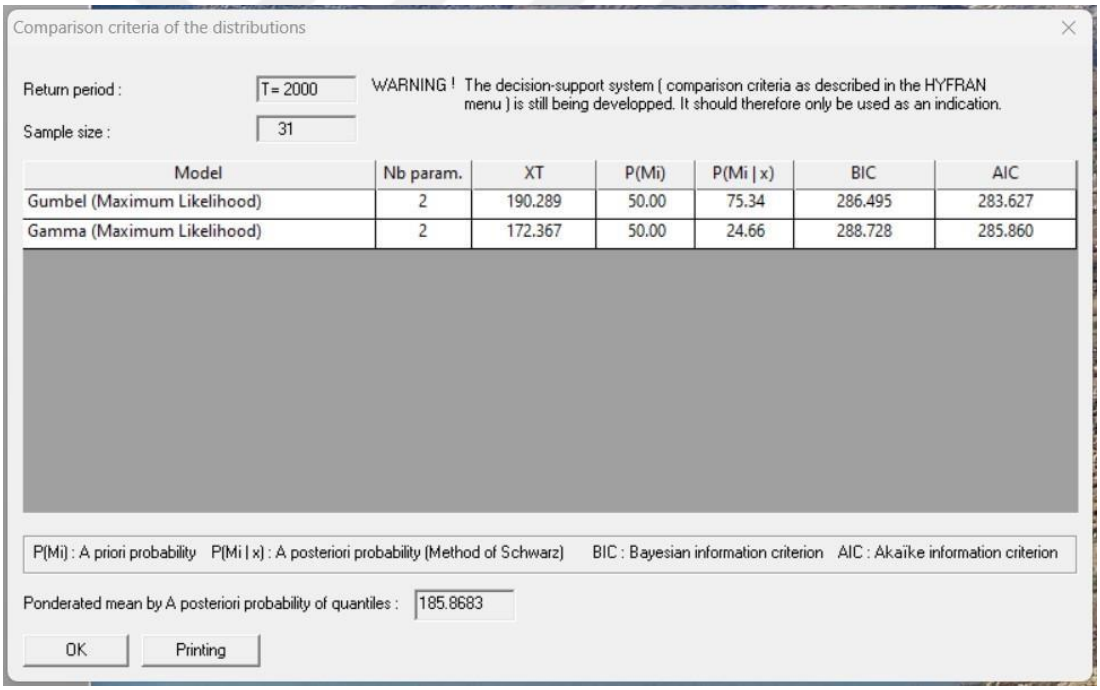

Figure 5.60: BIC and AIC, and the Maximum Estimated 24 Hrs. Rainfall (4)

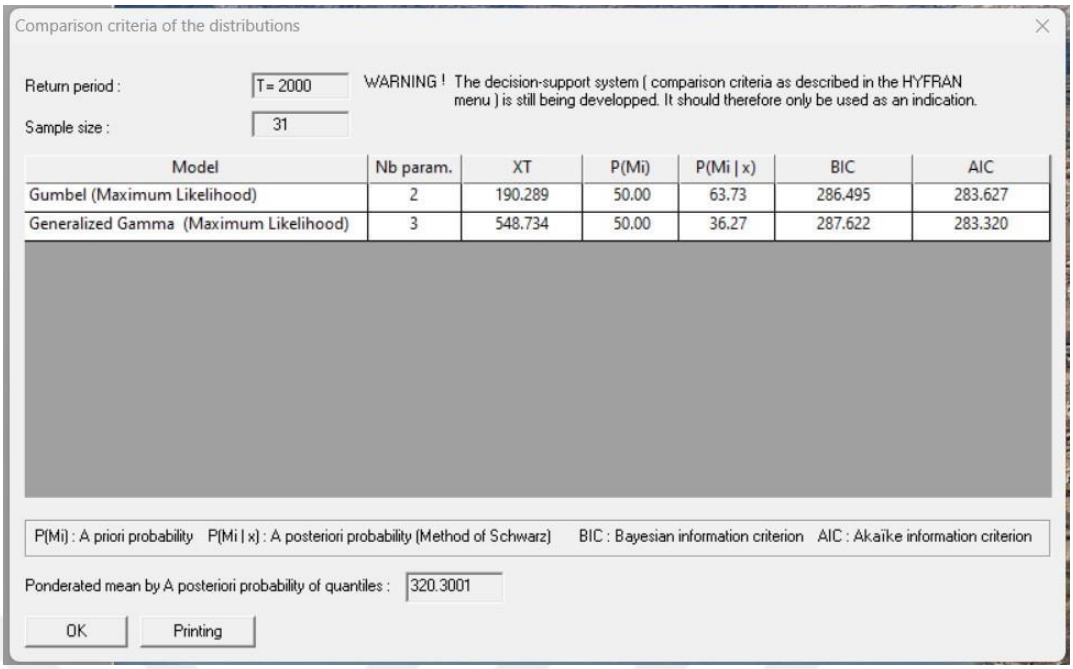

Figure 5.61: BIC and AIC, and the Maximum Estimated 24 Hrs. Rainfall (5)

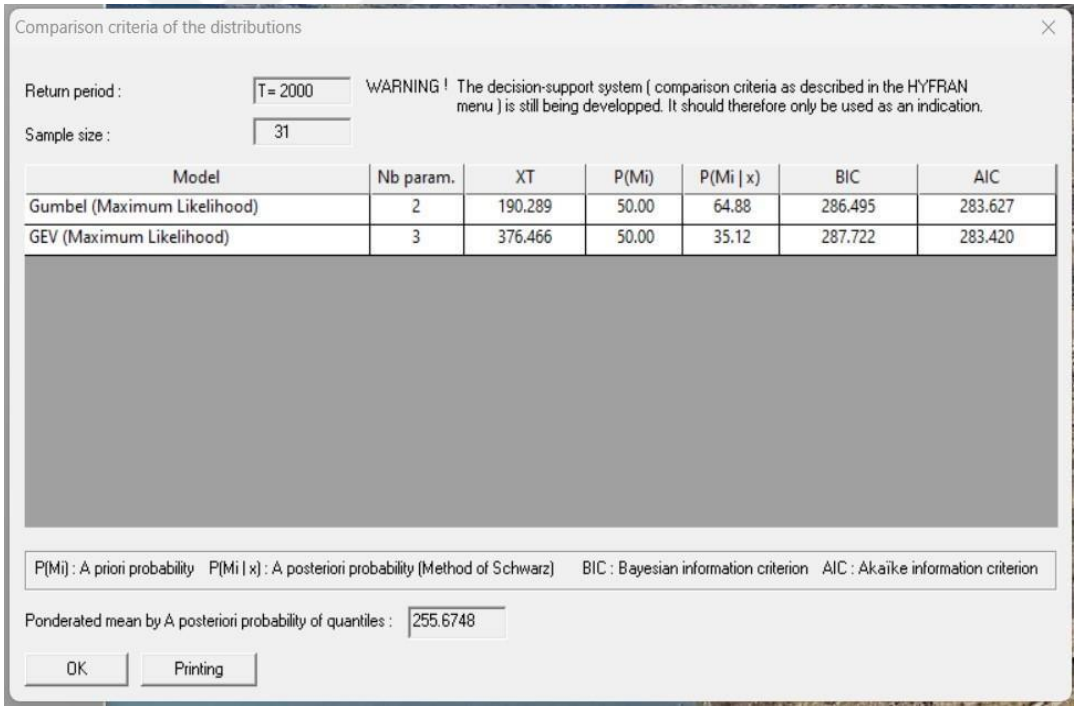

Figure 5.62: BIC and AIC, and the Maximum Estimated 24 Hrs. Rainfall (6)

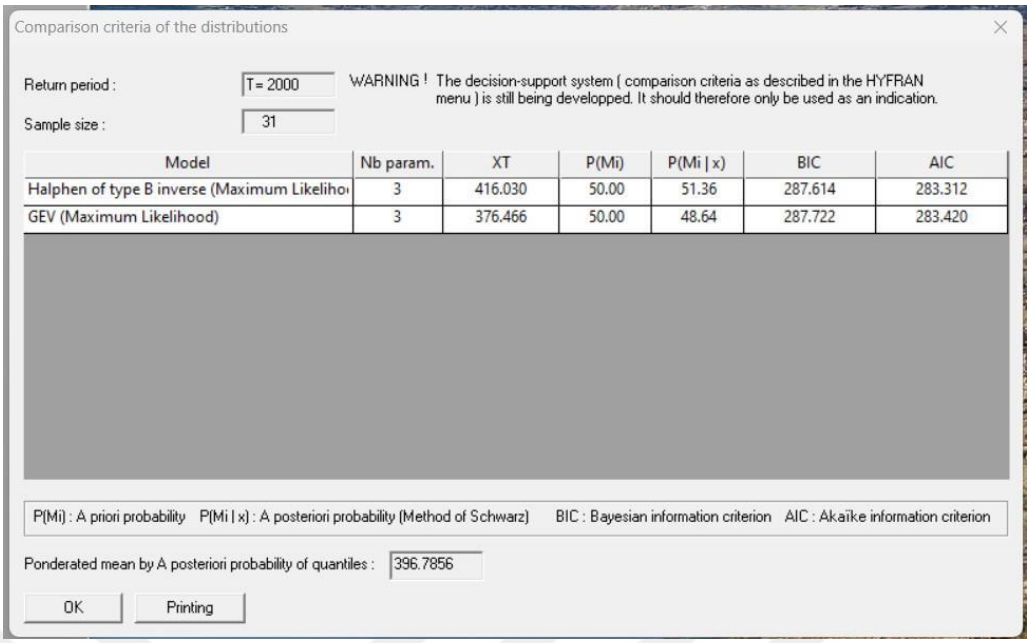

Figure 5.63: BIC and AIC, and the Maximum Estimated 24 Hrs. Rainfall (7)

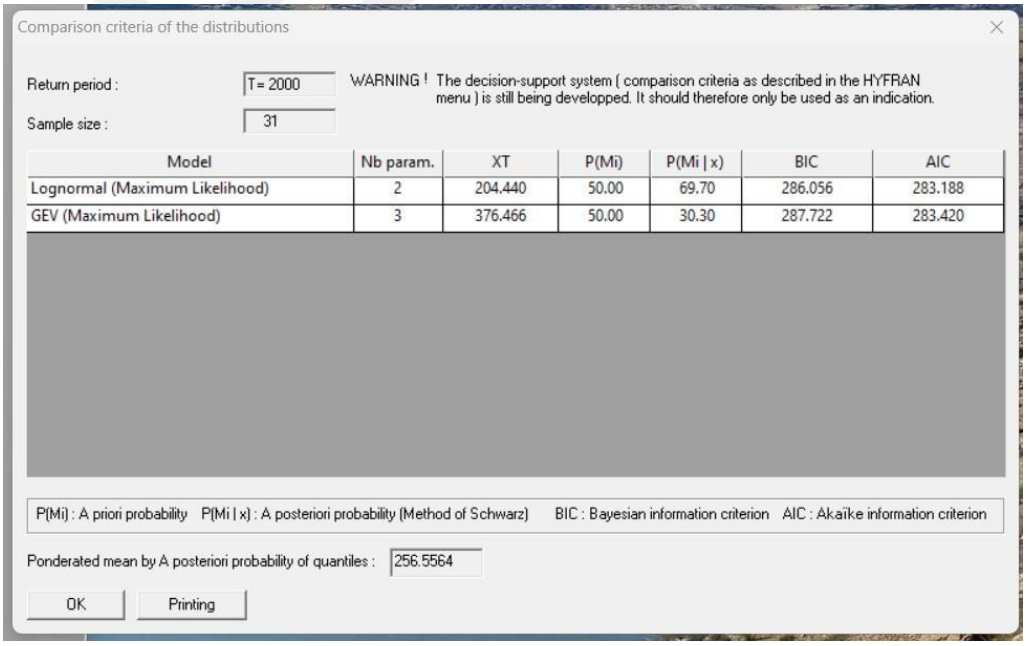

Figure 5.64: BIC and AIC, and the Maximum Estimated 24 Hrs. Rainfall (8)

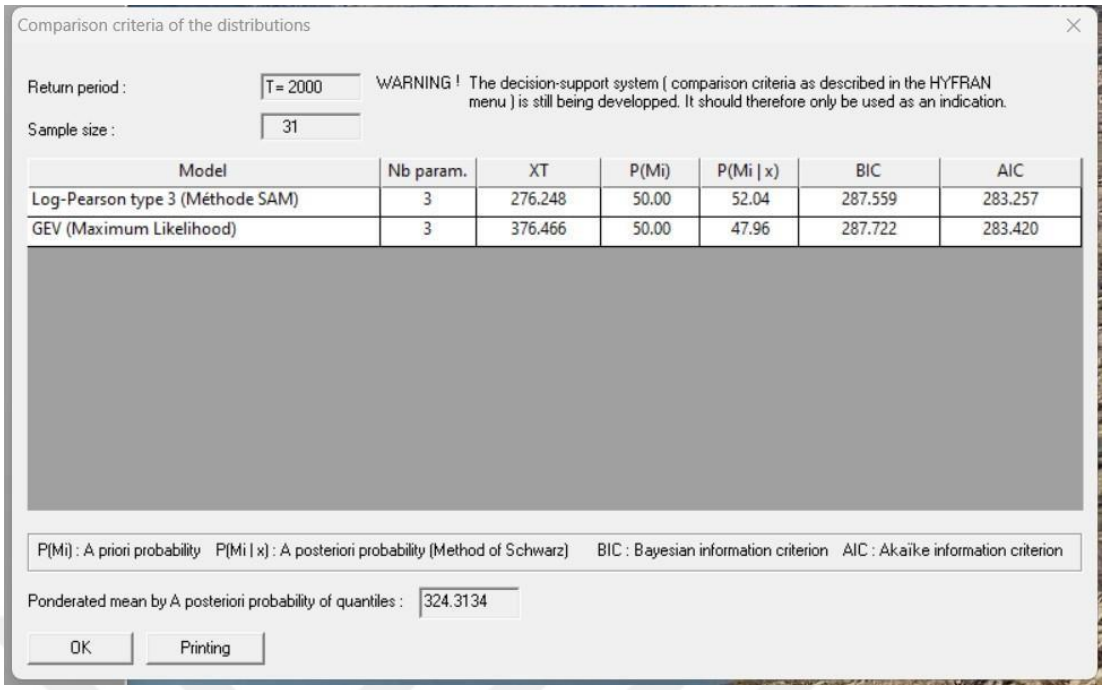

Figure 5.65: BIC and AIC, and the Maximum Estimated 24 Hrs. Rainfall (9)

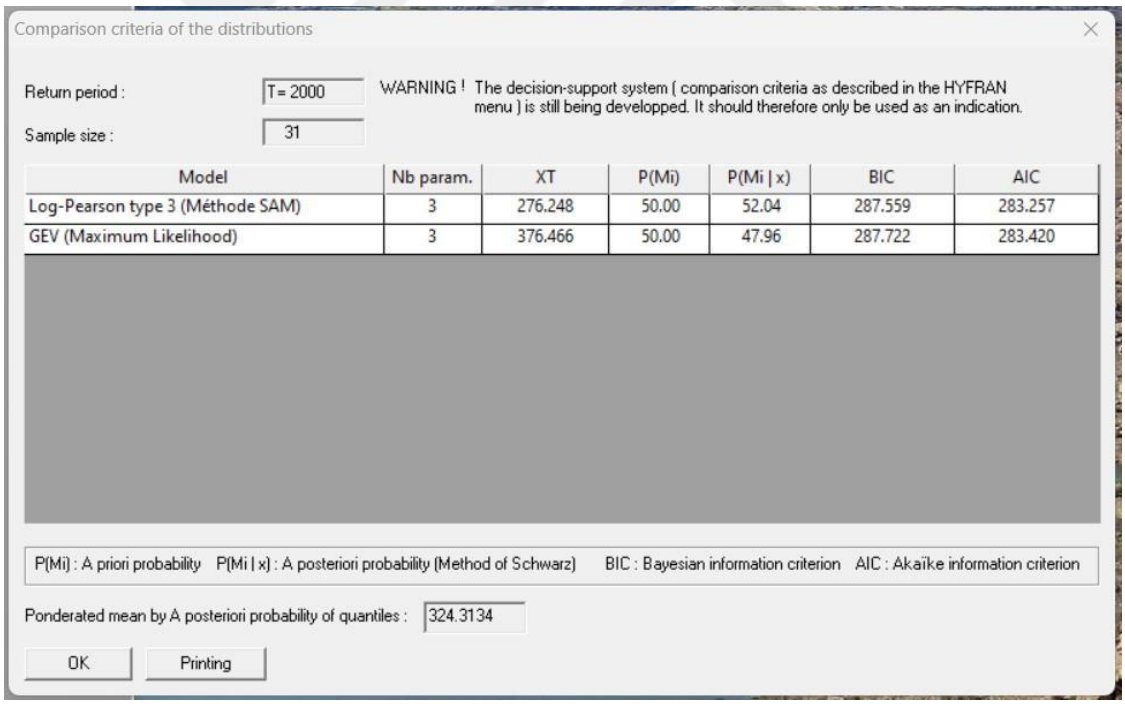

Figure 5.66: BIC and AIC, and the Maximum Estimated 24 Hrs. Rainfall (10)

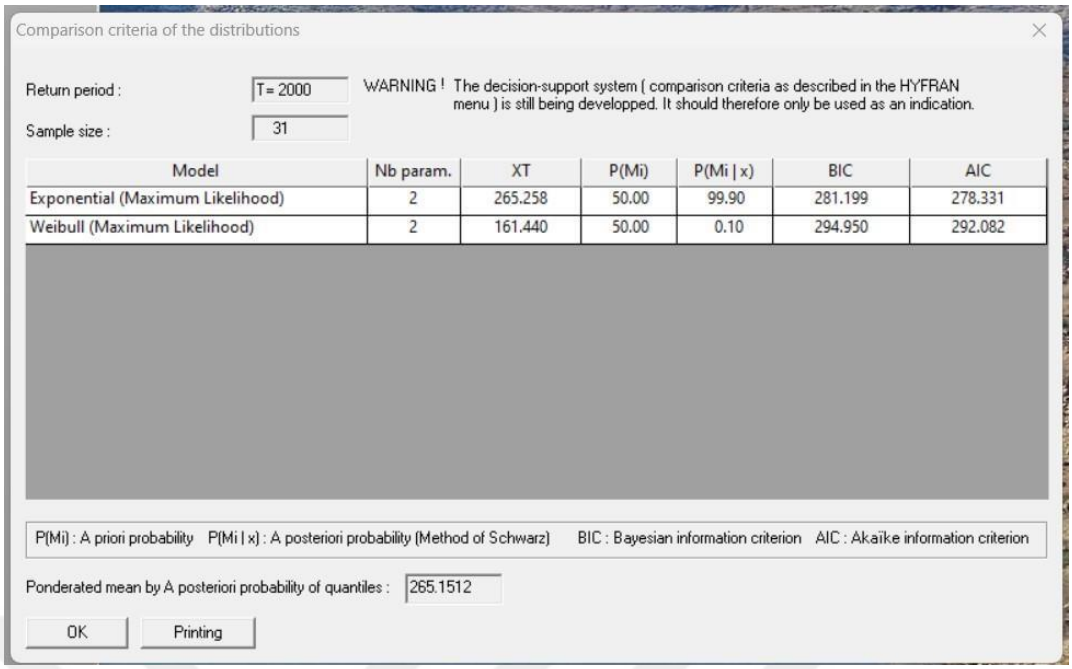

Figure 5.67: BIC and AIC, and the Maximum Estimated 24 Hrs. Rainfall (11)

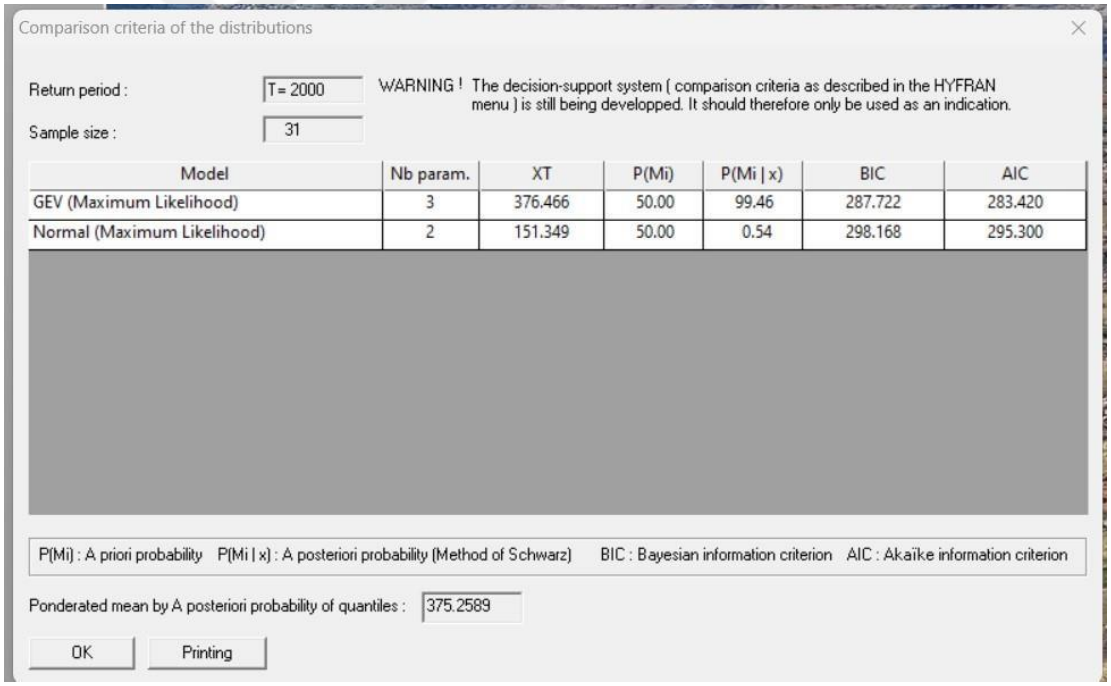

Figure 5.68: BIC and AIC, and the Maximum Estimated 24 Hrs. Rainfall (12)

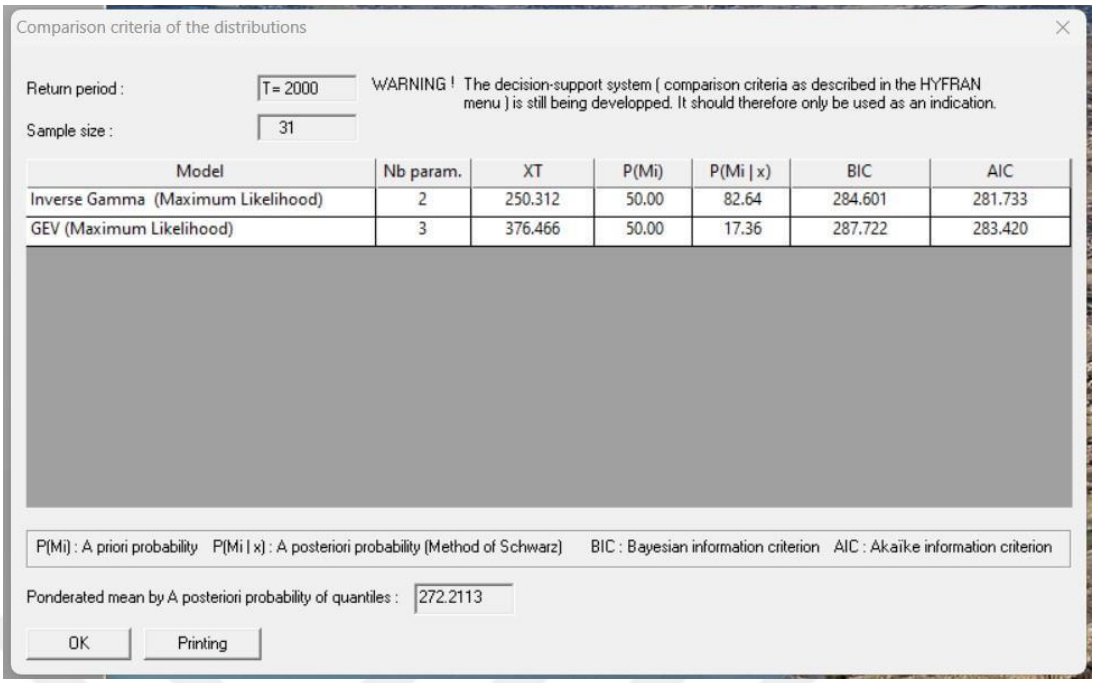

Figure 5.69: BIC and AIC, and the Maximum Estimated 24 Hrs. Rainfall (13)

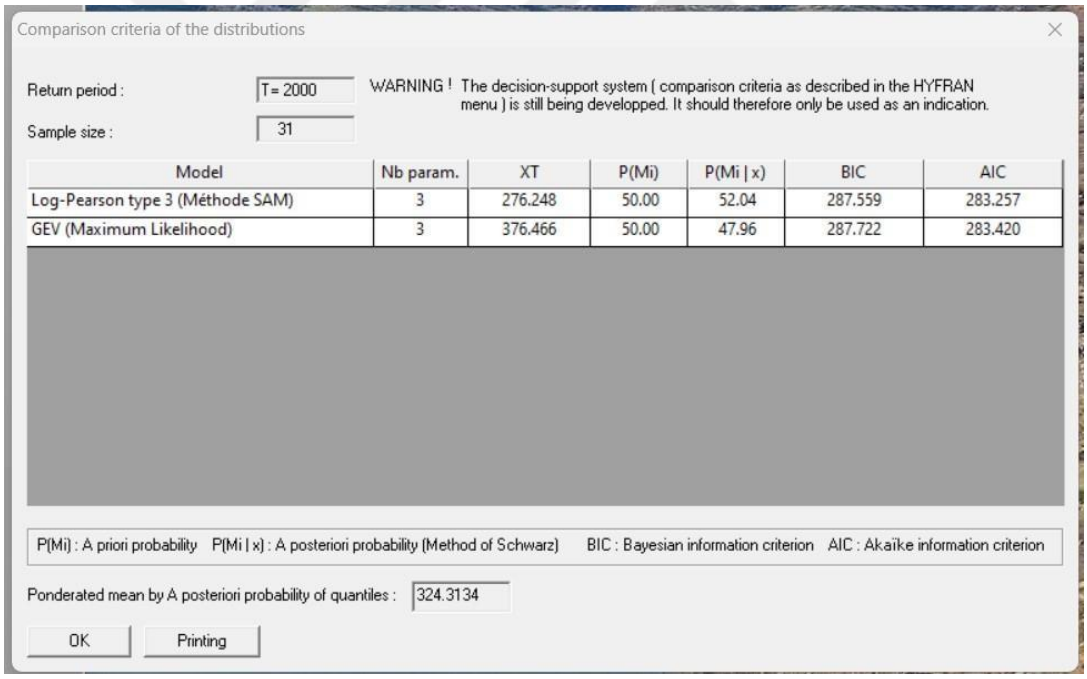

Figure 5.70: BIC and AIC, and the Maximum Estimated 24 Hrs. Rainfall (14)

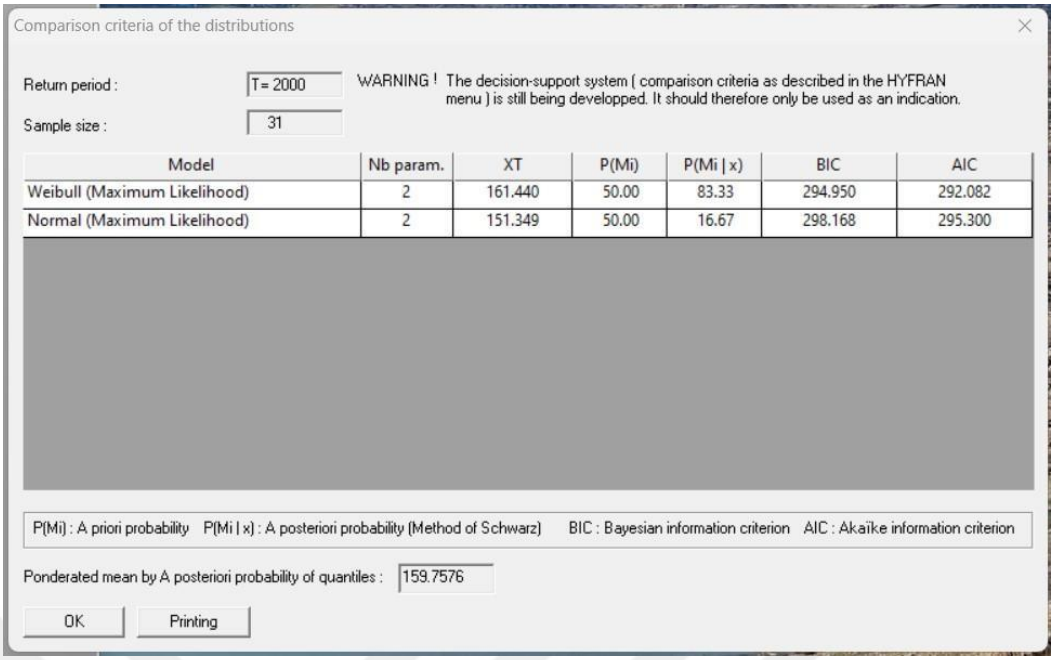

Figure 5.71: BIC and AIC, and the Maximum Estimated 24 Hrs. Rainfall (15)

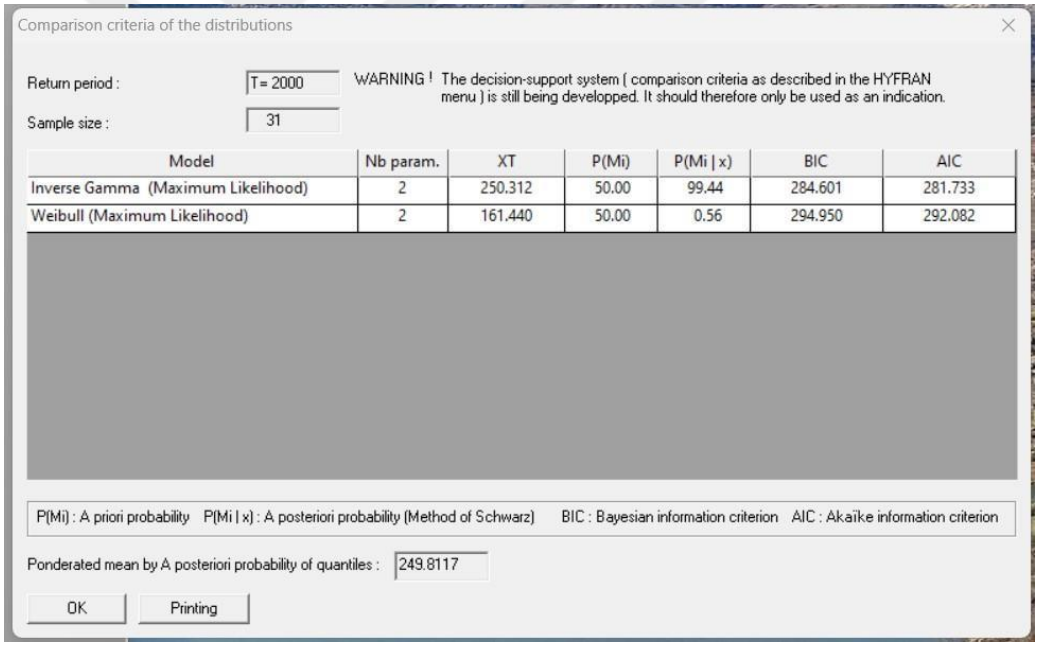

Figure 5.72: BIC and AIC, and the Maximum Estimated 24 Hrs. Rainfall (16)

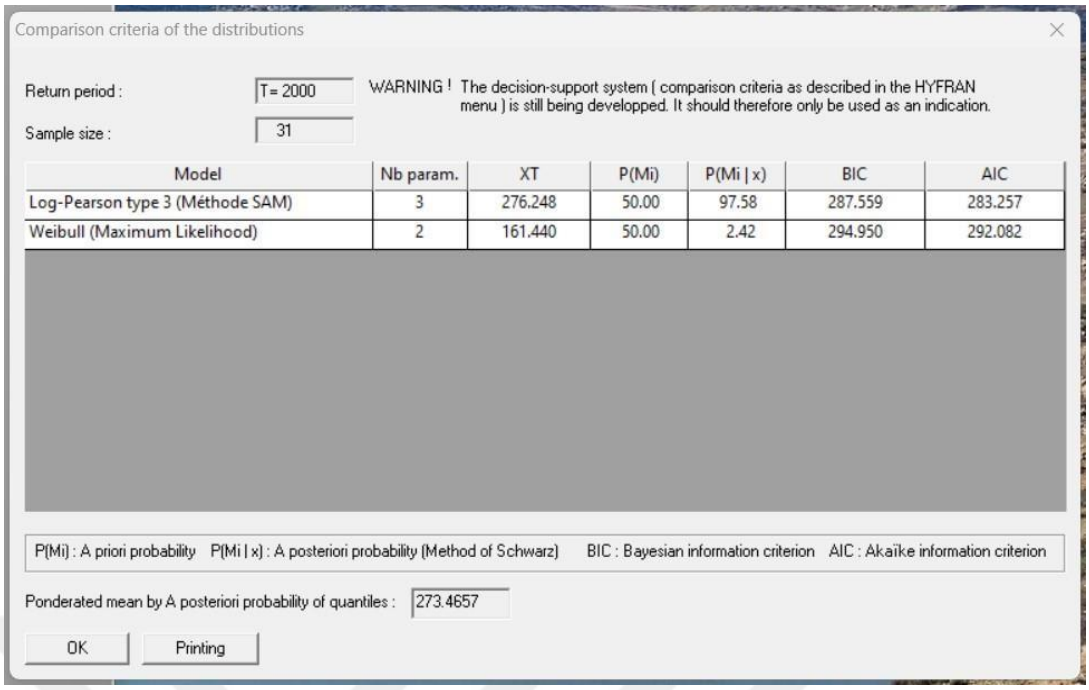

Figure 5.73: BIC and AIC, and the Maximum Estimated 24 Hrs. Rainfall(17)

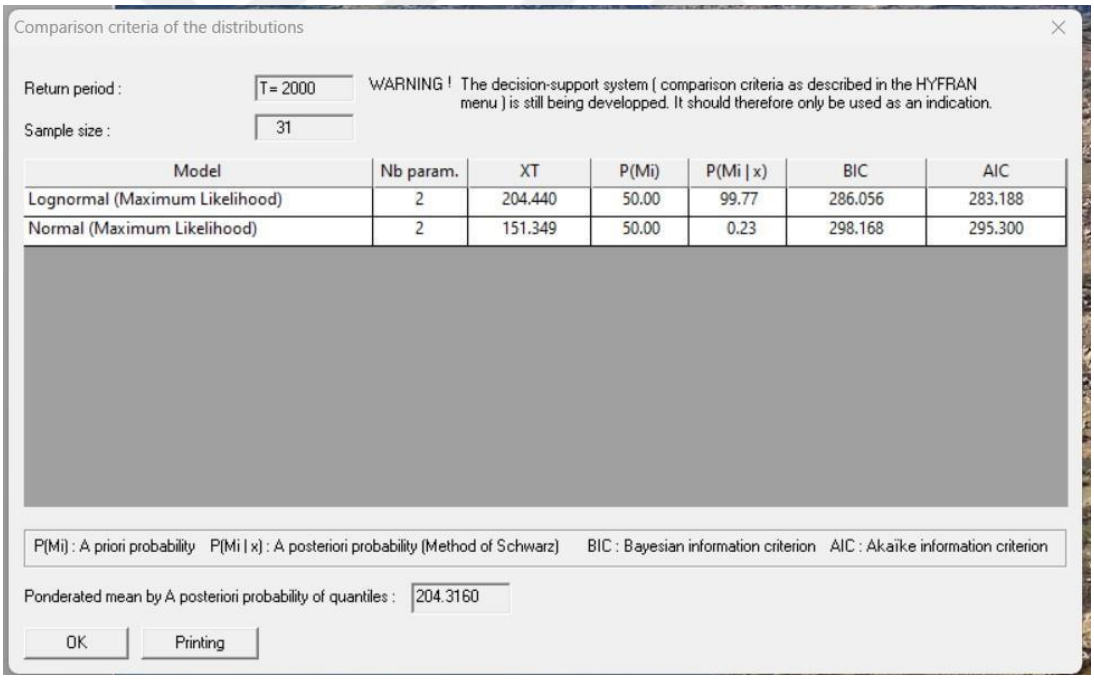

Figure 5.74: BIC and AIC, and the Maximum Estimated 24 Hrs. Rainfall (18)

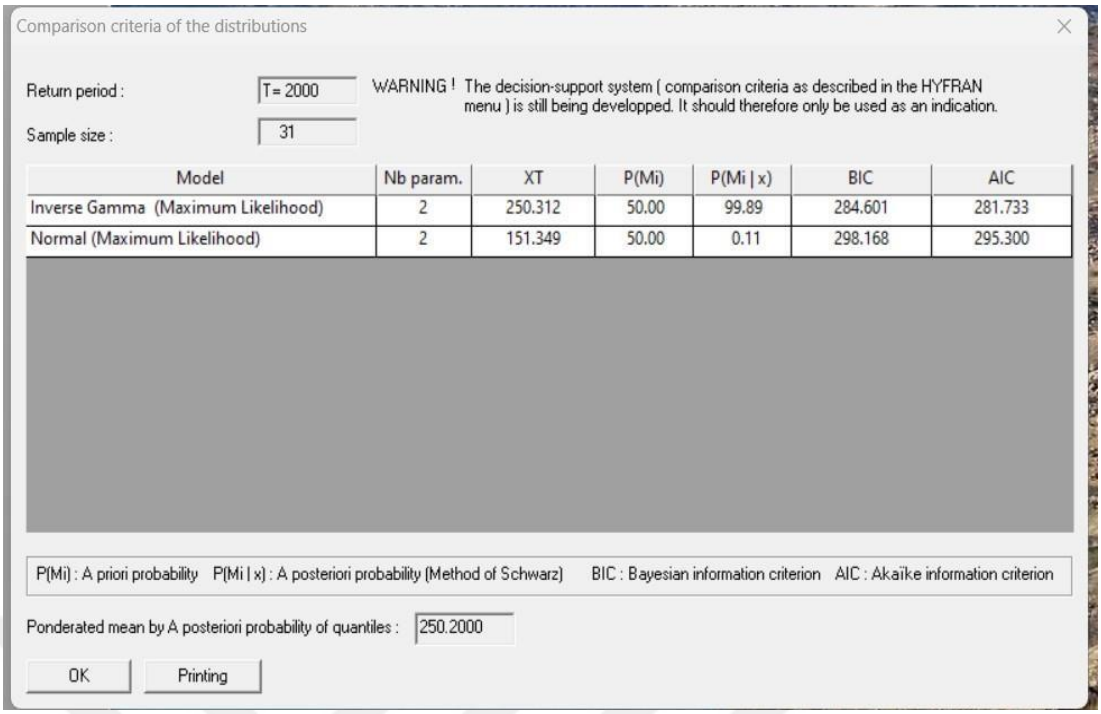

Figure 5.75: BIC and AIC, and the Maximum Estimated 24 Hrs. Rainfall (19)

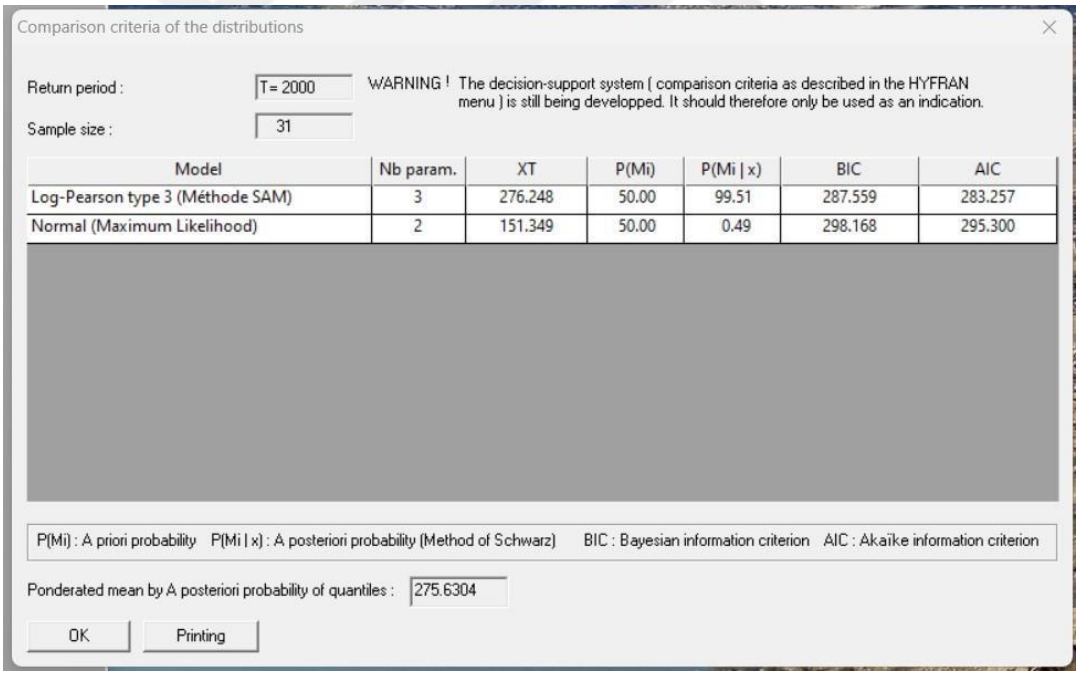

Figure 5.76: BIC and AIC, and the Maximum Estimated 24 Hrs. Rainfall (20)

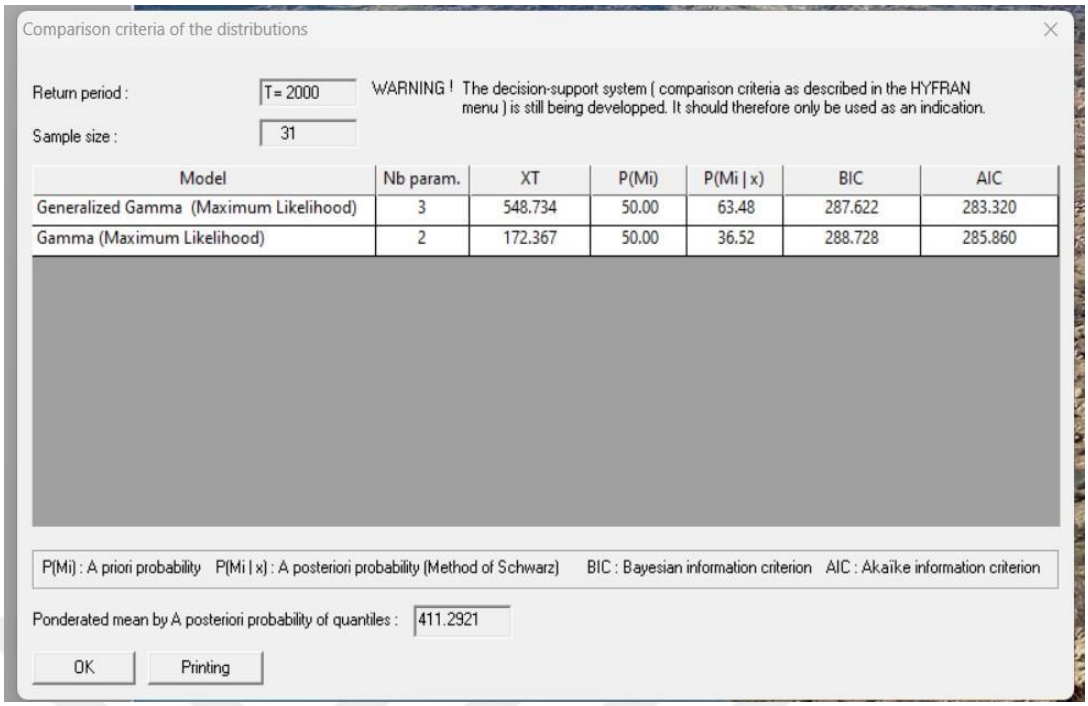

Figure 5.77: BIC and AIC, and the Maximum Estimated 24 Hrs. Rainfall (21)

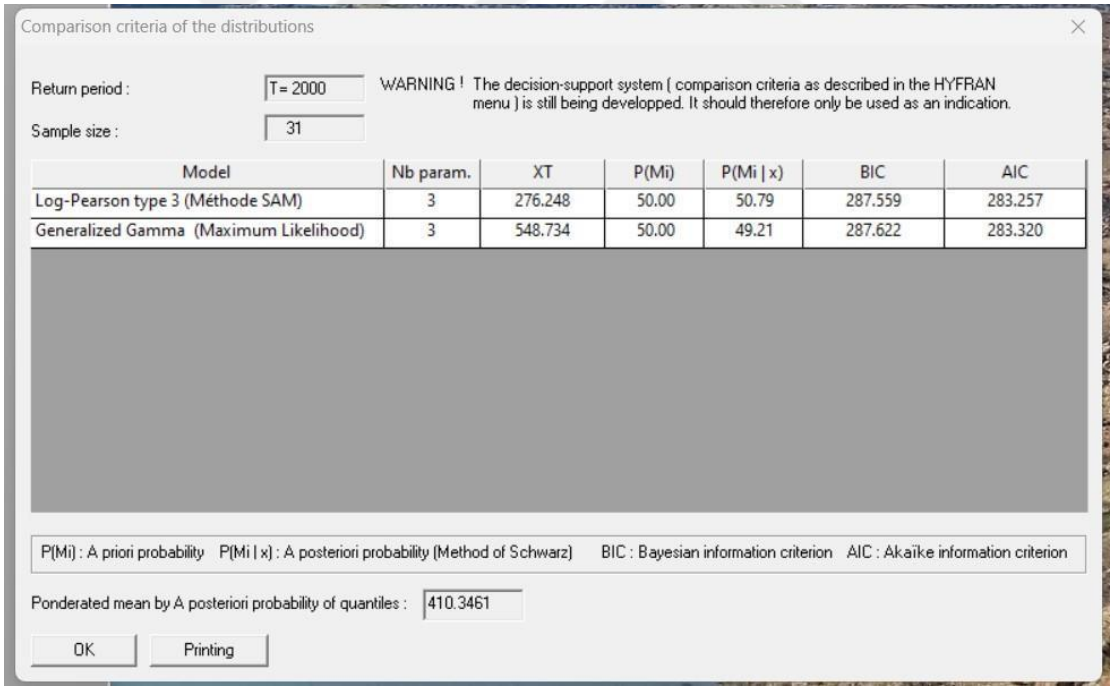

Figure 5.78: BIC and AIC, and the Maximum Estimated 24 Hrs. Rainfall (22)

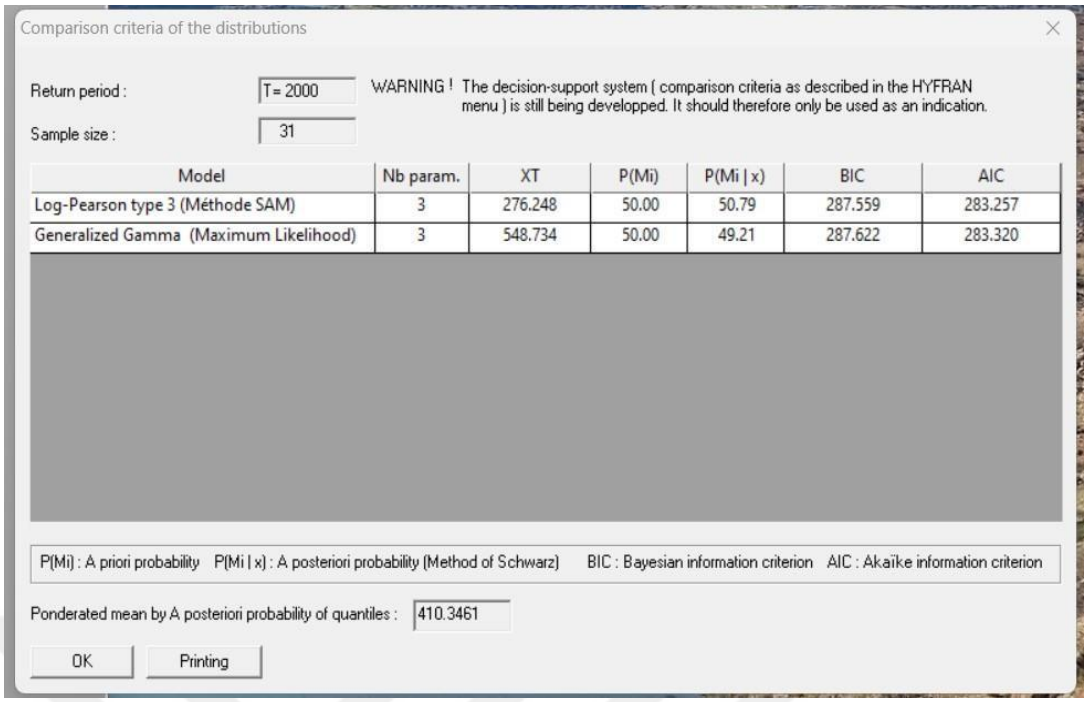

Figure 5.79: BIC and AIC, and the Maximum Estimated 24 Hrs. Rainfall (23)

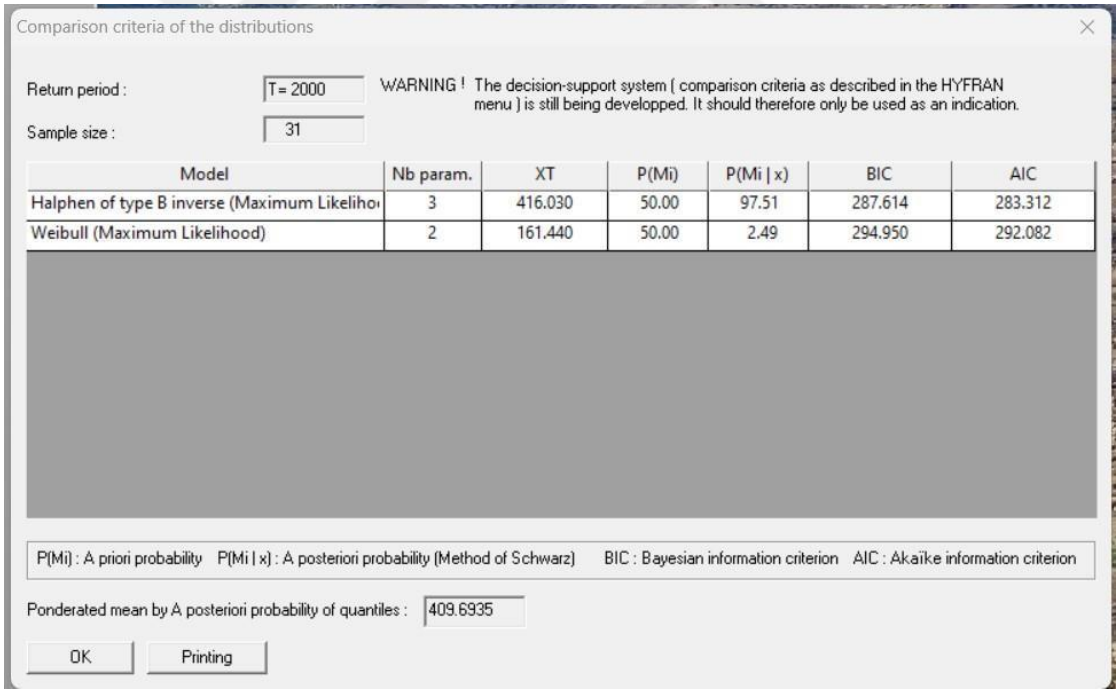

Figure 5.80: BIC and AIC, and the Maximum Estimated 24 Hrs. Rainfall (24)

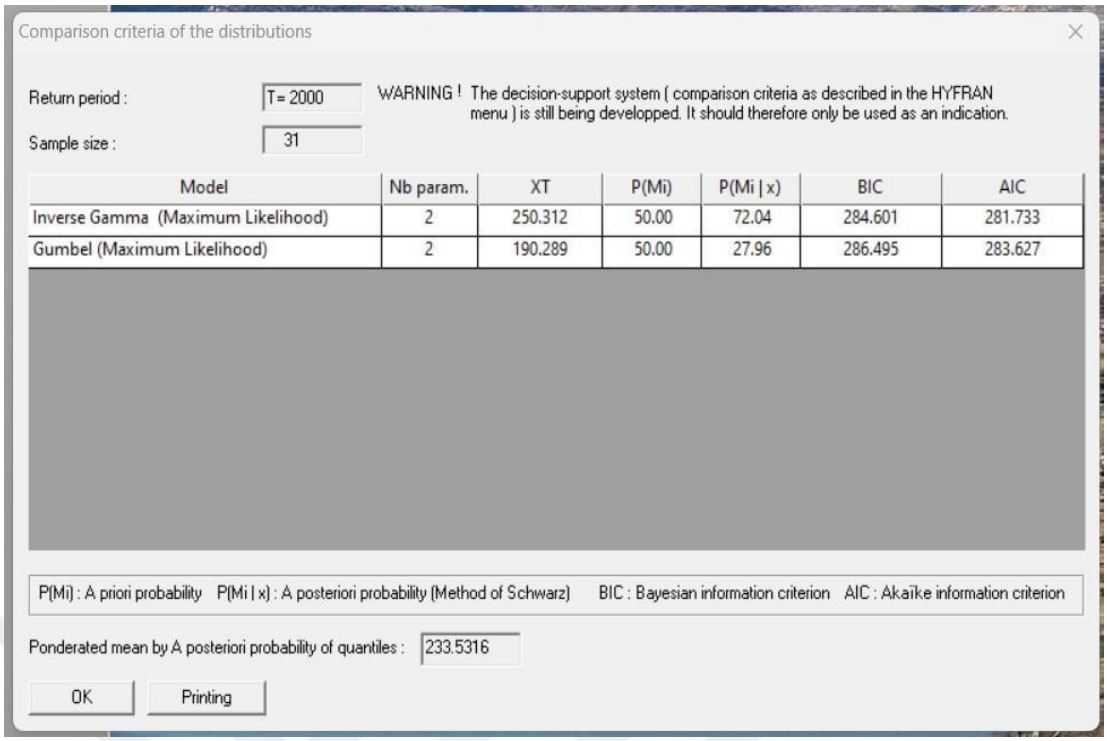

Figure 5.81: BIC and AIC, and the Maximum Estimated 24 Hrs. Rainfall(25)

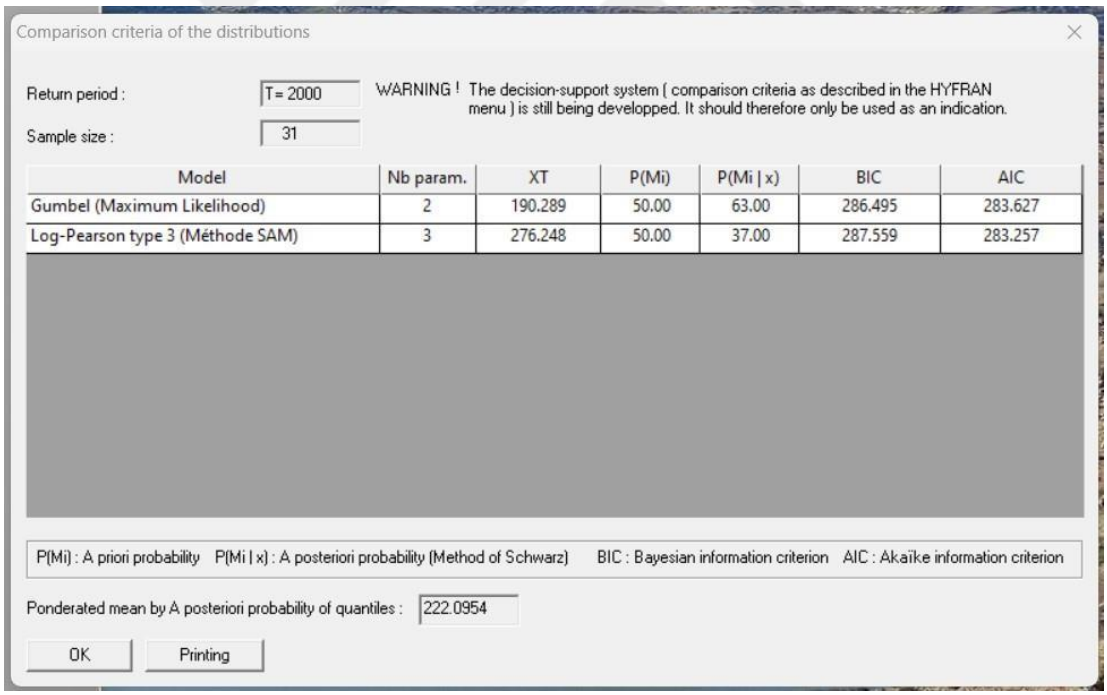

Figure 5.82: BIC and AIC, and the Maximum Estimated 24 Hrs. Rainfall (26)

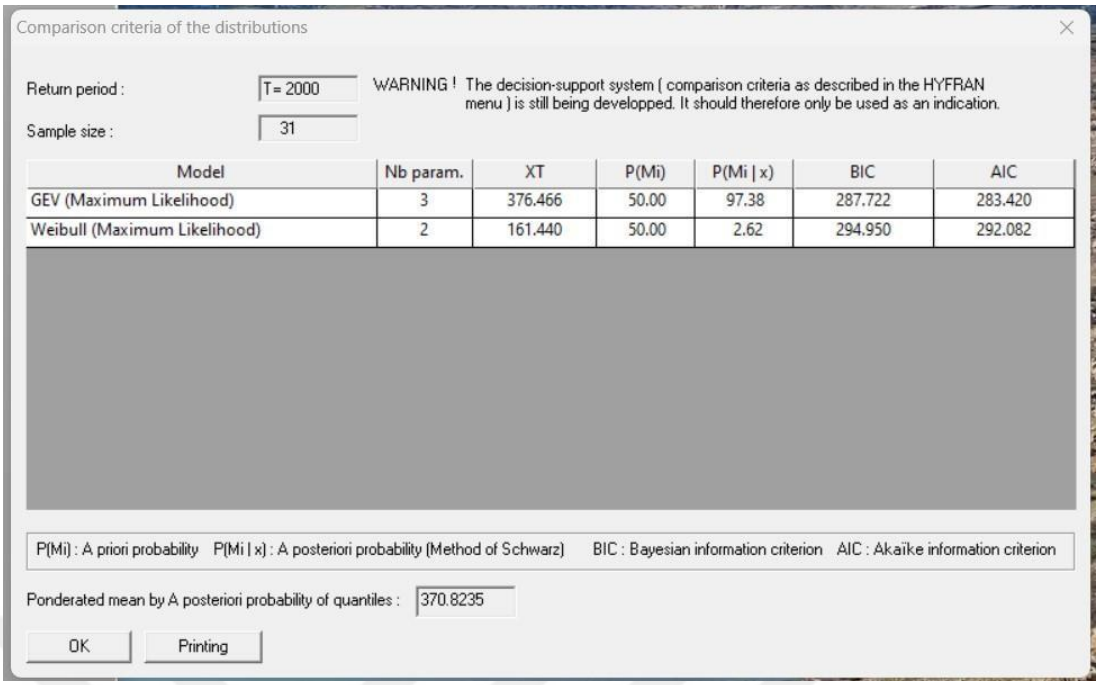

Figure 5.83: BIC and AIC, and the Maximum Estimated 24 Hrs. Rainfall (27)

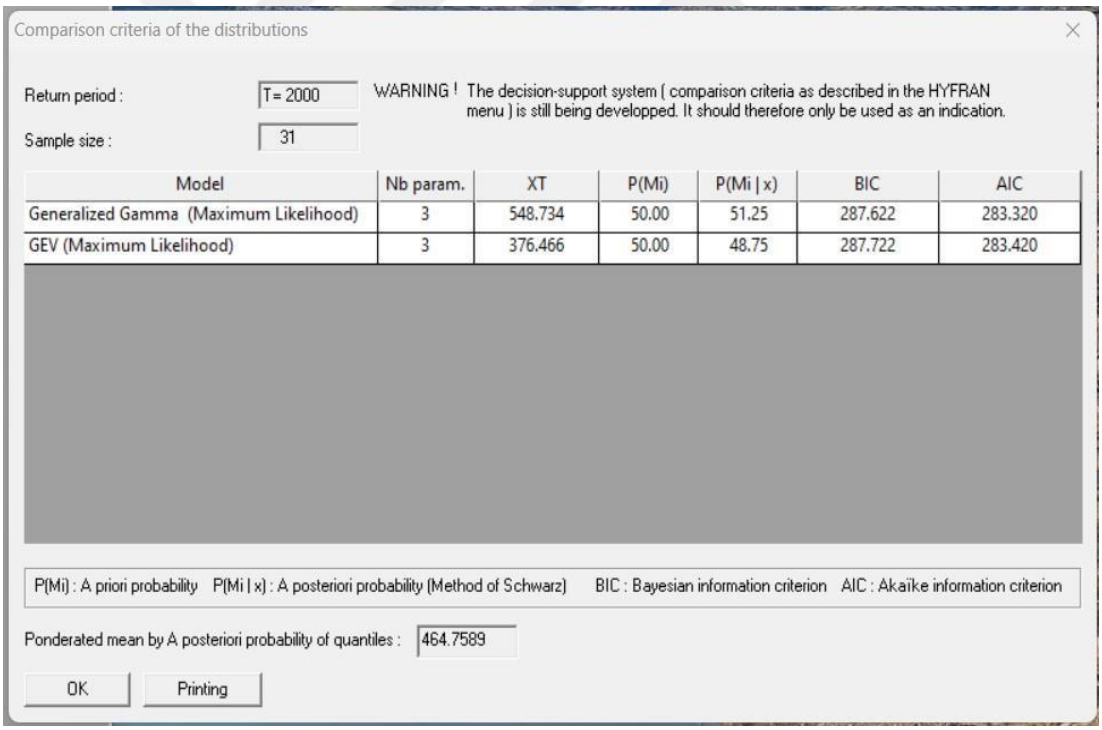

Figure 5.84: BIC and AIC, and the Maximum Estimated 24 Hrs. Rainfall (28)

5.4 Khanas Dam Characteristics

Type of Khanas dam: earth fills the dam with

Core Clay Height of the dam; 34.5 m

The length of the dam is 150 m

Width of the Crest: 6.0 m

U/S Side Slopes: 1(V):3(H)

D/S Side Slopes: 1(V):2.5(H)

Dam Crest Elevation: 484.5 m.a.s.l.

Normal Freeboard: 6.25 m

Minimum Freeboard: 2.12 m

Spillway crest level: 478.25 m.a.s.l. (Normal Water Level)

Maximum Flood Design Elevation: 482.38 m.a.s.l.

Spillway width: 50 m

Spillway length: 220 m

Spillway channel slope: 13 %

Maximum design flood discharge: 947 m3/s

Intake Elevation: 465.49 m.a.s.l.

Storage Capacity: 7,000,000 m3

Dead Storage: 1,000,000 m3

Table (5.2) shows the results of all methods for 5, 10, 15, 20, 25, 50, 100, 200, 1000, and 2000 years return Periods, and the best result, as explained before, is the Exponential (Maximum Likelihood) method, and the maximum estimated 24 hrs. rainfall is (265) mm for the return Period (2000) years.

Table 5.2: Results of all Methods

#	Model	Maximum Daily Rainfall (mm)									
		Return Period (Year)									
		5	10	15	20	25	50	100	200	1000	2000
1	Exponential (Maximum Likelihood)	81.2	103	115	124	131	152	173	195	244	265
2	GEV (Maximum Likelihood)	77.7	96	108	117	124	150	179	214	318	376
3	Gumbel (Maximum Likelihood)	78.6	92.3	100	105	110	123	135	148	178	190
4	Weibull (Maximum Likelihood)	85.7	99.2	106	110	114	123	132	139	155	161
5	Halphen of Type B Inverse (Maximum Likelihood)	77.9	95.5	107	115	122	144	170	199	339	416
6	Normal (Maximum Likelihood)	85.2	97.1	103	107	110	118	125	132	146	151
7	Lognormal (Maximum Likelihood)	80	94.7	103	109	113	127	141	155	189	204
8	3- Parameter Lognormal (Maximum Likelihood)	78.7	98.4	111	120	127	152	179	210	291	332
9	Gamma (Maximum Likelihood)	81.3	94.6	102	107	110	121	131	141	163	172
10	Inverse Gamma (Maximum Likelihood)	78.5	94.5	104	111	116	134	153	173	225	250
11	Log-Person Type 3 (Maximum Likelihood)	78.5	95.3	106	113	119	139	160	183	245	246

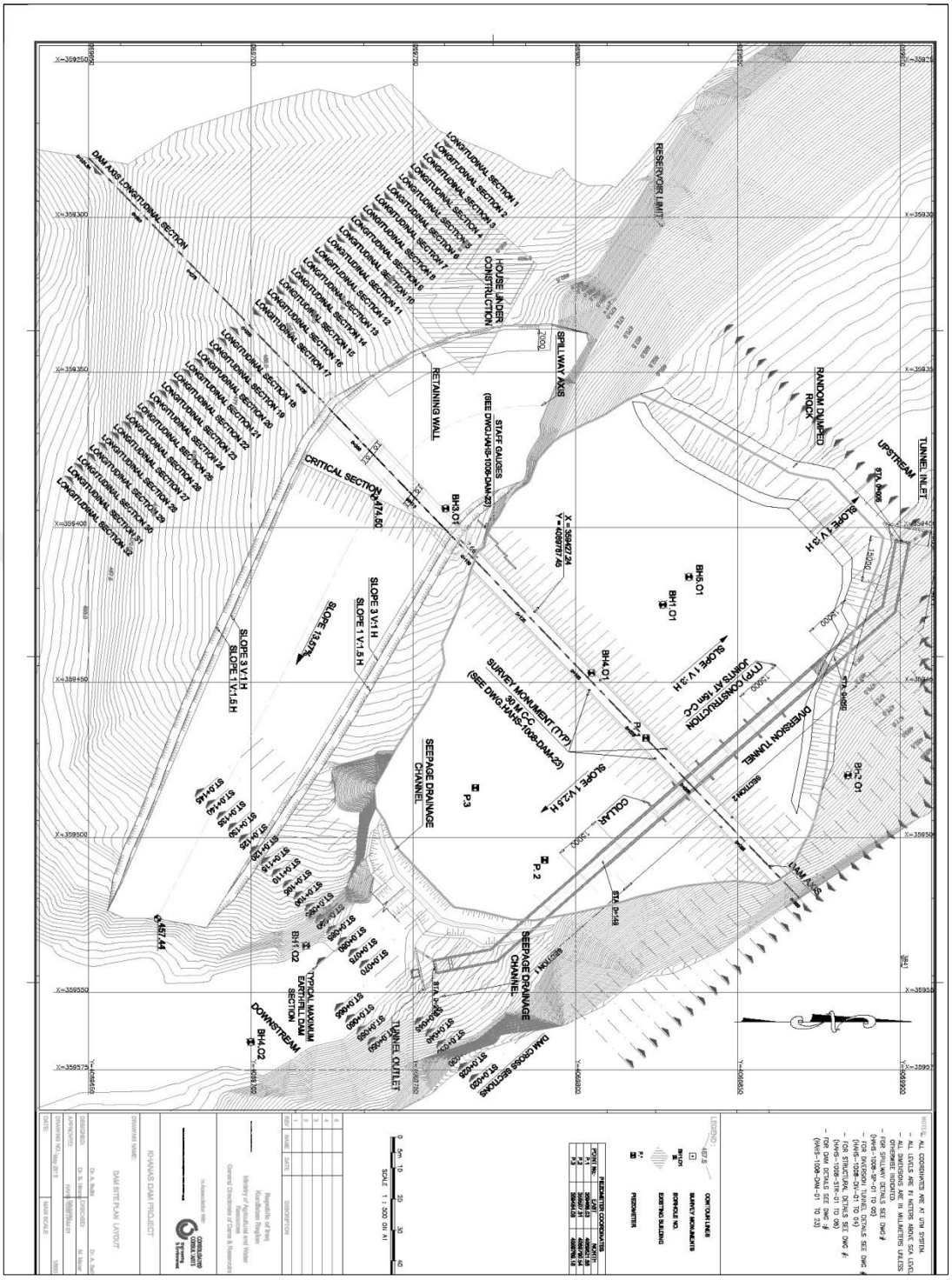

Figure 5.85: Khanas Dam Spillway According To Original Design

5.5 Peak Discharge Calculation by SCS (Soil Conservation Service)

5.5.1 Surface runoff calculation

The SCS model (soil conservation service) has been used to calculate the maximum runoff volume, based on the following equation, in order to estimate the amount of runoff for the reservoir site during the maximum daily rainfall.

$Q= (P-0.2S)^2 / (P+0.8S)$

Where:

Q: is the daily runoff in (mm).

P: is the daily rainfall in (mm).

P=190 mm from table(5.2)

S: is the monthly quantity of losses expressed in millimetres, which may be computed from: S= (25400/ CN) -254

CN: Is a number representing a runoff curve that depends on three variables (soil type, cover type, and initial moisture level), The reservoir catchments' CN was evaluated using a table developed by the soil conservation agency, which took into account the differences between mountainous and agricultural land cover.

CN: This is a number representing a runoff curve that depends on the soil type, the kind of cover, and the amount of moisture present beforehand.

The reservoir catchments' CN was evaluated using a table compiled by the soil conservation agency, and the overall basin's CN was based on the relative complexity of its land cover in terms of mountainous terrain and arable land.

CN =70 (According to Khanas dam Original design)

S= (25400/ 70) -254

S=108.86

$Q= (265-0.2(108.86))^2 / (265+0.8(108.86))$

Q = 59159.859/352.088

Q= 168.025 mm

Using the maximum 24-hour rainfall data in above, the maximum possible Flood

discharge

Q peak = 0.0208 * A* Q / Tp

In which Qpeak is in m^3/s

A is the catchment area in hectares.

Q is in (cm)

Khanas Dam Catchment

Area =530.3 km^2 (From figure 5.2 Ch 3, which was prepared by using GIS ArcMap)
And Tp in an hour

The time to peak (Tp) in an hour can be computed by using the following formula

$Tp= 0.6Tc + \sqrt{Tc}$

Where;

Tc: Time of Concentration in hr

Tc in minutes = $0.01947\ L0.77\ S^{-0.385}$ (Kirpich eq.)

L in meter

S = Slope ($\Delta h/L$) = 0.01 m/m

Tc=0.01947 (30000^0.77 $(0.01)^{-0.385}$

Tc= 321 minutes

Tc= 5.35 hr

$Tp = 0.6(5.35) + \sqrt{5.35}$

Tp =7.42 hr

Q = 168.025 mm

= (168.025/10) * Tp

= 16.8025* 7.42

= 124.68 mm

Q peak = 0.0208 * (530300000/10000) * (124.68 /10) / 7.42

Q peak = 1,853.44 m^3/s

5.5.2 Evaluations of Khanas dam as follows

According to the design Maximum flood discharge = 947 m^3/s, While according to our analysis Maximum flood discharge = 1,853.44 m^3/s, which means Khanas Dam spillway design is unsafe.

Table (5.3) showing comparison between Results obtained by HYFRAN Software and results obtained be researcher (Suzan Nazmy Hussein), results are: - Estimated maximum 24 hours Rainfall using HYFRAN Software for return period, 5, 10, 20, 50, 100. 200, 1000, and 2000 years, While, the researcher obtained results of estimated maximum 24 hours Rainfall using Program prepared using Visual Basic6, for the same returnperiods, the measure of the goodness of fit of a model (R2)between results taken as shown in table and figure is 0.9999

The program prepared by me (SUZAN NADMY HUSSEIN) using visual basic 6 using the Gumbel method for estimation of maximum rainfall easily and accurately, then comparison with the Gumbel method (Method of Moment) shown best-fit curve with (R2) = 0.999 as shown in figure (5.86), (5.87), and (5.88), and table (5.3) with the Program prepared by the researcher as shown in the link below:

https://drive.google.com/file/d/1SePBbR26KbU7R8wTQv5BKmutnm9Ni1W/view?usp=shar e_link

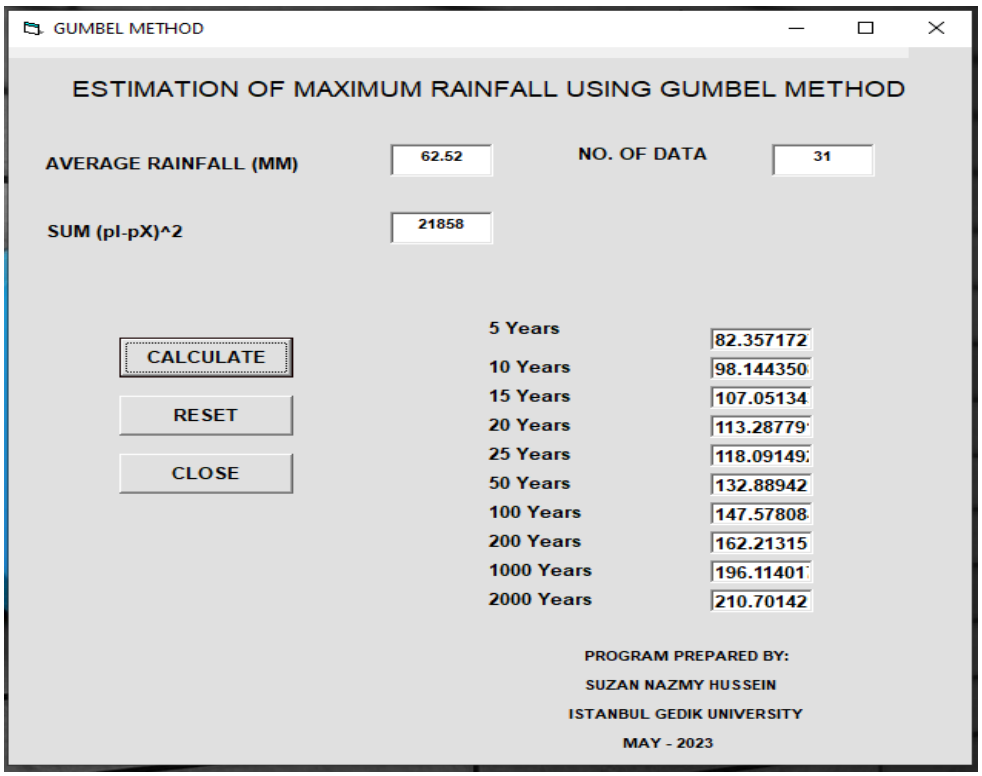

Figure 5.86: Gumbel Method For Estimation Maximum Rainfall

The Program created by me in Visual Basic 6 started with downloading the Program, then the form designed as shown in figure, then the code programmed for each cell, and after that by clicking “Run” we test the program and the code shown below:

```
Private Sub Command1_Click( )
Av = Val(Text3.Text)
 No = Val(Text2.Text)
Y = Val(Text14.Text)
SD = Sqr(((Y) / (No - 1)))
 K1 = -Sqr(6)
 K2 = 3.142857143
K3 = 0.557
Tr1 = 5
 Tr2 = 10
 Tr3 = 15
Tr4 = 20
Tr5 = 25
Tr6 = 50
 Tr7 = 100
Tr8 = 200
 Tr9 = 1000
 Tr10 = 2000
 K4 = Tr1 / (Tr1 – 1)
K5 = Tr2 / (Tr2 - 1)
K6 = Tr3 / (Tr3 - 1)
 K7 = Tr4 / (Tr4 - 1)
 K8 = Tr5 / (Tr5 - 1)
 K9 = Tr6 / (Tr6 - 1)
```

K10 = Tr7 / (Tr7 - 1)

K11 = Tr8 / (Tr8 - 1)

K12 = Tr9 / (Tr9 - 1)

K13 = Tr10 / (Tr10 – 1)

L1 = Log(K4) / Log(2.71828)

L11 = Log(L1) / Log(2.71828)

L2 = Log(K5) / Log(2.71828)

L22 = Log(L2) / Log(2.71828)

L3 = Log(K6) / Log(2.71828)

L33 = Log(L3) / Log(2.71828)

L4 = Log(K7) / Log(2.71828)

L44 = Log(L4) / Log(2.71828)

L5 = Log(K8) / Log(2.71828)

L55 = Log(L5) / Log(2.71828)

L6 = Log(K9) / Log(2.71828)

L66 = Log(L6) / Log(2.71828)

L7 = Log(K10) / Log(2.71828)

L77 = Log(L7) / Log(2.71828)

L8 = Log(K11) / Log(2.71828)

L88 = Log(L8) / Log(2.71828)

L9 = Log(K12) / Log(2.71828)

L99 = Log(L9) / Log(2.71828)

L10 = Log(K13) / Log(2.71828)

L1010 = Log(L10) / Log(2.71828)

KK1 = (K1 / K2) * (K3 + L11)

```
KK2 = (K1 / K2) * (K3 + L22)
KK3 = (K1 / K2) * (K3 + L33)
KK4 = (K1 / K2) * (K3 + L44)
KK5 = (K1 / K2) * (K3 + L55)
KK6 = (K1 / K2) * (K3 + L66)
KK7 = (K1 / K2) * (K3 + L77)
KK8 = (K1 / K2) * (K3 + L88)
KK9 = (K1 / K2) * (K3 + L99)
KK10 = (K1 / K2) * (K3 + L1010)
A = Av + KK1 * SD
B = Av + KK2 * SD
C = Av + KK3 * SD
D = Av + KK4 * SD
E = Av + KK5 * SD
F = Av + KK6 * SD
G = Av + KK7 * SD
H = Av + KK8 * SD
I = Av + KK9 * SD
J = Av + KK10 * SD
Text4.Text = A
Text5.Text = B
Text6.Text = C
Text7.Text = D
Text8.Text = E
Text9.Text = F
Text10.Text = G
```

```
 Text11.Text = H
Text12.Text = I
 Text13.Text = J
 End Sub
Private Sub Command2_Click( )
 Text2.Text = ""
Text3.Text = ""
Text4.Text = ""
Text5.Text = ""
Text6.Text = ""
 Text7.Text = ""
 Text8.Text = ""
Text9.Text = ""
Text10.Text = ""
 Text11.Text = ""
 Text12.Text = ""
 Text13.Text = ""
 Text14.Text = ""
End Sub
Private Sub Command3_Click( )
End
 End Sub
```

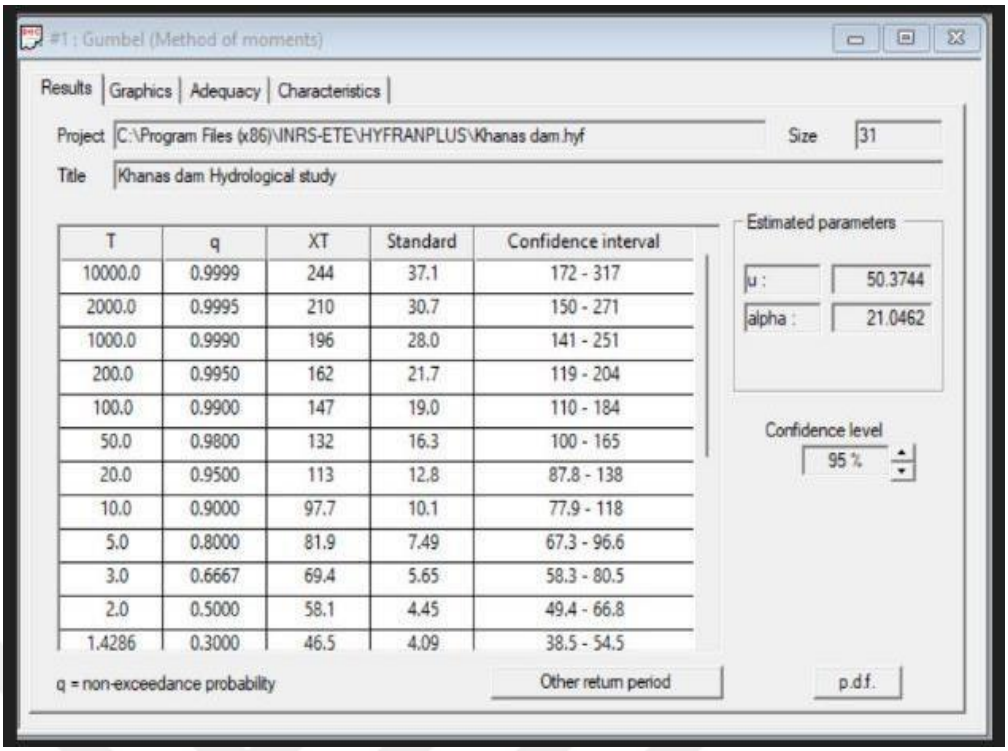

Figure 5.87: Gumbel Method For Estimation Maximum Rainfall

Table 5.3: Gumbel Method For Estimation Maximum Rainfall

	Return Period (Year)							
Method	5	10	20	50	100	200	1000	2000
HYFRAN	81.8	97.7	113	132	147	162	196	210
SUZAN PROGRAM	82.36	98.14	113.29	132.89	147.58	162.21	196.11	210.7

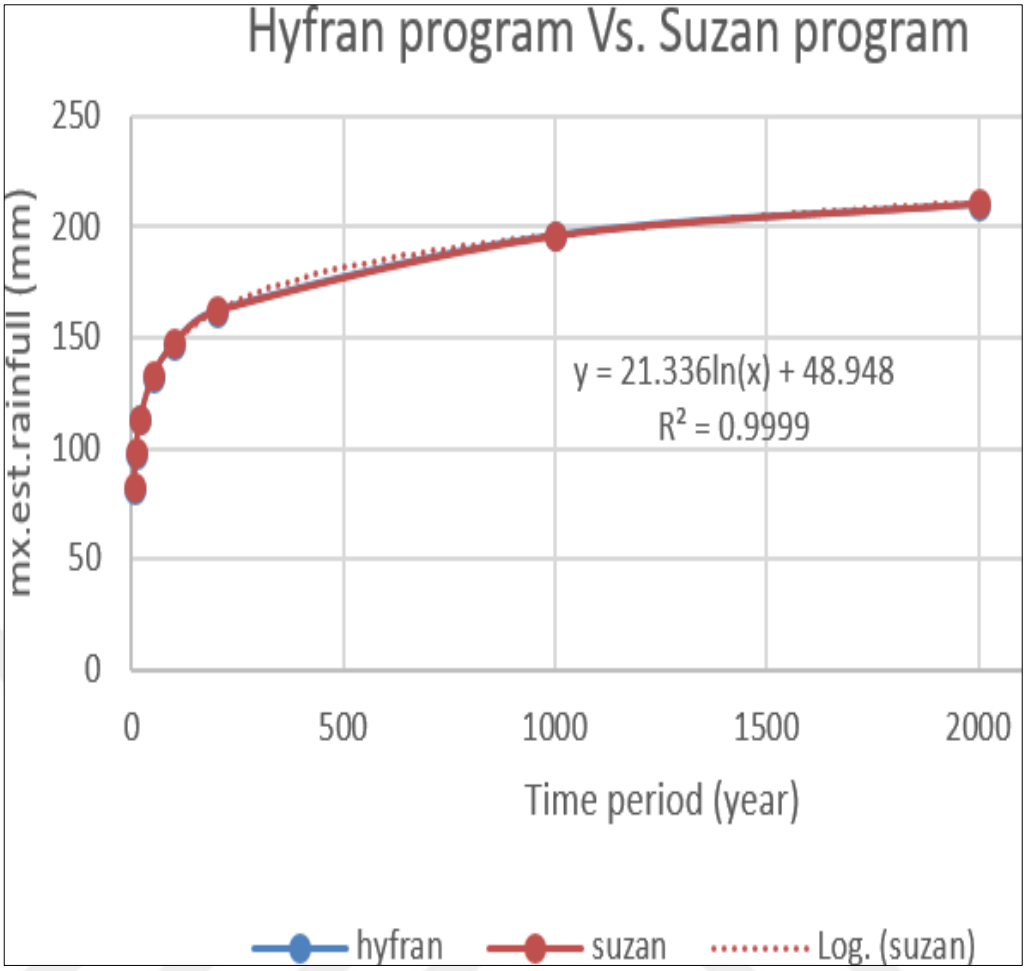

Figure 5.88: Gumbel Method For Estimation Maximum Rainfall

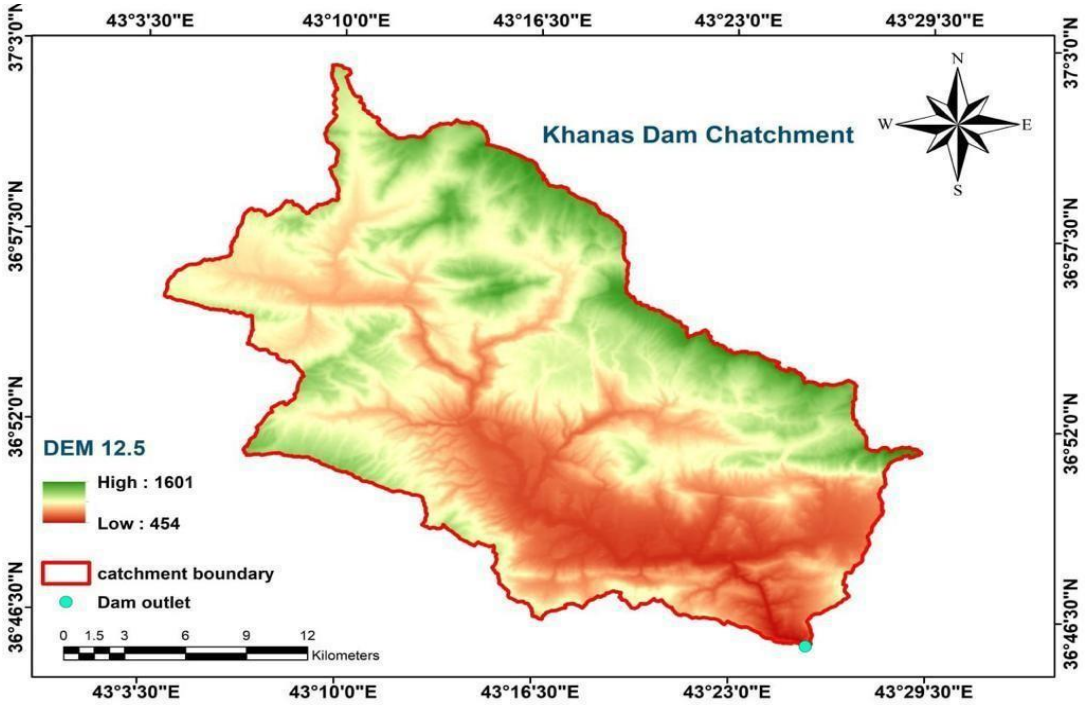

Figure 5.89: Khanas Dam Catchment

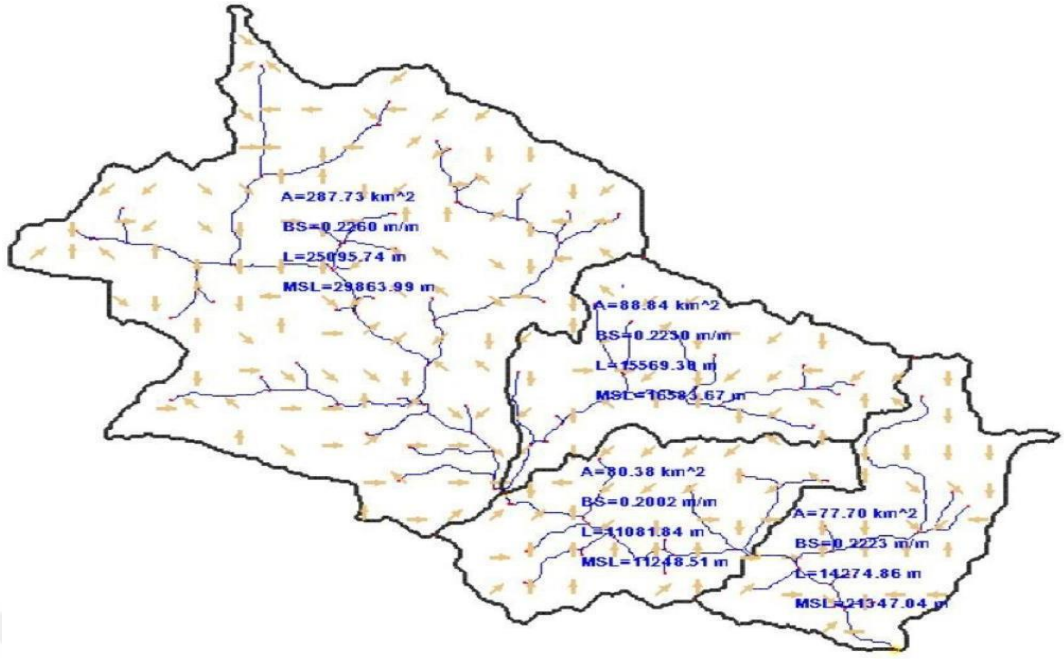

Figure 5.90: By Researcher Suzan Hussein By Watershed Modelling System (WMS)

Using Watershed Modelling System (WMS 8.1), the basin is divided into four sub-basins (indicating the direction of water) as shown in Figure (5.89), having characteristics as shown in Table (5.4):

Table 5.4: Total Catchment Area Using This Software

Sub-catchment area no.	Area (km2)	BS (m/m)	L (M)	MSL (m)
Sub-catchment area No.1	287.73	0.2260	25095.74	29863.99
Sub-catchment area No. 2	88.84	0.2230	15569.38	16583.67
Sub-catchment area No. 3	80.38	0.2002	11081.84	11248.51
Sub-catchment area No.4	77.7	0.2223	14274.86	24347.04

The total catchment area using this software is (534.65) km2

6. CONCLUSION AND RECOMMENDATION

6.1 Summary

After analyzing rainfall data using Hyfran software by 11 models, the best one according to our analyzing data using comparison by AIC and BIC is the Exponential (maximum likelihood) model and the maximum estimated rainfall for 24 hours is (265) mm and the maximum flood discharge according to our research is (1,853.44) m3/s for return period (2000) years (for the same return period of Khanas dam original design).

6.2 Conclusion

HYFRAN – PLUS software was used for estimating maximum daily rainfall in (mm/day) values at many different return periods for 5, 10, 15, 20, 25, 50, 100, 200, 1000, and 2000 years as shown in table no.1 from maximum daily values of Duhok meteorological station from 1991 to 2022 as shown in figure (5.1), (5.2), and (5.3).

Using the DEM map, which is explained in Figure (5.89). And figure (5.90), the stream through the watershed is delineated using GIS program, and the water basin is classified into four sub-basins.

In this study, hydrological parameters that affect floods in Khanas dam catchment area are studied; three types of parameters affecting floods are considered, i.e. meteorological (Climate), morphological, and geological factors. The study area is located in the east of Duhok Governorate, in Khanas Village (Archeological area). Maximum daily rainfall values of Duhok meteorological station from 1991 to 2022 were used in this study. The daily maximum values of rainfall for different return periods for 5, 10, 15, 20, 25, 50, 100, 200, 1000, and 2000 years are computed using HYFRAN, WMS and ArcGIS software are used to determine the total drainage basin characteristics that affect the area, and peak discharge of flood estimated using SCS method for Khanas dam and equal to (1,853.44) m^3/s, while, the maximum flood estimated in Khanas dam design is (947) m^3/s for (2000) years return periods;

therefore the Spillway is unsafe to pass maximum flood according to our research, and it will be at risk. The hydraulic structure of Khanas dam Spillway is unsafe and at risk because of Spillway hydraulic structure dimensions (50 m wide with freeboard 4.13 m at maximum design flood). The catchment area of Khanas Dam is (534.65) km2, and the annual inflow of the Gomel River is about (23) million cubic meters according to the original design project, while the maximum storage capacity of the Khanas dam lake is (7) million cubic meters, as shown in figure (5.2). Therefore, the flood in the Spillway structure happens in the winter season annually.

There are also some of the following things:

1. The hydraulic structure of Khanas dam Spillway is unsafe and at risk because of Spillway hydraulic structure dimensions (50) m wide with a freeboard of 4.13 m at maximum design flood) and it doesn't have the adequacy to pass flood safely according to the original design.
2. The Project don't have a manual of operation and maintenance with original design.
3. According to the original design, there is no stilling at the end of the spillway to dissipate the water energy; therefore, it must be constructed as soon as possible.

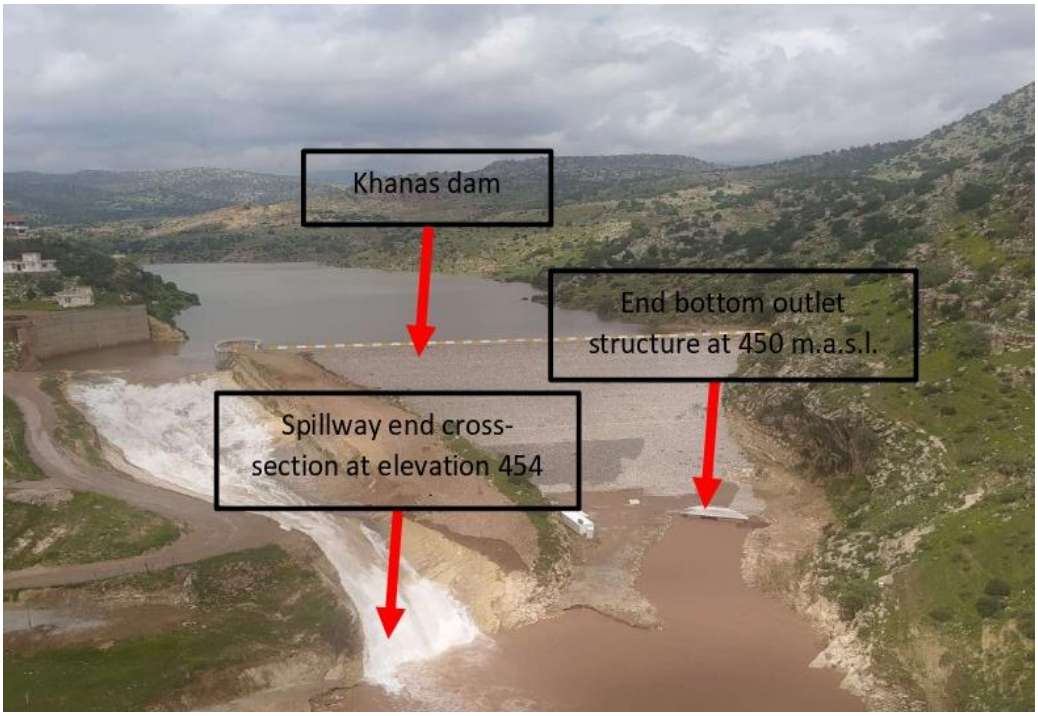

Figure 6.1: Khanas Dam In Flood Case

1. The catchment area of Khanas Dam is (530.3) km2, and the annual inflow of the Gomel River is about (23) million cubic meters according to the original design of the project, while the maximum storage capacity of the Khanas dam lake is (7) million cubic meters. Therefore, the flood in the Spillway structure happens in the winter season annually.
2. In our research, after reviewing the Spillway design layout and cross-sections of the Khanas dam original design showed that the Spillway cross-section end is higher than the bottom outlet structure by more than (4) m; therefore, we expected the backwater to happen (in flood case), in (13/04/2023) this situation happened as shown in the picture below:

6.3 Recommendations

1. It is necessary to make an emergency spillway at the right abutment of the dam.
2. It is very important to the lining of the spillway structure by reinforced concrete from
3. the beginning to the end Spillway channel.
4. In our opinion, it is necessary for the design of any dam spillway structure to be Constructed in hard rock or using a reinforced concrete structure and, as possible, as far away from the alignment of the spillway to the dam body, not the same as executed is Khanas Dam.
5. The Project must have a manual of operation and maintenance, with good supervision, at least in the winter season.
6. It is necessary to install a metrological station at least once to collect data to analyze for the best Operation of the dam.
7. It is important to construct at least two dams upstream of Khanas dam because of the largest catchment area and the smallest storage capacity of Khanas dam for controlling the flood.
8. It is very important to save Khanas Archeological and Sennacherib channels downstream of the Khanas dam.

9. It’s very important for and dam project to have Operation and Maintenance Manual, and should be mention to:

- Bottom Outlet, which contain gates and Valves, how it will be open=d and closed, what is the discharge for every opening verse lake water level, also, what kind of maintenance needed for gates and Valves and when.
- Piezometers and other sensors in dam body, must be shown the locations with coordinates and how it will be measuring with analyzing the data.
- Geodetic Network, must be explained with all Benchmarks and Pillars, locations with coordinates, and when it will be measured and how.
- Spillway, must be explained, how to measure the spillway discharge.
- Water Balance of the dam must be explained.
- If there is any leakage on the dam body or, in left or right abutment, how will controlled.

According to my investigation of the sediments being brought to the dam, the kind of sediment is Suspended sediment, and the effects of sediment on the dam are tow effects: The amount of sediment carried into a reservoir is at its highest during floods. This reduces the reservoir's storage capacity, and sediment affect Turbines in Hydropower Dams that making cavitation on Gates and Valves in Bottom Outlets.

The default life expectancy of the dam is 40 years, when check dams constructed in valleys, Sediment will be reduced and the life expected of the dam will increase about 18% when the operation of the dam is controlled by technical staff, maybe can decreasing sediment by opening valves in flood case.

REFERENCES

Abdulqadir Mohammed Salih, The Engineer (A step in the design for irrigation, water resources, and civil Engineers), Published by VNG International NGO, Iraq, Duhok Governorate, 2020.

Adamo, N., Al-Ansari, N., Sissakian, V., Laue, J., & Knutsson, S. (2020). Dam Safety: General Considerations. Journal of Earth Sciences and Geotechnical Engineering, 10(6), 1-21.

Athani, S. S., Solanki, C. H., & Dodagoudar, G. R. (2015). Seepage and stability analyses of earth dam using finite element method. Aquatic Procedia, 4, 876-883.

Arora, K. R. (2004). Irrigation, water power and water resources engineering. Standard Publisher Distributors.

Andreini, M., Gardoni, P., Pagliara, S., & Sassu, M. (2019). Probabilistic models for the erosion rate in embankments and reliability analysis of earth dams. Reliability Engineering & System Safety, 181, 142-155.

Awad, M., Khanna, R., Awad, M., & Khanna, R. (2015). Support vector machines for classification. Efficient Learning Machines: Theories, Concepts, and Applications for Engineers and System Designers, 39-66.

Barebohar Preventive Proposed Dam Design, Iraq-Duhok Governorate, 2022, VNG International NGO.

Barbu, A., & Zhu, S. C. (2020). Monte Carlo Methods (Vol. 35, p. 36). Singapore: Springer Singapore.

Bai, H., Ma, D., & Chen, Z. (2013). Mechanical behaviour of groundwater seepage in karst collapse pillars. Engineering Geology, 164, 101-106.

Bhaskar, P., Puppala, A. J., & Boluk, B. (2022). Influence of unsaturated hydraulic properties on transient seepage and stability analysis of an earthen dam. International Journal of Geomechanics, 22(7), 04022105.

Bect, J., Li, L., & Vazquez, E. (2017). Bayesian subset simulation. SIAM/ASA Journal on Uncertainty Quantification, 5(1), 762-786.

Betz, W., Papaioannou, I., Beck, J. L., & Straub, D. (2018). Bayesian inference with subset simulation: strategies and improvements. Computer Methods in Applied Mechanics and Engineering, 331, 72-93.

Breitung, K. W. (2006). Asymptotic approximations for probability integrals. Springer.

Coyne & Bellier, " Khazer – Gomel Project " Committees Comments on The Hydrological study, 1978

Chow, V.T, "Applied Hydrology" McGraw Hill Book Company Inc, New York, N. Y, 1988.

Chen, Q., & Chang, L. Y. (2011). Probabilistic slope stability analysis of a 300 m high embankment dam. In Geo-Risk 2011: Risk Assessment and Management (pp. 452-459).

Chen, C., Zhang, L. M., & Chang, D. S. (2016). Stress-strain behaviour of granular soils subjected to internal erosion. Journal of Geotechnical and Geoenvironmental Engineering, 142(12), 06016014.

Devi, D. D. L., & Anbalagan, R. (2017). Study on slope stability of earthen dams by using GeoStudio software. International Journal of advanced research, ideas and Innovations in Technology, 3(6), 408-414.

El Methni, J., Gardes, L., Girard, S., & Guillou, A. (2012). Estimation of extreme quantiles from heavy and light-tailed distributions. Journal of Statistical Planning and Inference, 142(10), 2735-2747.

Emmerich, M. T., & Deutz, A. H. (2018). A tutorial on multiobjective optimization: fundamentals and evolutionary methods. Natural Computing, 17, 585-609.

Fattah, M. Y., Al-Labban, S. N., & Salman, F. A. (2014). Seepage analysis of a zoned earth dam by finite elements. International Journal of Civil Engineering and Technology (IJCIET), 5(8), 128-139.

Feng, K., Lu, Z., Pang, C., & Yun, W. (2018). Efficient numerical algorithm of profuse reliability analysis: an application to wing box structure. Aerospace Science and Technology, 80, 203-211.

Froehlich, D. C. (2008). Embankment dam breach parameters and their uncertainties. Journal of Hydraulic Engineering, 134(12), 1708-1721.

Fu, G., Deo, R., Ji, J., & Kodikara, J. (2021). Failure assessment of reinforced rock slopes subjected to bolt corrosion considering correlated multiple failure modes. Computers and Geotechnics, 132, 104029.

General Directorate of Agriculture, Duhok, Meteorological Department. Master Thesis, The Climate of Duhok Governorate, Dlear Aziz Taha B.A. College of Social Science University koya, 2013." Ministry of Irrigation/Iraq" Design Manual of Irrigation and drainage.

Gholampoor, M. H. (2017, October). Reliability Analysis of Internal Erosion in Embankment Dam. In ISRM 3rd Nordic Rock Mechanics Symposium-NRMS 2017. OnePetro.

Goodarzi, E., Shui, L. T., Ziaei, M., & Haghizadeh, A. (2010). Estimating the Probability of failure due to internal erosion with event tree analysis. European Journal of Geotechnical Engineering, 935-948.

Guo, X., Dias, D., Carvajal, C., Peyras, L., & Breul, P. (2019). A comparative study of different reliability methods for high dimensional stochastic problems related to earth dam stability analyses. Engineering Structures, 188, 591-602.

Hadigol, M., & Doostan, A. (2018). Least squares polynomial chaos expansion: A review of sampling strategies. Computer Methods in Applied Mechanics and Engineering, 332, 382-407.

Hanson, G. J., Tejral, R. D., Hunt, S. L., & Temple, D. M. (2010, April). Internal erosion and impact of erosion resistance. In Proceedings of the 30th US Society on Dams annual meeting and conference (pp. 773-784).

Hasan, K. N., Preece, R., & Milanović, J. V. (2019). Existing approaches and trends in uncertainty modelling and probabilistic stability analysis of power systems with renewable generation. Renewable and Sustainable Energy Reviews, 101, 168-180.

Kanning, W., Bocovich, C., Schweckendiek, T., & Mooney, M. A. (2015). Incorporating observations to update the piping reliability estimate of the Francis levee. In Geotechnical Safety and Risk V (pp. 861-866). IOS Press.

KRG, Ministry of Agriculture and Water Resources, General Directorate of Dams and Water Resourses Feasibility study of GaliBandawa Dam, Barzan Engineering Consultant Berau, 2012.

Ksubramanya " Engineering Hydrology" McGraw Hill Book Company Inc, New York, N. Y, 1999.

Larry, W. "Water Resources Engineering" John Wiley & Sons, Inc., 2005.

Linsly, R. K. "Water Resources Engineering" McGraw Hill Book Company Inc, New York, N. Y, 1986.

Liang, R.Y. & Nusier, Osama & Husein Malkawi, Abdallah. (1999). A reliability-based approach for evaluating the slope stability of embankment dams. Engineering Geology. 54. 271-285. 10.1016/S0013-7952(99)00017-4.

Li, D., Li, Z., & Gao, Z. (2019). Quadrature-based moment methods for the population balance equation: An algorithm review. Chinese Journal of Chemical Engineering, 27(3), 483-500.

Li, N., Zhang, D. Q., Liu, H. T., & Li, T. J. (2021). Optimal design and strength reliability analysis of pressure shell with grid sandwich structure. Ocean Engineering, 223, 108657.

Martin, T. E., & McRoberts, E. C. (1999, January). Some considerations in the stability analysis of upstream tailings dams. In Proceedings of the sixth international conference on Tailings and mine waste (Vol. 99, pp. 287-302). Rotterdam, Netherlands: AA Balkema.

Melchers, R. E., & Beck, A. T. (2018). Structural reliability analysis and prediction. John Wiley & Sons.

Mouyeaux, A., Carvajal, C., Bressolette, P., Peyras, L., Breul, P., & Bacconnet, C. (2018). Probabilistic stability analysis of an earth dam by Stochastic Finite Element Method based on field data. Computers and Geotechnics, 101, 34-47.

Nusier, Osama & Alawneh, Ahmed & Husein Malkawi, Abdallah. (2002). Remedial measures to control seepage problems in the Kafrein dam, Jordan. Bulletin of Engineering Geology and the Environment. 61. 145-152. 10.1007/s100640100131.

Papaioannou, I., Geyer, S., & Straub, D. (2019). Improved cross entropy-based importance sampling with a flexible mixture model. Reliability Engineering & System Safety, 191, 106564.

Priadko, I. N., Mushchanov, V. P., Bartolo, H., Vatin, N. I., & Rudnieva, I. N. (2016). Improved numerical methods in reliability analysis of suspension roof joints. Magazine of Civil Engineering, (5 (65)), 27-41.

Poce, V. M. " Engineering Hydrology, Principle and Practice" Prentice Hall, 1989.

Punmia, B. C. " Irrigation and Water Power Engineering" Laxmi Publications(P) LTD, New Delhi, 1992.

Ribas, J. R., Severo, J. C. R., Guimaraes, L. F., & Perpetuo, K. P. C. (2021). A fuzzy FMEA assessment of hydroelectric earth dam failure modes: A case study in Central Brazil. Energy Reports, 7, 4412-4424.

Richards, K. S., & Reddy, K. R. (2005). Slope failure of embankment dam under extreme flooding conditions: comparison of limit equilibrium and continuum models. In Slopes and retaining structures under seismic and static conditions (pp. 1-12).

Sachpazis, C. I. (2013). Detailed slope stability analysis and assessment of the original Carsington earth embankment dam failure in the UK. Published in, 18.

Sengupta, A., & Upadhyay, A. (2009). Locating the critical failure surface in a slope stability analysis by genetic algorithm. Applied Soft Computing, 9(1), 387-392.

Sica, S., Pagano, L., & Rotili, F. (2019). Rapid drawdown on earth dam stability after a strong earthquake. Computers and Geotechnics, 116, 103187.

Siacara, A. T., Napa-García, G. F., Beck, A. T., & Futai, M. M. (2020). Reliability analysis of earth dams using direct coupling. Journal of Rock Mechanics and Geotechnical Engineering, 12(2), 366-380.

Schöbi, R. (2019). Surrogate models for uncertainty quantification in the context of imprecise probability modelling. IBK Bericht, 505.

Sun, Y., Chang, H., Miao, Z., & Zhong, D. (2012). Solution method of an overtopping risk model for earth dams. Safety Science, 50(9), 1906-1912.

Refaiy, A. R., AboulAtta, N. M., Saad, N. Y., & El-Molla, D. A. (2021). Modelling the effect of downstream drain geometry on seepage through earth dams. Ain Shams Engineering Journal, 12(3), 2511-2531.

Tan, X., Wang, X., Khoshnevisan, S., Hou, X., & Zha, F. (2017). Seepage analysis of earth dams considering spatial variability of hydraulic parameters. Engineering Geology, 228, 260-269.

Vakili, Amir & Selamat, Mohamad & Mohajeri, Parsa & Moayedi, Hossein. (2018). A Critical Review on Filter Design Criteria for Dispersive Base Soils. Geotechnical and Geological Engineering. 36. 10.1007/s10706-018-0453-7.

Wang, L., Wu, C., Tang, L., Zhang, W., Lacasse, S., Liu, H., & Gao, L. (2020). Efficient reliability analysis of earth dam slope stability using extreme gradient boosting method. Acta Geotechnica, 15, 3135-3150.

Wu, Z., Chen, C., Lu, X., Pei, L., & Zhang, L. (2020). Discussion on the allowable safety factor of slope stability for high rockfill dams in China. Engineering geology, 272, 105666.

Zhu, Z., & Du, X. (2016). Reliability analysis with Monte Carlo simulation and dependent Kriging predictions. Journal of Mechanical Design, 138(12).

Zuev, K. (2015). Subset simulation method for rare event estimation: an introduction. arXiv preprint arXiv:1505.03506.

Zou, Yuhua & Zou, Yu & Tang, Min & He, Chang. (2014). Modelling the construction of a high embankment dam. KSCE Journal of Civil Engineering. 18. 10.1007/s12205-014-0180-4.

RESUME

Suzan Nazmy HUSSEIN

EDUCATION:

- Bachelor :2011, Kirkuk University, Civil Engineering Department ,College of Kirkuk-Iraq.
- Tomer : 2021 , Turkish Language ,Alanya Alaaddin Keykubat University.
- Russian langue study: 2022, in Russian language Online Academy
- Master :2023, Istanbul Gedik University, Civil Engineering.

Job:

- Assistant engineer at the Engineering Depaetment in Kirkuk Electricity Directorate (2013-2018) in Iraq

Languages:

- Arabic
- Turkish
- English
- Turkman
- Sorani-Kurdish
- Russian

Microsoft programs:

- Microsoft office (Excel, Word, Power Point, One Drive)
- Hyrfran plus (Hydrological frequency analysis)
- GIS ArcMap
- WMS (watershed modelling system)
- Autocad Civil 3D
- Matlab
- Best fit
- Visual Basic 6
- Google Earth Pro
- Surfer